AWARD NUMBER: W81XWH-11-1-0819

TITLE: An Implantable Neuroprosthetic Device to Normalize Bladder Function after SCI

PRINCIPAL INVESTIGATOR: Changfeng Tai, PhD

CONTRACTING ORGANIZATION: University of Pittsburgh
Pittsburgh, PA 15213-3320

REPORT DATE: December 2014

TYPE OF REPORT: Final

PREPARED FOR: U.S. Army Medical Research and Materiel Command
Fort Detrick, Maryland 21702-5012

REPORT DOCUMENTATION PAGE

Form Approved
OMB No. 0704-0188

1. REPORT DATE	2. REPORT TYPE	3. DATES COVERED
December 1, 2014	Final report	9/22/2011-9/21/2014

4. TITLE AND SUBTITLE
An Implantable Neuroprosthetic Device to Normalize Bladder Function after SCI

5a. CONTRACT NUMBER

5b. GRANT NUMBER
W81XWH-11-1-0819

5c. PROGRAM ELEMENT NUMBER

6. AUTHOR(S)
Changfeng Tai, PhD

E-Mail:cftai@pitt.edu

5d. PROJECT NUMBER

5e. TASK NUMBER

5f. WORK UNIT NUMBER

7. PERFORMING ORGANIZATION NAME(S) AND ADDRESS(ES)

University of Pittsburgh
3520 Fifth Ave
Pittsburgh, PA 15213-3320

8. PERFORMING ORGANIZATION REPORT NUMBER

9. SPONSORING / MONITORING AGENCY NAME(S) AND ADDRESS(ES)

U.S. Army Medical Research and Materiel Command
Fort Detrick, Maryland 21702-5012

10. SPONSOR/MONITOR'S ACRONYM(S)

11. SPONSOR/MONITOR'S REPORT NUMBER(S)

12. DISTRIBUTION / AVAILABILITY STATEMENT

Approved for Public Release; Distribution Unlimited

13. SUPPLEMENTARY NOTES

14. ABSTRACT
The long-term goal of our project is to develop a novel neuroprosthetic device to restore the functions of the urinary bladder for SCI people without further damaging the nervous system. Advanced technologies in electrical and computer engineering will be applied to design the novel neuroprosthetic device. Based on our previous studies, we propose in this project to use pudendal nerve stimulation and blockade to restore both continence and micturition after SCI. Our strategy does not require sacral posterior root rhizotomy, preserves the spinal reflex functions of the bowel and sexual organs, and more importantly provides the opportunity for SCI people to benefit from any advance in neural regeneration and repair techniques in the future. During the last 3 years, we have successfully designed and developed a wireless controlled, wireless charged, small implantable stimulator for pudendal nerve stimulation and/or block, and tested its functionality in animal experiments using cats. These results have laid the foundation for us to further design and develop an implantable stimulator for human application in the future.

15. SUBJECT TERMS
Spinal cord injury, micturition, bladder, stimulator, block

16. SECURITY CLASSIFICATION OF:			17. LIMITATION OF ABSTRACT	18. NUMBER OF PAGES	19a. NAME OF RESPONSIBLE PERSON
a. REPORT	b. ABSTRACT	c. THIS PAGE			USAMRMC
Unclassified	Unclassified	Unclassified	Unclassified	70	19b. TELEPHONE NUMBER *(include area code)*

Table of Contents

Page

1. Introduction

The long-term goal of our project is to develop a novel neuroprosthetic device to restore the functions of the urinary bladder for SCI people without further damaging the nervous system. Advanced technologies in electrical and computer engineering will be applied to design the novel neuroprosthetic device. Based on our previous studies [1-4], we propose in this project to use pudendal nerve stimulation (PNS) and blockade to restore both continence and micturition after SCI. Our strategy does not require sacral posterior root rhizotomy, preserves the spinal reflex functions of the bowel and sexual organs, and more importantly provides the opportunity for SCI people to benefit from any advance in neural regeneration and repair techniques in the future. During the last 3 years, we have successfully designed and developed a wireless controlled, wireless charged, small implantable stimulator for pudendal nerve stimulation and/or block, and tested its functionality in animal experiments using cats. These results have laid the foundation for us to further design and develop this implantable stimulator into human application in the future.

2. Keywords

Spinal cord injury, micturition, bladder, stimulator, block

3. Overall Project Summary

During the 3 last years, we have made significant progresses on all 3 tasks proposed in our original grant applications. Task #1: Design and develop an implantable stimulator to activate and/or block the pudendal nerves. Task #2: Test the implantable stimulator in awake chronic SCI animals. Task #3: Data analysis and publishing the results.

Task #1: Design and develop an implantable stimulator to activate and/or block the pudendal nerves

(a). The design of the implantable stimulator system

Our previous studies [1-4] in anesthetized chronic SCI cats showed that blocking pudendal nerves using high-frequency (6-10 kHz) biphasic electrical current could relax the external urethral sphincter (EUS) and significantly improve voiding efficiency. Meanwhile our studies in animals [2-4] also showed that electrical stimulation of pudendal afferent pathways at different stimulation frequencies could either inhibit (1-10 Hz) or excite (20-40 Hz) the bladder. Therefore, we hypothesize that both continence and micturition functions could be restored after SCI by electrical stimulation and/or blockade of the pudendal

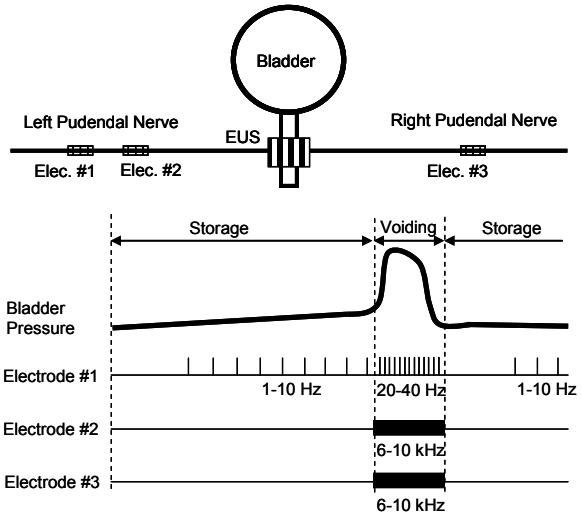

Figure 1: Our strategy to restore normal functions of the lower urinary tract after SCI. EUS – External Urethral Sphincter.

nerves. During urine storage phase, an implanted stimulator will activate the pudendal nerve at a frequency of 1-10 Hz to inhibit bladder activity and treat the bladder overactivity. When voiding is intended, the same stimulator will switch the pudendal nerve stimulation to 20-40 Hz to induce a strong bladder contraction, and at the same time it will also apply 6-10 kHz stimulation bilaterally to block pudendal nerve conduction, relax EUS, and prevent detrusor sphincter dyssynergia (see Fig.1). Using large laboratory equipment and computer to generate the required stimulation waveforms, we have successfully tested this novel pudendal nerve stimulation strategy in anesthetized chronic SCI cats and published the results [2-4].

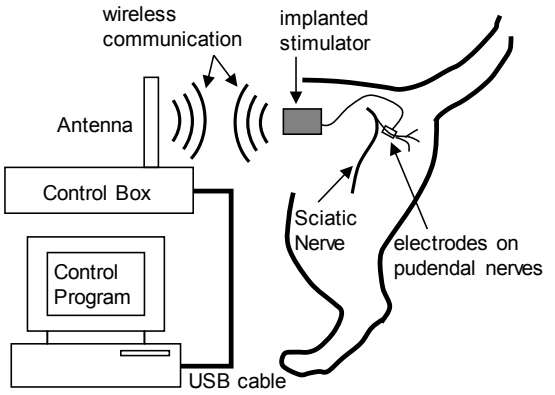

Figure 2: Wireless control system for the implanted stimulator.

This grant is aimed at developing a small implantable stimulator to further test our stimulation methods in awake chronic SCI cats, providing preclinical evidence and equipment support for a future clinical trial. We propose to develop a small stimulator (see Fig.2) that can be implanted on the back of a cat, while the output channels of the stimulator are controlled wirelessly via an external controller that receives commands and stimulation parameters from a computer running a control program. In addition, the implantable stimulator has to be wirelessly charged across the skin so that it can be powered continuously for a long-term chronic application. Fig.3 shows our final design of the implantable stimulator which includes an implanted stimulator, an external control device, and an external charging device. This final report will summarize our development of the implantable stimulator as shown in Figs.1-3.

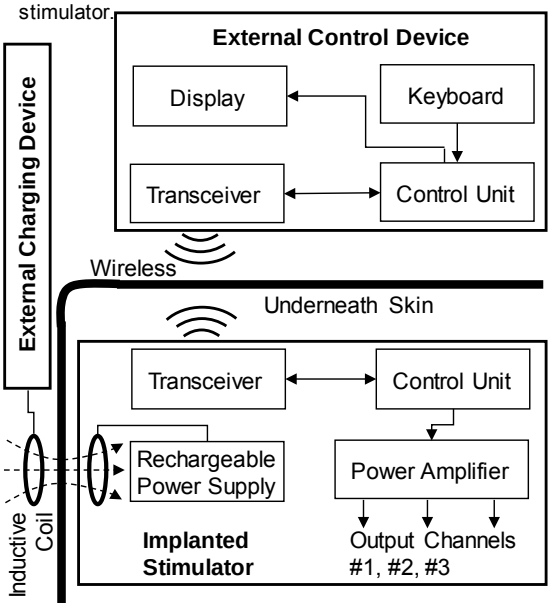

Figure 3: The proposed neuroprosthetic device.

(b). The development of the implantable stimulator system

With the DOD grant support, we were able to develop the wireless controlled, wireless charged, small implantable stimulator in the last 3 years. We have gone through several design and development circles to identify the problems and improve the stimulator design. The first prototype of the implantable stimulator is shown in Fig.4. The purpose of this first prototype is to determine: (1) the effectiveness of the transcutaneous wireless

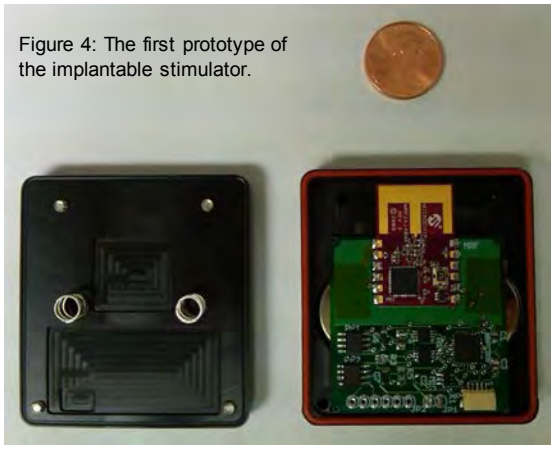

Figure 4: The first prototype of the implantable stimulator.

communication, and (2) whether the output power amplifiers are strong enough to activate or block the pudendal nerve. Preliminary tests were performed by implanting the stimulator underneath the skin (Fig.2) in 3 anesthetized cats with the output channels connected to 3 electrodes as shown in Fig.1. Via wireless communication the computer program successfully controlled the implanted stimulator that delivered 5 Hz, 20 Hz, and 10 kHz electrical pulses to the pudendal nerves (Fig.5). The output power amplifiers generated enough electrical currents to significantly increase bladder capacity with 5 Hz pudendal nerve stimulation (Fig.5A), and induce efficient (88%) low pressure (<40 cmH_2O) voiding with 20 Hz stimulation combined with 10 kHz nerve block (Fig.5B). This first prototype is powered by 2 button batteries (see Fig.4) that are not rechargeable.

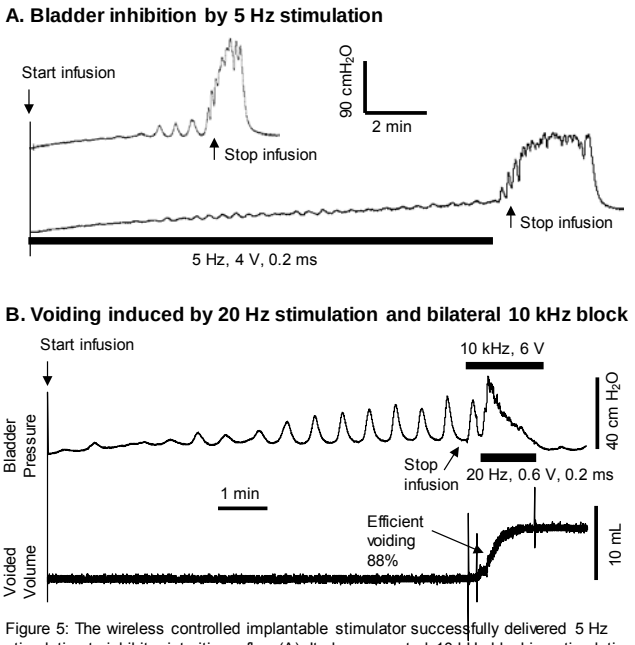

Figure 5: The wireless controlled implantable stimulator successfully delivered 5 Hz stimulation to inhibit micturition reflex (A). It also generated 10 kHz blocking stimulation together with 20 Hz stimulation, and induced efficient voiding of 88% (B).

Fig.6 shows our second prototype of the implantable stimulator with wireless charging ability. This second prototype includes a small (4x 5.5 x 1.4 cm) implantable stimulator that can be wirelessly controlled by an external USB controller (see Fig.6). This small implantable stimulator can also be charged externally through a wireless charging device (not shown in Fig.2). We also developed the software for computer to send control signal via the USB controller to wirelessly control the 3 output channels of the implantable stimulator. One channel provides the low frequency output (1-100 Hz, 0-11 V) for bladder inhibition or excitation (i.e. channel #1 in Fig.1). The other 2 channels provide the high frequency output (5k-20k Hz, 0-11 V) for pudendal nerve block (i.e. channels #2-3 in Fig.1). We have

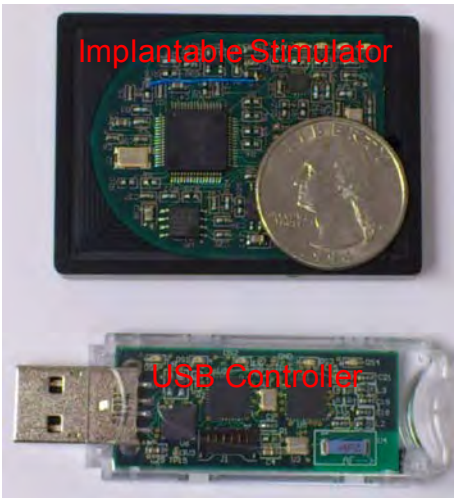

Figure 6: The implantable stimulator and USB controller.

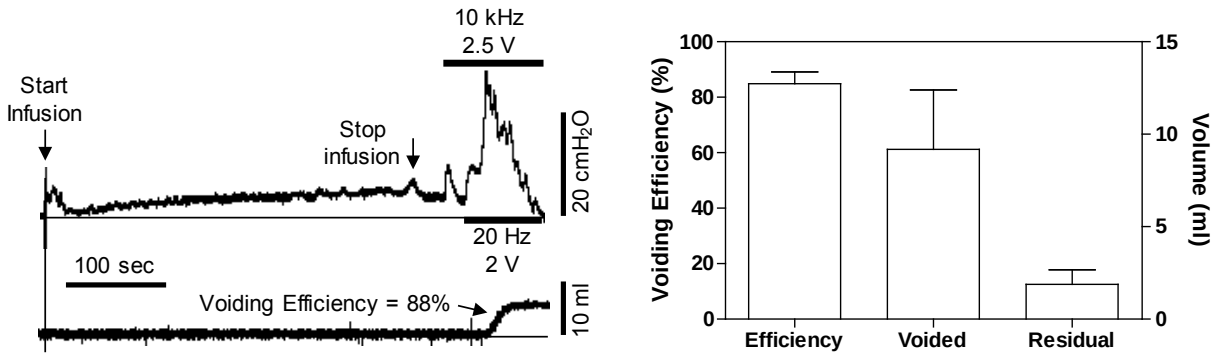

Figure 7: Efficient voiding induced in anesthetized cats by the implantable stimulator.

successfully tested this implantable stimulator in 6 anesthetized cats. Efficient voiding (>80%, Fig.7) was induced in the 6 cats by wireless control through the USB controller using a computer. Fig.7 (left) shows that 10 kHz pudendal nerve block combined with 20 Hz pudendal nerve stimulation induced efficient voiding (88%) in an anesthetized cat, while Fig.7 (right) shows the summarized results from the 6 cats.

However, when we implanted this second prototype of the stimulator as shown in Fig.6 in awake freely moving chronic SCI cats, we encountered following problems: 1. failure to recharge the battery in one animal; 2. failure to block the pudendal nerve and failure to recharge the battery in another animal. We found that the charging circuit of the stimulator could generate heat to increase the surface temperature of the Li-ion rechargeable battery to about 45 ˚C. At this temperature, most Li-ion rechargeable battery will be damaged. To fix this problem, we have re-designed the packaging method so that the stimulator circuits and the rechargeable battery were separately packaged (see Fig.8A). We also found that the failure to block the pudendal nerve was due to the interaction between the low frequency and the high frequency channels, because we used a single cuff electrode with 5 leads to deliver both low and high frequency stimulations to the pudendal nerve. To solve this problem, we now used 2 separate cuff electrodes (one bipolar and one tripolar, i.e., the electrode #1 and #2 in Fig.8A) to deliver the low and high frequency stimulations and implanted the 2 cuff electrodes on the pudendal nerve at least 1 cm apart (see Stim. A and Stim. B1 in Fig.8B). In order to make sure that these problems are now solved, we tested the new design in 5 cats under anesthesia. These tests are mainly designed to confirm the functionality of the re-designed stimulator before we move forward to implant it in awake SCI cats for chronic testing.

A. Implantable Stimulator

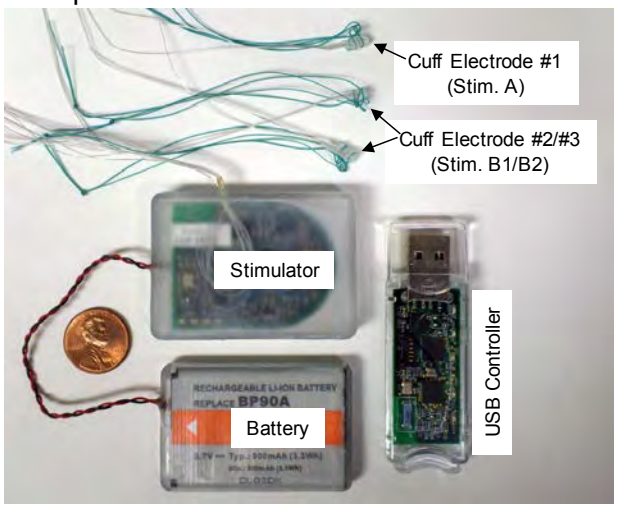

B. Experimental Setup

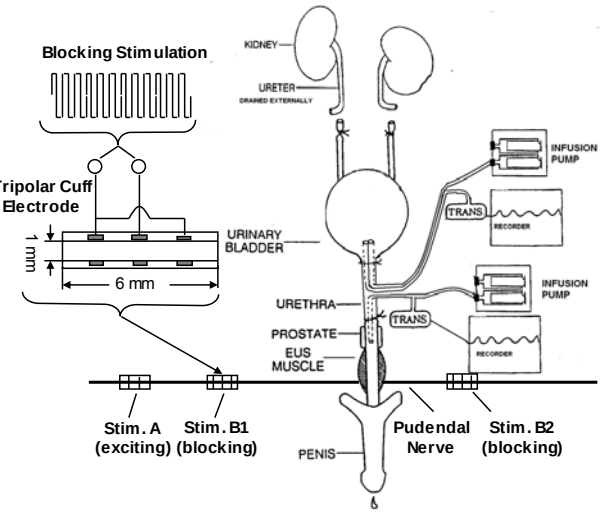

Fig.8. The implantable stimulator (A) and the locations of cuff electrodes implanted on the pudendal nerves in the cat (B). EUS – External Urethral Sphincter.

Fig.8A shows a picture of the re-designed implantable stimulator (dimensions: 5.6x4.0x0.8 cm) connected to a rechargeable battery (3.7 V and 900 mAh; dimensions:

5.4x3.6x0.6 cm). The stimulator has 2 output channels providing charge-balanced rectangular pulses (1-100 Hz, 0-11 V, 0.05-0.2 ms) to the bipolar cuff electrode #1 (i.e., Stim. A in Fig.8B) and a high frequency (5-20 kHz, 0-11 V) biphasic square waveform (see Fig.8B) to the tripolar cuff electrodes #2 and #3 (i.e., Stim. B1 and B2 in Fig.8B). The stimulator can be wireless controlled within a 2-meter distance by a USB controller that is connected to a USB port of a portable computer (the computer is not shown). The computer software can set stimulation parameters for each output channel and turn on/off each channel by wireless communication between the implanted stimulator and the USB controller. The stimulator and battery are implanted underneath the skin on the left side of the lower back of the cat along the sacral spine (see Fig.2). The battery can be charged by the charging circuitry in the stimulator that can be powered wirelessly across the skin by an external charging coil. At the beginning of each experiment, the battery was fully charged from 2.8 V to 3.7 V in about 15-20 minutes and it could run for the entire experiment (5-6 hours) with repeated stimulation. After removing the stimulator and battery from the animal at the end of experiment, the battery power lasted for about 2-3 days before the stimulator stopped functioning and lost communication with the USB controller due to a low battery level (<2.8 V). Although the stimulator was not used to stimulate/block the pudendal nerve once it was removed from the animal, it is estimated that the battery should still be able to power the stimulator for the same amount of time (2-3 days) if it were used for pudendal nerve stimulation (PNS) and/or block. This is because the electrical power used by PNS/block is only a very small portion of the total power consumption by the electrical circuits including wireless communication, microprocessor, and the output amplifiers. Therefore, it is expected

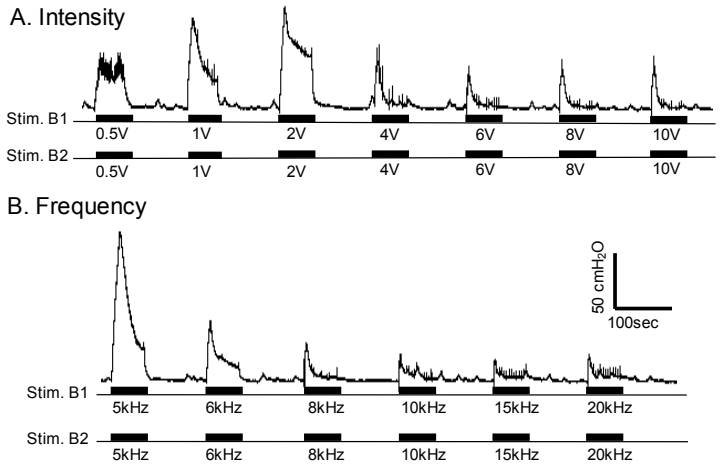

Fig.9. Urethral pressure induced by the high frequency biphasic electrical stimulation applied bilaterally on the pudendal nerves. A. Different intensities at 10 kHz frequency. B. Different frequencies at 6 V intensity. The urethral infusion rate is 1 ml/min. The black bars under the pressure traces indicate the stimulation duration.

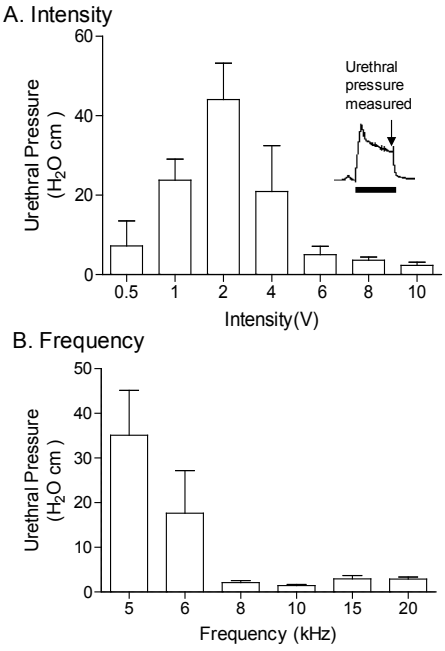

Fig.10. Urethral pressure measured at the end of high frequency biphasic electrical stimulation. A. Different intensities at 10 kHz frequency. B. Different frequencies at 6-10 V intensity. N = 5 cats. The inserted figure in A shows the time point for urethral pressure measurement.

that the implantable stimulator will continuously function after chronic implantation in SCI cats as long as we continue to charge it for 15-20 minutes every day.

A total of 5 cats were used to test this stimulator under anesthetized condition. Fig.8B shows the experimental setup. The temperature of the animal was maintained at 35 ˚C to 37 ˚C using a heating pad. The ureters were cut and drained externally. A double lumen catheter (5F) was inserted into the bladder through a small incision in the proximal urethra and secured by a ligature (Fig.8B). One lumen of the catheter was attached to a pump to infuse the bladder with saline, and the other lumen was connected to a pressure transducer to monitor the bladder activity. Another catheter (5F) was also inserted at the same site in the proximal urethra but directed toward the distal urethra and secured by a ligature (Fig.8B). This catheter was attached to an infusion pump and to a pressure transducer via a T connector. The pudendal nerves were accessed posteriorly in the sciatic notch lateral to the tail. The three cuff electrodes (NCE112/113, MicroProbes Inc., Gaithersburg, MD) as shown in Fig.8A were tunneled underneath the skin from the stimulator to the exposed pudendal nerves and were placed around the left and right pudendal nerves as shown in Fig.8B. After implanting the stimulator, the battery, and the cuff electrodes, the muscle and skin were closed by sutures.

Pudendal nerve block by high frequency biphasic stimulation: The high frequency biphasic PNS waveform generated by the implanted stimulator successfully blocked pudendal nerve conduction and eliminated the PNS evoked EUS contraction when applied bilaterally on the pudendal nerves (Figs.9-12). The high frequency biphasic PNS applied bilaterally at 10 kHz for 60 sec at locations Stim. B1 and Stim. B2 (Fig.8B) activated the pudendal nerves, induced a strong EUS contraction, and caused large increases in urethral pressure at intensities of 0.5-2 V (Fig.9A and Fig.10A). However, as the intensity was increased the urethral pressure response

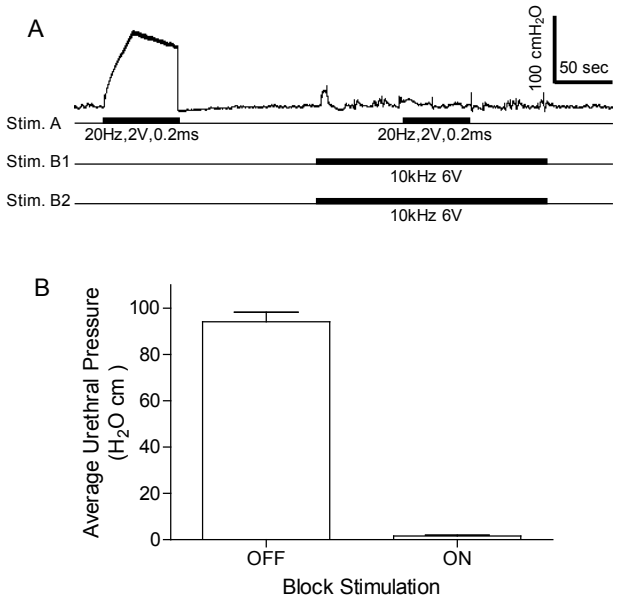

Fig.11. High frequency biphasic electrical stimulation blocked the pudendal nerves and eliminated the urethral pressure increase induced by pudendal nerve stimulation. A. High frequency stimulation delivered to Stim. B1 and Stim. B2 (see Fig.1B) completely blocked the urethral pressure increase induced by Stim. A. The black bars under pressure trace indicate the stimulation duration. B. Average urethral pressure measured during Stim. A when the high frequency stimulation was either on or off. Stim. A: frequency 20 Hz, pulse width 0.2 ms, intensity 2-5 V. Stim. B1/B2: frequency 6-15 kHz, intensity 6-10 V. N = 5 cats.

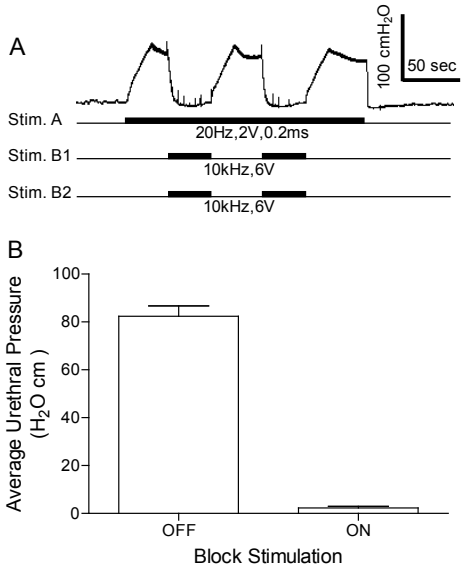

Fig.12. High frequency biphasic stimulation blocked the pudendal nerves and completely reduced the urethral pressure induced by pudendal nerve stimulation. A. High frequency stimulation delivered to Stim. B1 and Stim. B2 (see Fig.1B) completely reduced the urethral pressure induced by Stim. A. The black bars under pressure trace indicate the stimulation duration. B. Average urethral pressure induced by Stim. A when the high frequency stimulation was either on or off. Stim. A: frequency 20 Hz, pulse width 0.2 ms, intensity 2-5 V. Stim. B1/B2: frequency 6-15 kHz, intensity 6-10 V. N = 4 cats.

gradually decreased in amplitude and duration, and became minimal (<5 cmH_2O) at the end of the 60 second high frequency stimulation when the intensity was 6-10 V (Fig.9A and Fig.10A). Within this range of intensities (6-10 V), the high frequency biphasic PNS also generated large urethral pressure responses at frequencies below 6 kHz, but the response was minimal (<5 cmH_2O) at the end of the 60 second stimulation once the frequency was increased above 6 kHz (Fig.9B and Fig.10B).

In order to show that the high frequency biphasic PNS blocked pudendal nerve conduction when the urethral pressure response was diminished at the end of the 60 second stimulation, a 20 Hz PNS (2-5 V, 0.2 ms) was applied at Stim. A (Fig.8B) central to the high frequency stimulation site to induce a maximal (70-100 cmH_2O) urethral pressure response (Fig.11 and Fig.12). This urethral response was completely blocked by the high frequency biphasic PNS (6-15 kHz, 6-10 V) (Fig.11 and Fig.12). The pudendal nerve conduction recovered quickly from the block once the high frequency PNS was terminated (Fig.12A).

Bladder excitation or inhibition by PNS: The implanted stimulator also generated rectangular pulses at the cuff electrode #1 (at Stim. A in Fig.8 A and B) that reflexively excited or inhibited the bladder depending on the frequency of stimulation (Fig.13 and Fig.14). Several CMGs were performed in each animal to determine the bladder capacity. In one group of experiments, 20-30 Hz PNS (2-8 V, 0.2 ms) induced a large amplitude (45.9±13.4 to 52.0±22 cmH_2O) sustained bladder contraction (Fig.13) when the bladder was filled to 90% of capacity. When the frequency was changed to 5 Hz, PNS (2-5 V, 0.2 ms) applied during CMG inhibited reflex micturition and significantly ($P<0.05$) increased bladder capacity to 176.5 ± 27.1% of the control capacity (8.2±1.9 ml) (Fig.14).

During the last 3 years, we designed, developed, and successfully tested the wireless controlled, wireless rechargeable,

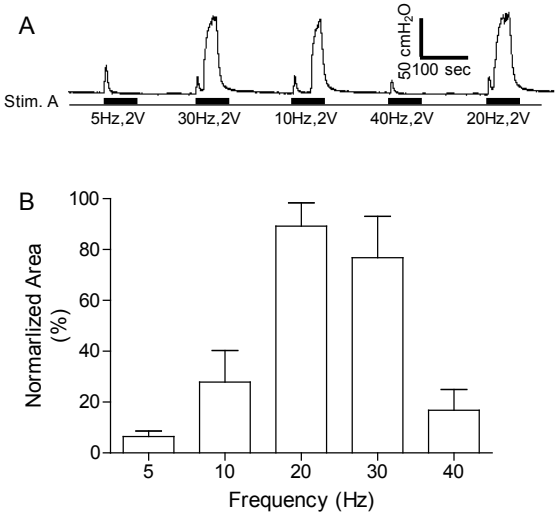

Fig.13. Bladder contraction induced by pudendal nerve stimulation at different frequencies. A. Bladder pressure trace. The black bars under pressure trace indicate the stimulation duration. B. Normalized area under bladder pressure curve during stimulation. The area under curve was normalized to the maximal response in each animal. Stim. A: frequency 20 Hz, pulse width 0.2 ms, intensity 2-8 V. N = 5 cats.

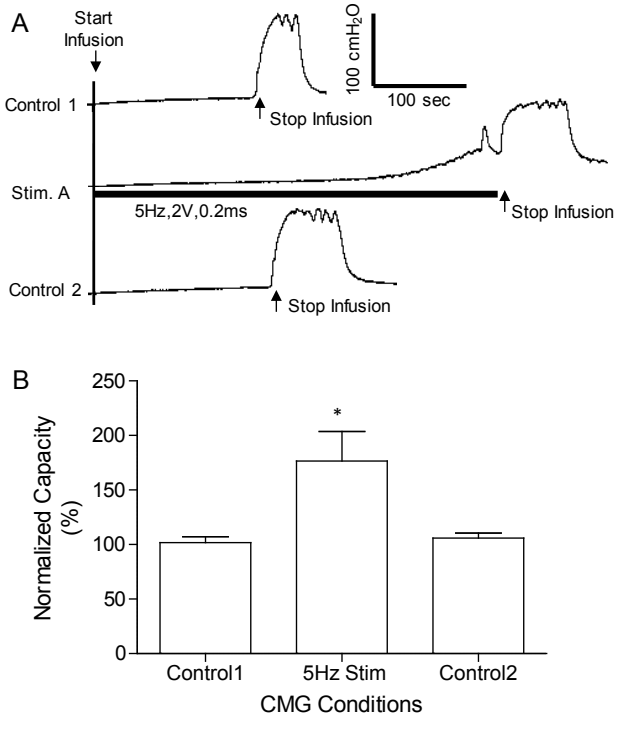

Fig.14. Bladder inhibition induced by 5 Hz pudendal nerve stimulation. A. Repeated CMG recordings. The black bar under the CMG trace indicate the stimulation duration. B. Normalized bladder capacity measured during different CMGs. The capacity was normalized to the measurement from control 1 CMG. * indicates significantly different from the control 1. Stimulation: frequency 5 Hz, pulse width 0.2 ms, intensity 2-5 V. N = 4 cats.

implantable stimulator that can now provide the required stimulation waveforms (see Fig.1) to: 1) block pudendal nerve conduction and relax the EUS (Figs.9-12), 2) induce a large sustained reflex bladder contraction (Fig.13), or 3) inhibit reflex bladder activity (Fig.14). These in vivo experiments in anesthetized cats establish the effectiveness of the implantable stimulator as well as the stimulation parameters.

Task #2: Test the implantable stimulator in awake chronic SCI animals

We have tested the implantable stimulator in 3 chronic SCI cats under awake conditions. After 2-3 month SCI, the cats were implanted with the pudendal nerve stimulator as shown in Figs.1-2. Then the stimulation tests were performed in the following 2-4 weeks. Under awake conditions, the bladder of chronic SCI cats was catheterized via the urethra using a double lumen balloon catheter with the balloon distended at the bladder neck to prevent leakage. Sterile saline was infused into the bladder via one lumen, and the bladder pressure was recorded via the other lumen. Starting from bladder empty, a cystometrogram (CMG) was performed with a slow infusion of the bladder (2-5 ml/min) while the cats sited quietly in a padded standard cat transportation carrier. The infusion was stopped once the large amplitude, long-duration micturition contraction was induced (see Fig.16) which was usually accompanied with hindlimb stepping movements in awake SCI animals. During the voiding experiments, the animals were lying on a table without a urethral catheter. A funnel was used to collect the voided urine. The initial bladder volume was the volume remaining in the bladder overnight or during the day. After stimulation induced voiding, the voided volume was recorded. Then, a small (3.5F) Tom cat catheter was inserted via the urethra into the bladder to withdraw the residual volume. The voiding efficiency was calculated using the voided volume divided by the initial volume.

With the implantable stimulator, we are now able to confirm that the frequency response in awake SCI cats is same as what was discovered in the anesthetized SCI cats. The most effective stimulation frequency to induce a strong, sustained bladder contraction is between 20-50 Hz with frequency below 10 Hz to be ineffective (see Fig.15). Meanwhile, at the effective frequency of 40 Hz the stimulation

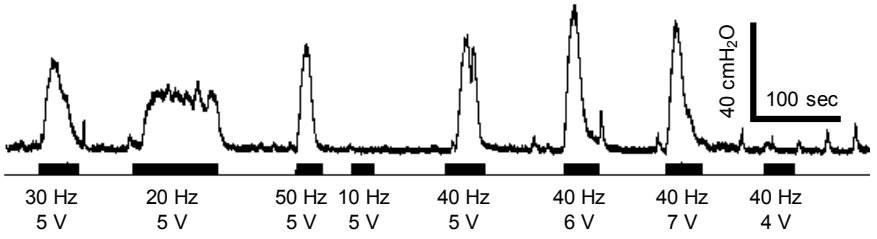

Fig.15. Bladder contractions induced by pudendal nerve stimulation at different frequencies and intensities in chronic SCI cat under awake conditions.

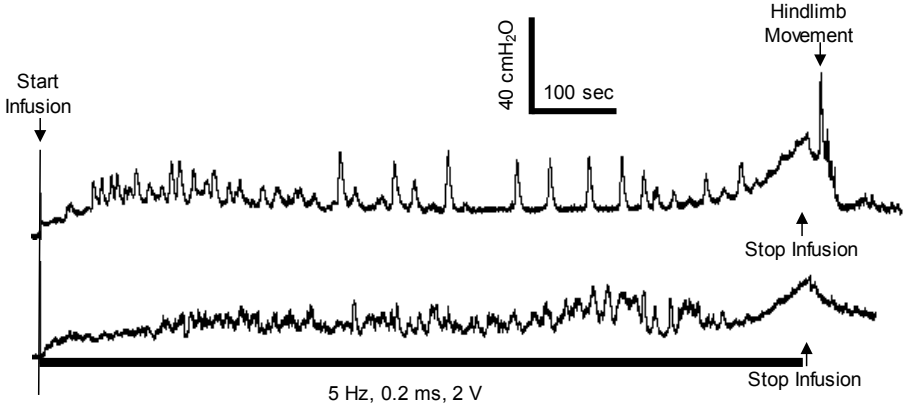

Fig.16. Pudendal nerve stimulation at 5 Hz suppressed the non-voiding contractions during slow infusion of the bladder in chronic SCI cat under awake conditions.

intensity must be greater than a threshold (4V in Fig.15) to be effective in inducing bladder contraction. In addition, at the low frequency of 5 Hz the pudendal nerve stimulation can successfully suppress the bladder overactivity and eliminate the non-voiding contractions during slow infusion of the bladder, i.e. during the storage phase (Fig.16). Voiding test was performed twice per day in the morning and in the afternoon for a 2-week period. The implanted stimulator induced voiding of average efficiency 89.4±2.1% in the morning and 73.1±4.2% in the afternoon (Fig.17). Since the residual volume is almost the same in the morning and in the afternoon (4.6±0.8 ml v.s. 4.6±0.7 ml), the difference between voiding efficiencies in the morning and afternoon is mainly caused by the total amount of urine accumulation in the bladder in the morning (39.2±2.0 ml) or afternoon (13.1±1.6 ml), not by the ineffectiveness of the stimulator.

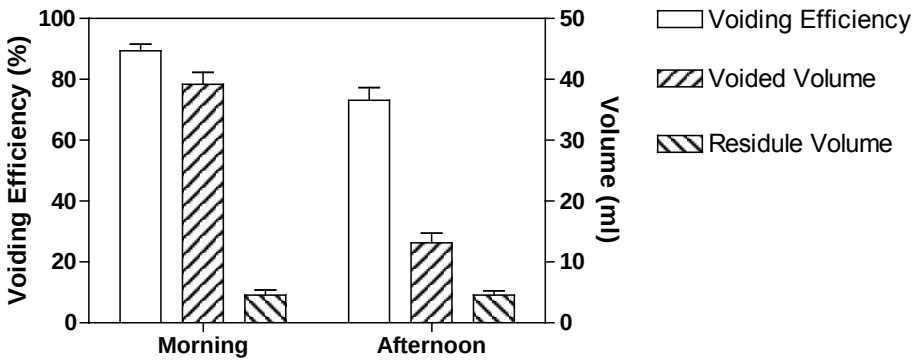

Fig.17. Voiding efficiency, voided volume, and residual volume induced by implantable stimulator in chronic SCI cat under awake conditions.

Task #3: Data analysis and publishing the results

We have analyzed the data obtained from animal experiments. In addition, we also performed computer modelling studies in order to understand the possible mechanisms of pudendal nerve stimulation/block. Our studies in the past 3 years have results in three publications (2 published papers and 1 submitted manuscript), four conference abstracts, and two invited presentations (1 international and 1 national). Please see section 6 and the appendices for details.

4. Key Research Accomplishments

- Successfully designed (Figs.1-3) and developed (Figs.4-14) a wireless charged, wireless controlled, small implantable stimulator to activate or block the pudendal nerves in cats.
- Tested the implantable pudendal nerve stimulator in chronic SCI cats under awake conditions (Figs.15-17).
- Confirmed the frequency response of pudendal nerve stimulation in chronic SCI cats under awake conditions without any influence of anesthesia. Low frequency (5 Hz) is inhibitory while high frequency (20-50 Hz) is excitatory (Figs.15-17), which is the foundation for our strategy (Fig.1) to be successful in restoring bladder function after SCI.

5. Conclusion

We have successfully developed a wireless controlled, wireless charged, small implantable stimulator for pudnedal nerve stimulation and block and successfully tested it in

cats. The results indicate that our pudendal nerve stimulation strategy (Fig.1) can be implemented using a fully implantable device with current technologies including wireless control and wireless charging technologies. These animal studies provided the scientific evidence to support further development of our strategy into human application. The success of our project will create a novel implantable neuroprosthesis to restore both continence and micturition functions for SCI people. It will fundamentally change the current medical treatments for the lower urinary tract dysfunctions after SCI. Daily urethral catheterization will not be the norm for SCI. Frequent infection of the lower urinary tract will be eliminated. The quality of life will be improved greatly for both SCI people and their family.

6. **Publications, Abstracts, and Presentations**

Peer-Reviewed Scientific Journals

[1] Guangning Yang, Jicheng Wang, Bing Shen, James R. Roppolo, William C. de Groat, **Changfeng Tai**, "Pudendal nerve stimulation and block by a wireless controlled implantable stimulator in cats", Neuromodulation, 17: 490-496, 2014.

[2] Shouguo Zhao, Guangning Yang, Jicheng Wang, James R. Roppolo, William C. de Groat, **Changfeng Tai**, "Effect of non-symmetric waveform on conduction block induced by high-frequency (kHz) biphasic stimulation in unmyelinated axon", Journal of Computational Neuroscience, 37: 377-386, 2014.

Manuscript Submitted

[1] Shouguo Zhao, Guangning Yang, Jicheng Wang, James R. Roppolo, William C. de Groat, **Changfeng Tai**. "Conduction block in myelinated axons induced by high-frequency (kHz) non-symmetric biphasic stimulation". Medical & Biological Engineering & Computing, 2014, submitted.

Abstracts

[1] Guangning Yang, Jicheng Wang, Bing Shen, James R. Roppolo, William C. de Groat, **Changfeng Tai**. "Pudendal nerve stimulation and block by a wireless-controlled implantable stimulator in cats". Military Health Service Research Symposium (MHSRS), Fort Lauderdale, FL, 2014.

[2] Guangning Yang, Jicheng Wang, James R. Roppolo, William C. de Groat, **Changfeng Tai**, "Simulation analysis of conduction block in unmyelinated axon after high-frequency electrical stimulation". 43nd Annual Meeting of Society for Neuroscience, San Diego, 2013.

[3] **Changfeng Tai**, "An implantable neuroprosthetic device to restore bladder function after SCI". Military Health System Research Symposium (MHSRS), Fort Lauderdale, Florida, 2012

[4] Jicheng Wang, Shouguo Zhao, James R. Roppolo, William C. de Groat, **Changfeng Tai**, "Mechanisms underlying non-monotonic block of unmyelinated axons by high-frequency biphasic stimulation". 42nd Annual Meeting of Society for Neuroscience, New Orleans, 2012.

Presentations / Invited Speakers

[1] A Novel Neuroprothesis to Restore Micturition and Continence after SCI
Symposium: Spinal Cord Injury and Tissue Regeneration Center Salzburg
Paracelsus Medical University
Salzburg, Austria, June, 2014

[2] Extra-Cellular Electrical Stimulation
State of the Science Symposium: Regenerative Medicine for Wounded, Injured, and Ill Veterans
Uniformed Services University of the Health Science
Walter Reed National Military Medical Center
Bethesda, MD, June, 2014

7. **Inventions, Patents and Licenses**

Nothing to report.

8. Reportable Outcomes

The wireless controlled, wireless charged, small stimulator suitable for implantation in cats is the reportable outcome of this grant support (see Fig.8A). This small implantable stimulator is now available in our lab and can be commercialized for other research purposes.

9. Other Achievements

Nothing to report.

10. **References**

[1] Changfeng Tai, James R. Roppolo and William C. de Groat , "Block of external urethral sphincter contraction by high frequency electrical stimulation of pudendal nerve", Journal of Urology, Vol.172, PP2069-2072, 2004.

[2] Changfeng Tai, Stanley E. Smerin, William C. de Groat and James R. Roppolo, "Pudendal-to-bladder reflex in chronic spinal cord injured cat", Experimental Neurology, Vol.197, PP225-234, 2006.

[3] Changfeng Tai, Jicheng Wang, Xianchun Wang, James R. Roppolo and William C. de Groat, "Voiding reflex in chronic spinal cord injured cats induced by stimulating and blocking pudendal nerves", Neurourology and Urodynamics, Vol.26, PP879-886, 2007.

[4] Changfeng Tai, Jicheng Wang, Xianchun Wang, William C. de Groat, and James R. Roppolo, "Bladder inhibition and voiding induced by pudendal nerve stimulation in chronic spinal cord injured cats", Neurourology and Urodynamics, Vol. 26, PP570-577, 2007.

11. **Appendices**

[1] Guangning Yang, Jicheng Wang, Bing Shen, James R. Roppolo, William C. de Groat, **Changfeng Tai**, "Pudendal nerve stimulation and block by a wireless controlled implantable stimulator in cats", Neuromodulation, 17: 490-496, 2014.

[2] Shouguo Zhao, Guangning Yang, Jicheng Wang, James R. Roppolo, William C. de Groat, **Changfeng Tai**, "Effect of non-symmetric waveform on conduction block induced by high-frequency (kHz) biphasic stimulation in unmyelinated axon", Journal of Computational Neuroscience, 37: 377-386, 2014.

[3] Shouguo Zhao, Guangning Yang, Jicheng Wang, James R. Roppolo, William C. de Groat, **Changfeng Tai**. "Conduction block in myelinated axons induced by high-frequency (kHz) non-symmetric biphasic stimulation". Medical & Biological Engineering & Computing, 2014, submitted.

[4] Guangning Yang, Jicheng Wang, Bing Shen, James R. Roppolo, William C. de Groat, **Changfeng Tai**. "Pudendal nerve stimulation and block by a wireless-controlled implantable stimulator in cats". Military Health Service Research Symposium (MHSRS), Fort Lauderdale, FL, 2014.

[5] Guangning Yang, Jicheng Wang, James R. Roppolo, William C. de Groat, **Changfeng Tai**, "Simulation analysis of conduction block in unmyelinated axon after high-frequency electrical stimulation". 43nd Annual Meeting of Society for Neuroscience, San Diego, 2013.

[6] **Changfeng Tai**, "An implantable neuroprosthetic device to restore bladder function after SCI". Military Health System Research Symposium (MHSRS), Fort Lauderdale, Florida, 2012

[7] Jicheng Wang, Shouguo Zhao, James R. Roppolo, William C. de Groat**, Changfeng Tai**, "Mechanisms underlying non-monotonic block of unmyelinated axons by high-frequency biphasic stimulation". 42nd Annual Meeting of Society for Neuroscience, New Orleans, 2012.

Received: August 21, 2013 Revised: September 20, 2013 Accepted: October 25, 2013

(onlinelibrary.wiley.com) DOI: 10.1111/ner.12136

Pudendal Nerve Stimulation and Block by a Wireless-Controlled Implantable Stimulator in Cats

Guangning Yang, BS*,†; Jicheng Wang, PhD*; Bing Shen, DVM*; James R. Roppolo, PhD‡; William C. de Groat, PhD‡; Changfeng Tai, PhD*,‡

Objective: The study aims to determine the functionality of a wireless-controlled implantable stimulator designed for stimulation and block of the pudendal nerve.

Materials and Methods: In five cats under α-chloralose anesthesia, the stimulator was implanted underneath the skin on the left side in the lower back along the sacral spine. Two tripolar cuff electrodes were implanted bilaterally on the pudendal nerves in addition to one bipolar cuff electrode that was implanted on the left side central to the tripolar cuff electrode. The stimulator provided high-frequency (5–20 kHz) biphasic stimulation waveforms to the two tripolar electrodes and low-frequency (1–100 Hz) rectangular pulses to the bipolar electrode. Bladder and urethral pressures were measured to determine the effects of pudendal nerve stimulation (PNS) or block.

Results: The maximal (70–100 cmH_2O) urethral pressure generated by 20-Hz PNS applied via the bipolar electrode was completely eliminated by the pudendal nerve block induced by the high-frequency stimulation (6–15 kHz, 6–10 V) applied via the two tripolar electrodes. In a partially filled bladder, 20–30 Hz PNS (2–8 V, 0.2 ms) but not 5 Hz stimulation applied via the bipolar electrode elicited a large sustained bladder contraction (45.9 ± 13.4 to 52.0 ± 22 cmH_2O). During cystometry, the 5 Hz PNS significantly ($p < 0.05$) increased bladder capacity to 176.5 ± 27.1% of control capacity.

Conclusions: The wireless-controlled implantable stimulator successfully generated the required waveforms for stimulation and block of pudendal nerve, which will be useful for restoring bladder functions after spinal cord injury.

Keywords: Block, cat, pudendal nerve, spinal cord injury, stimulation

Conflict of Interest: Dr. Tai is the inventor of a pending patent application related to this study. The other authors reported no conflicts of interest.

INTRODUCTION

After spinal cord injury (SCI) above the lumbosacral level, the coordinated action between bladder and external urethral sphincter (EUS) disappears (1). Instead, the bladder and EUS contract simultaneously (termed detrusor sphincter dyssynergia or DSD), which generates high bladder pressure, prevents complete elimination of urine, and requires daily urethral catheterization (1,2). High bladder pressure can cause vesicoureteral reflux and renal failure in the long term. Frequent urethral catheterization can cause low urinary tract infection (2). In addition, detrusor overactivity (DO) induces poor bladder storage function and frequent incontinence (1,2). Currently, no medication can treat both DSD and DO. However, in the 1970s, Brindley and his team developed an implantable sacral anterior root stimulator to restore bladder function after SCI. This system is now commercially available (Finetech Medical Limited, Welwyn Garden City, Hertfordshire, UK) and has been implanted in more than 2000 SCI persons around the world (3). It requires sacral posterior root rhizotomy to prevent DO and DSD, which is destructive and irreversible and results in the loss of reflex sexual and defecation functions (3).

Our previous studies (4–6) in chronic SCI cats under anesthesia have revealed a frequency-dependent pudendal-to-bladder spinal reflex. Pudendal nerve stimulation (PNS) at 5 Hz can inhibit reflex bladder activity and increase bladder capacity, but at 20 Hz it can excite the bladder and induce a large bladder contraction (4–6). In addition, our previous studies (7–9) in cats have shown that high-frequency (>6 kHz) biphasic stimulation can block the pudendal nerve and completely relax the EUS. When the 20 Hz PNS was combined with high-frequency pudendal nerve block in anesthetized chronic SCI cats, a large bladder contraction was induced simultaneously with an EUS relaxation, resulting in efficient voiding (10).

Address correspondence to: Changfeng Tai, PhD, Department of Urology, University of Pittsburgh, 700 Kaufmann Building, Pittsburgh, PA 15213, USA. Email: cftai@pitt.edu

* Department of Urology, University of Pittsburgh, Pittsburgh, PA, USA;
† Department of Biomedical Engineering, Beijing Jiaotong University, China; and
‡ Department of Pharmacology and Chemical Biology, University of Pittsburgh, Pittsburgh, PA, USA.

For more information on author guidelines, an explanation of our peer review process, and conflict of interest informed consent policies, please go to http://www.wiley.com/bw/submit.asp?ref=1094-7159&site=1

Sources of financial support: The DOD Spinal Cord Injury Research Program (SCIRP) under contract number W81XWH-11-1-0819, and the NIH under grants DK-094905, DK-068566, DK-090006, and DK-091253.

a. Implantable Stimulator

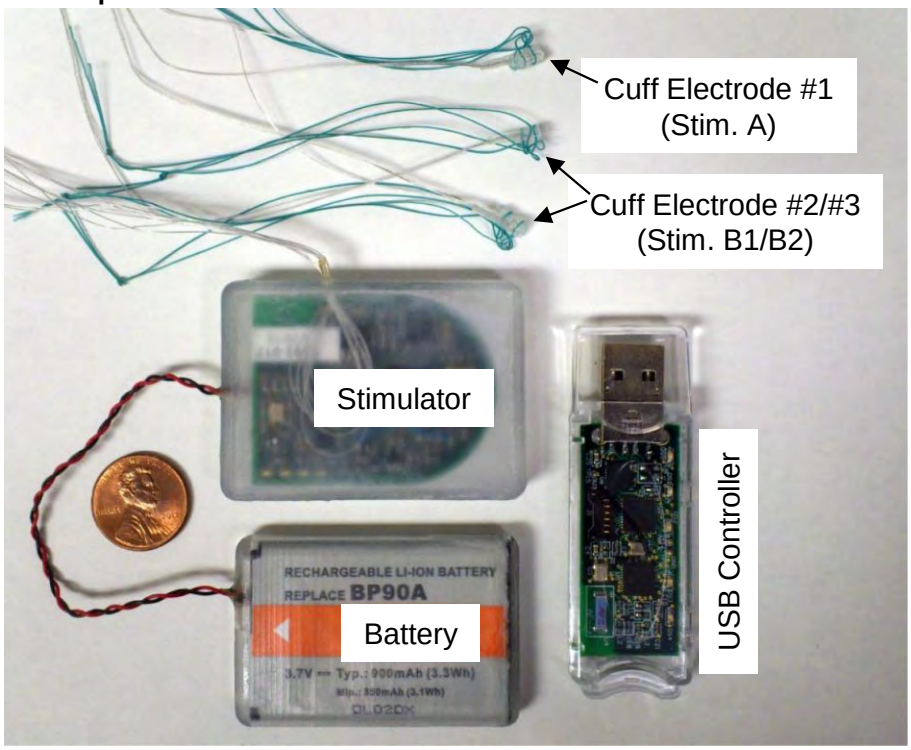

b. Experimental Setup

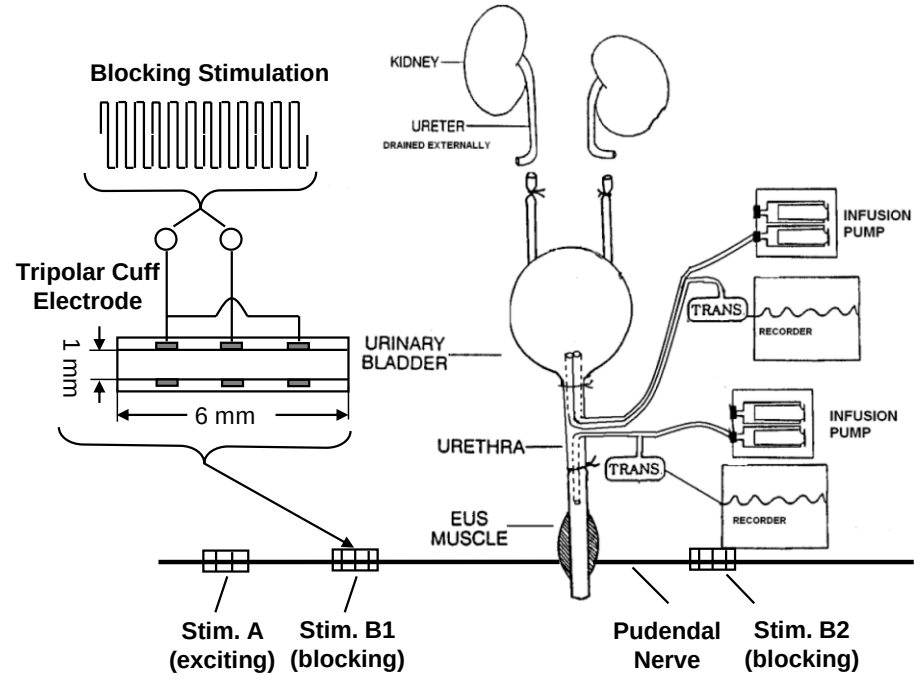

Figure 1. The implantable stimulator (a) and the locations of cuff electrodes implanted on the pudendal nerves in the cat (b). EUS—external urethral sphincter.

These results indicate that both micturition and continence functions could be restored after SCI by stimulation and block of the pudendal nerve, which will not require a dorsal root rhizotomy and thereby preserving the residual reflexes for bowel and sexual functions after SCI.

However, to test the stimulation/block strategy in a future clinical trial to restore bladder functions after SCI, an implantable stimulator is needed to generate the required 5 Hz and 20 Hz PNS as well as the high-frequency (>6 kHz) biphasic waveform for pudendal nerve block. Currently, such an implantable stimulator is not commercially

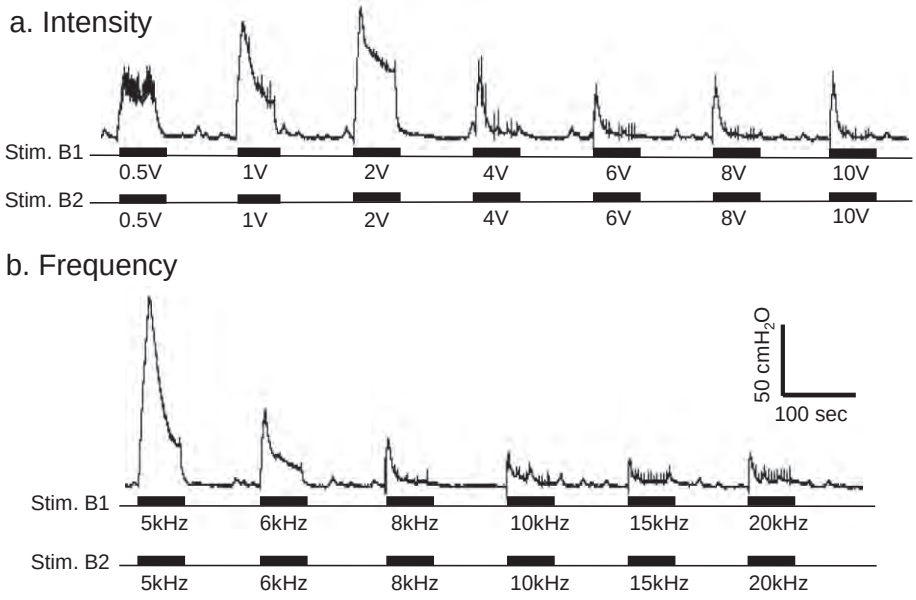

Figure 2. Urethral pressure induced by the high-frequency biphasic electrical stimulation applied bilaterally to the pudendal nerves. (a) Different intensities at 10 kHz frequency. (b) Different frequencies at 6 V intensity. The urethral infusion rate is 1 mL/min. The black bars under the pressure traces indicate the stimulation duration. The calibration bars are for both (a) and (b). The Y-calibration bar indicates the urethral pressure in 50 cmH_2O and the X-calibration bar indicates the time in 100 sec.

available. Therefore, in this study we designed and constructed a small, wireless-controlled, battery-powered, implantable stimulator, and showed in anesthetized cats that it can generate the required stimulation waveforms to reflexively excite or inhibit the bladder and block axonal conduction in the pudendal nerve. This study represents the first step in developing a device for future testing in awake chronic SCI animals, and eventually in SCI human subjects.

MATERIALS AND METHODS

The Animal Care and Use Committee at the University of Pittsburgh approved all protocols involving the use of animals in this study. Figure 1a shows a picture of the implantable stimulator (dimensions: $5.6 \times 4.0 \times 0.8$ cm) connected to a rechargeable battery (3.7 V and 900 mAh; dimensions: $5.4 \times 3.6 \times 0.6$ cm). The stimulator has two output channels providing charge-balanced rectangular pulses (1–100 Hz, 0–11 V, 0.05–0.2 ms) to the bipolar cuff electrode #1 (i.e., Stim. A in Fig. 1b) and a high-frequency (5–20 kHz, 0–11 V) biphasic square waveform (see Fig. 1b) to the tripolar cuff electrodes #2 and #3 (i.e., Stim. B1 and B2 in Fig. 1b). The stimulator can be wireless controlled within a two-meter distance by a USB controller that is connected to a USB port of a portable computer (the computer is not shown). The computer software can set stimulation parameters for each output channel and turn on/off each channel by wireless communication between the implanted stimulator and the USB controller. The stimulator and battery are implanted underneath the skin on the left side of the lower back of the cat along the sacral spine. The battery can be charged by the charging circuitry in the stimulator that can be powered wirelessly across the skin by an external charging coil (not shown). At the beginning of each experiment, the battery was fully charged from 2.8 V to 3.7 V in about 15–20 min and it could be run for the entire experiment (five to six hours) with repeated stimulation. At the end of the experiment, the battery, stimulator, and electrodes were removed from the animal.

A total of five cats (three females and two males, 2.9 to 3.3 kg) were used in this study. Isoflurane (2–5% in O_2) was used to anesthetize the animals during surgery and then replaced by α-chloralose anesthesia (65 mg/kg i.v. and supplemented as needed) during data collection. The temperature of the animal was maintained at 35°C to 37°C using a heating pad. The ureters were cut and drained externally in order to accurately measure the bladder capacity when bladder was infused through a catheter in the urethra. A double lumen catheter (5F) was inserted into the bladder through a small incision in the proximal urethra and secured by a ligature (Fig. 1b). One lumen of the catheter was attached to a pump to infuse the bladder with saline, and the other lumen was connected to a pressure transducer to monitor the bladder activity. Another catheter (5F) was also inserted at the same site in the proximal urethra but directed toward the distal urethra and secured by a ligature (Fig. 1b). This catheter was attached to an infusion pump and to a pressure transducer via a T connector. The pudendal nerves were accessed posteriorly in the sciatic notch lateral to the tail. The three cuff electrodes (NCE112/113, MicroProbes Inc., Gaithersburg, MD, USA), as shown in Figure 1a, were tunneled underneath the skin from the stimulator to the exposed pudendal nerves and were placed around the left and right pudendal nerves as shown in Figure 1b. After implanting the stimulator, the battery, and the cuff electrodes, the muscle and skin were closed by sutures.

Three tests were performed in this study to determine the ability for the implanted stimulator to 1) block the pudendal nerve; 2) induce large bladder contraction; or 3) inhibit the micturition reflex. In the first test ($N = 5$ cats), the urethra was infused continuously with saline at a rate of 1–2 mL/min. Back pressure in the urethral perfusion system caused by EUS contraction was recorded via the pressure transducer (Fig. 1b). First, the high-frequency biphasic PNS at 10 kHz was applied to both Stim. A and Stim. B sites (see Fig. 1b) at different intensities (0.5–10 V) to determine the effective intensities for pudendal nerve block. Then, using an intensity effective in blocking the nerve at 10 kHz, different frequencies

(5–20 kHz) were tested to determine the threshold and optimal frequencies for pudendal nerve block. Finally, the high-frequency biphasic stimulation determined to be effective in blocking the pudendal nerve conduction was applied to block the maximal EUS contraction induced by the 20 Hz PNS applied at Stim. A (Fig. 1b). In the second test ($N = 5$ cats), a cystometrogram (CMG) was performed to determine the bladder capacity (i.e., the volume necessary to induce a large micturition contraction, > 30 cm H_2O). Then the bladder was infused to about 90% of its capacity and PNS (2–8 V, 0.2 ms) of different frequencies (5–40 Hz) was applied at Stim. A (Fig. 1b) to determine the optimal frequency for inducing a large (>30 cmH_2O) bladder contraction. In the third test ($N = 4$ cats), repeated CMGs were performed to determine the bladder capacity. Each CMG consisted of a slow infusion of saline (1–2 mL/min) starting with an empty bladder until the first micturition contraction occurred. Initially, two or three control CMGs were performed without PNS to determine the control bladder capacity and evaluate reproducibility. Then PNS (5 Hz, 2–5 V, 0.2 ms) was applied at Stim. A (Fig. 1b) during the CMG to increase bladder capacity. A control CMG without stimulation was also performed after the PNS CMG.

To quantify the PNS inhibitory effect, the bladder capacity measured during each CMG was normalized to the measurement during the first control CMG. Bladder contraction amplitude and area under bladder contraction curve were measured to determine the excitatory PNS effect. Urethral pressure induced by 20 Hz PNS was measured to determine the effect of high-frequency block. The data from different animals are presented as mean ± standard error. One-way ANOVA followed by Dunnett multiple comparison was used to detect statistical significance ($p < 0.05$).

RESULTS

Pudendal Nerve Block by High-Frequency Biphasic Stimulation

The high-frequency biphasic PNS waveform generated by the implanted stimulator successfully blocked pudendal nerve conduction and eliminated the PNS-evoked EUS contraction when applied bilaterally on the pudendal nerves (Figs. 2–5). The high-frequency biphasic PNS applied bilaterally at 10 kHz for 60 sec at locations Stim. B1 and Stim. B2 (Fig. 1b) activated the pudendal nerves, induced a strong EUS contraction, and caused large increases in urethral pressure at intensities of 0.5–2 V (Figs. 2a and 3a). However, as the intensity was increased, the urethral pressure response gradually decreased in amplitude and duration, and became minimal (<5 cmH_2O) at the end of the 60-sec high-frequency stimulation when the intensity was 6–10 V (Figs. 2a and 3a). Within this range of intensities (6–10 V), the high-frequency biphasic PNS generated large urethral pressure responses at frequencies below 6 kHz, but the response was minimal (<5 cmH_2O) at the end of the 60-sec stimulation once the frequency was increased above 6 kHz (Figs. 2b and 3b).

In order to show that the high-frequency biphasic PNS blocked pudendal nerve conduction when the urethral pressure response was diminished at the end of the 60-sec stimulation, a 20 Hz PNS (2–5 V, 0.2 ms) was applied at Stim. A (Fig. 1b) central to the high-frequency stimulation site to induce a maximal (70–100 cmH_2O) urethral pressure response (Figs. 4 and 5). This urethral response was completely blocked by the high-frequency biphasic PNS (6–15 kHz, 6–10 V) (Figs. 4 and 5). The pudendal nerve conduction recovered quickly from the block once the high-frequency PNS was terminated (Fig. 5a).

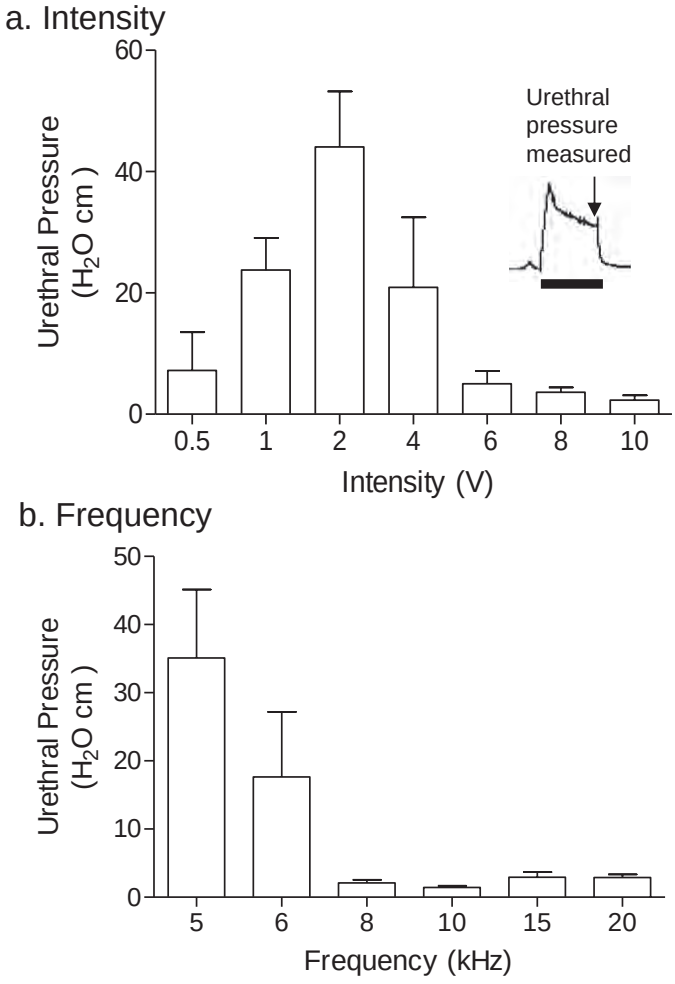

Figure 3. Urethral pressure measured at the end of high-frequency biphasic electrical stimulation. (a) Different intensities at 10 kHz frequency. (b) Different frequencies at 6–10 V intensity. $N = 5$ cats. The inserted figure in (a) shows the time point for urethral pressure measurement.

Bladder Excitation or Inhibition by PNS

The implanted stimulator also generated rectangular pulses at the cuff electrode #1 (at Stim. A in Fig. 1a,b) that reflexively excited or inhibited the bladder depending on the frequency of stimulation (Figs. 6 and 7). Several CMGs were performed in each animal to determine the bladder capacity. In one group of experiments, 20–30 Hz PNS (2–8 V, 0.2 ms) induced a large amplitude (45.9 ± 13.4 to 52.0 ± 22 cmH_2O) sustained bladder contraction (Fig. 6) when the bladder was filled to 90% of capacity. When the frequency was changed to 5 Hz, PNS (2–5 V, 0.2 ms) applied during CMG inhibited reflex micturition and significantly ($p < 0.05$) increased bladder capacity to 176.5 ± 27.1% of the control capacity (8.2 ± 1.9 mL) (Fig. 7).

DISCUSSION

In this study, we constructed and successfully tested an implantable, wireless-controlled, rechargeable battery-powered stimulator that can provide the required stimulation waveforms to 1) block pudendal nerve conduction and relax the EUS (Figs. 2–5); 2) induce a large sustained reflex bladder contraction (Fig. 6); or 3) inhibit

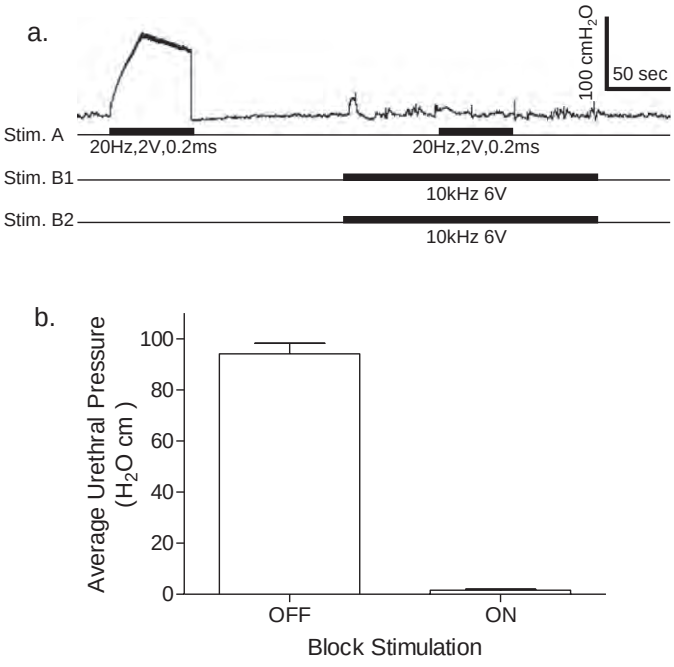

Figure 4. High-frequency, biphasic electrical stimulation of the pudendal nerves bilaterally blocked the urethral pressure increase induced by 20 Hz unilateral pudendal nerve stimulation. (a) A typical representation of the block effect. High-frequency stimulation delivered to Stim. B1 and Stim. B2 (see Fig. 1b) completely blocked the urethral pressure increase induced by Stim. A. The black bars under pressure trace indicate the stimulation duration. The Y-calibration bar indicates urethral pressure in 100 cmH_2O and the X-calibration bar indicates the time in 50 sec. (b) Average urethral pressure measured during Stim. A when the high-frequency stimulation was either on or off. Stim. A: frequency 20 Hz, pulse width 0.2 ms, intensity 2–5 V. Stim. B1/B2: frequency 6–15 kHz, intensity 6–10 V. $N = 5$ cats. A total of 17 tests were performed in five cats, with two to five tests in each cat.

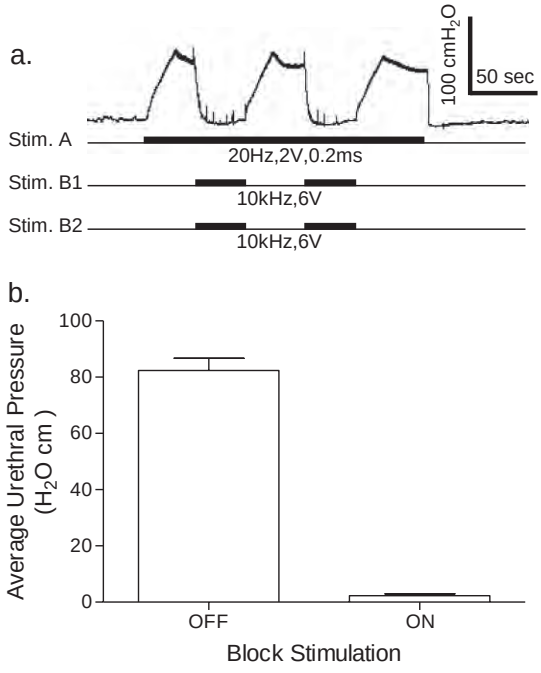

Figure 5. High-frequency biphasic stimulation of the pudendal nerves bilaterally completely blocked the increase in urethral pressure induced by unilateral pudendal nerve stimulation. (a) Records from one female cat showing the representative block of the response elicited by Stim. A during bilateral pudendal nerve stimulation (Stim. B1 and Stim. B2). High-frequency stimulation delivered to Stim. B1 and Stim. B2 (see Fig. 1b) blocked the urethral pressure induced by Stim. A. The black bars under pressure trace indicate the stimulation duration. The Y-calibration bar indicates the urethral pressure in 100 cmH_2O and the X-calibration bar indicates the time in 50 sec. (b) Average urethral pressure induced by Stim. A when the high-frequency stimulation was either on or off. Stim. A: frequency 20 Hz, pulse width 0.2 ms, intensity 2–5 V. Stim. B1/B2: frequency 6–15 kHz, intensity 6–10 V. $N = 4$ cats. A total of eight tests were performed in four cats, with one to three tests in each cat.

reflex bladder activity (Fig. 7). These acute *in vivo* experiments in anesthetized normal cats establish the effectiveness of the device as well as stimulation parameters that will be used in future long-term experiments to modulate abnormal lower urinary tract function in awake chronic SCI cats. In the chronic experiments, the 5 Hz PNS will be used to inhibit bladder overactivity and to promote urine storage. However, to elicit voiding, the 5 Hz PNS will be switched to 20 Hz to induce a sustained bladder contraction and at the same time a high-frequency (6–10 kHz) pudendal nerve block will be used to relax the EUS and prevent DSD, so that efficient, low-pressure voiding can be induced.

The elimination of EUS contraction by the high-frequency stimulation as shown in Figures 4 and 5 is due to the block of pudendal nerve conduction. It is not due to EUS fatigue caused by the stimulation, because a previous study (9) showed that the EUS could still contract if the Stim. A (Fig. 1b) was moved to a location distal to the high-frequency blocking stimulation. Our previous studies (7,8) have shown that the EUS contraction was gradually reduced as the stimulation frequency increased from 1 kHz to 10 kHz. A complete block of EUS contraction could only be achieved at 6 kHz and above. Therefore, we designed the stimulator to provide 5–20 kHz for pudendal nerve block (Fig. 2b). In the present study, the high-frequency blocking stimulation was applied bilaterally on the pudendal nerves (Fig. 1b) to block an excitatory pudendal-to-pudendal reflex (10,11) that can be triggered by afferent axonal volleys elicited by Stim. A that in turn can elicit efferent activity on the contralateral as well as the ipsilateral pudendal nerves to cause an EUS contraction. In addition, bilateral block of the pudendal nerves would be needed to control DSD after chronic SCI because afferent activity elicited by bladder contractions can generate pudendal efferent activity and EUS contractions bilaterally. Therefore, in this study, we implanted the blocking electrodes bilaterally on the pudendal nerves (Stim. B1 and B2 in Fig. 1b) to mimic the conditions when the implantable stimulator is used to restore bladder functions after chronic SCI. Our approach combining pudendal nerve stimulation and block is different from the approach used in other studies (12,13) that attempted to induce a reflex bladder contraction without an EUS contraction by selectively stimulating pudendal afferent nerves without stimulating efferent nerves. However, activation of pudendal afferent nerves will reflexively activate pudendal efferent nerves through an excitatory pudendal-to-pudendal reflex (10,11). In addition, the bladder contraction induced by pudendal afferent stimulation will produce pudendal efferent activity and EUS contraction due to DSD after SCI. This is why we positioned the electrodes bilaterally on the whole pudendal nerve to completely block pudendal efferent activity and relax the EUS.

The high-frequency blocking stimulation generated by the implantable stimulator produced a reversible block of the pudendal nerve. Pudendal nerve conduction recovered quickly once the

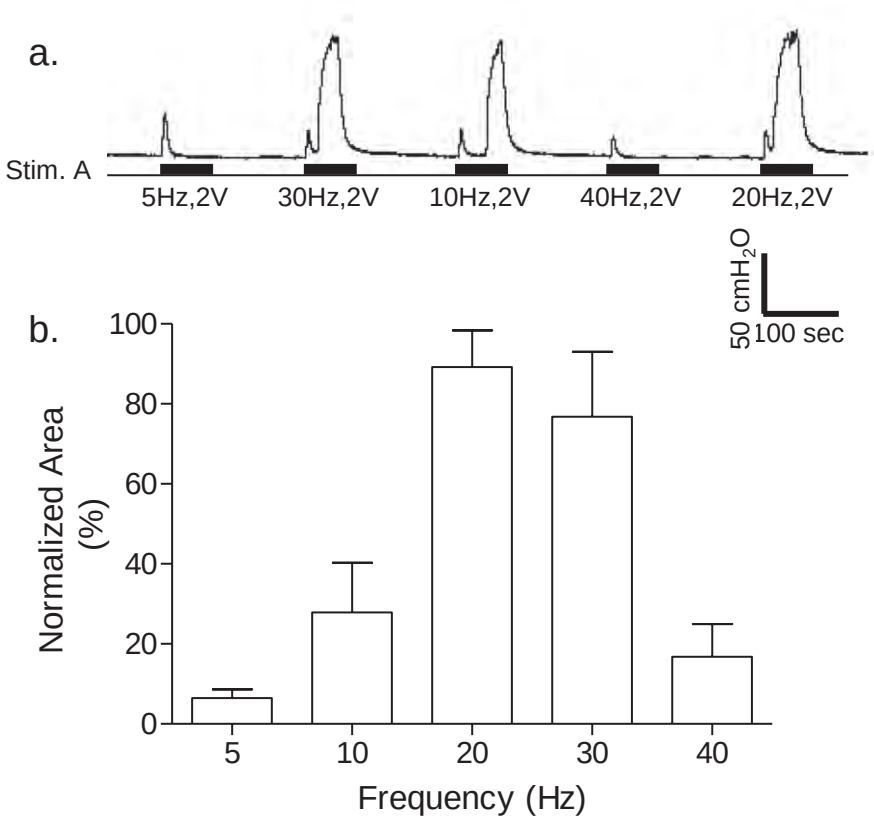

Figure 6. Bladder contractions induced by pudendal nerve stimulation at different frequencies. (a) Increase in bladder pressure elicited by unilateral pudendal nerve stimulation (Stim. A). The black bars under pressure trace indicate the stimulation duration. The Y-calibration bar indicates bladder pressure in 50 cmH_2O and the X-calibration bar indicates the time in 100 sec. (b) Normalized area under bladder pressure curve during stimulation. The area under curve was normalized to the maximal response in each animal. Stim. A: frequency 20 Hz, pulse width 0.2 msec, intensity 2–8 V. *N* = 5 cats.

high-frequency blocking stimulation was off (Fig. 5), indicating that the stimulation was safe and no nerve damage was induced. It is worth noting that the quick recovery from pudendal nerve block as shown in Figure 5 was achieved even after repeatedly (>14 times, see Figs. 2 and 4) applying the high-frequency blocking stimulation of 1–3 min duration for a total duration greater than 15 min. In clinical applications to restore micturition function after SCI, the high-frequency blocking stimulation will be applied about three to five times per day for only 1–2 min each time during voiding. Therefore, the possibility of pudendal nerve damage caused by the high-frequency blocking stimulation should be minimal. In addition, the safety of high-frequency blocking stimulation has also been verified by recent clinical studies to block the vagus nerve for diabetes treatment (14,15). The reversibility from pudendal nerve block is not only important for safety reasons but also necessary for maintaining continence function during urine storage.

About 15–20 min were needed to fully charge the battery wirelessly across the skin. After each charging, the battery successfully powered the stimulator in the animal for the entire experimental period (five to six hours). After removing the stimulator and battery from the animal at the end of experiment, the battery power lasted for about two to three days before the stimulator stopped functioning and lost communication with the USB controller due to a low battery level (<2.8 V). Although the stimulator was not used to stimulate/block the pudendal nerve once it was removed from the animal, it is estimated that the battery should still be able to power the stimulator for the same amount of time (two to three days) if it were used for PNS/block. This is because the electrical power used by PNS/block is only a very small portion of the total power consumption by the electrical circuits, including wireless communication, microprocessor, and the output amplifiers. Therefore, it is expected that the implantable stimulator will continuously function after chronic implantation in SCI cats as long as we continue to charge it for 15–20 min every day.

Currently there is a commercially available, implantable stimulator (InterStim, Medtronic Inc., Minneapolis, MN, USA) that stimulates the sacral S3 root to treat overactive bladder (OAB) (16). It has also been used to stimulate the pudendal nerve for the treatment of OAB or interstitial cystitis (IC) (17,18). However, the InterStim stimulator does not generate kHz frequencies and cannot be used to block the pudendal nerve and prevent DSD. Our stimulator is designed to treat both DO (5 Hz) and DSD (20 Hz + kHz) after SCI by stimulating and/or blocking the pudendal nerves. Although our stimulator could potentially be used for OAB or IC treatment, the kHz stimulation generated by our stimulator would be unnecessary for this purpose. As pudendal nerve also innervates the penis and anal sphincter in addition to the EUS, our pudendal nerve stimulator might have other potential applications to induce defecation, ejaculation, or penile erection, etc. However, before these applications become possible, the responses from these visceral organs to PNS will have to be determined.

This study only tested the functionality of the implantable stimulator. The durability can only be tested when the stimulator is implanted in awake chronic SCI cats in our future experiments. Although many improvements on this prototype stimulator may have to be implemented as our study progresses, this study is the

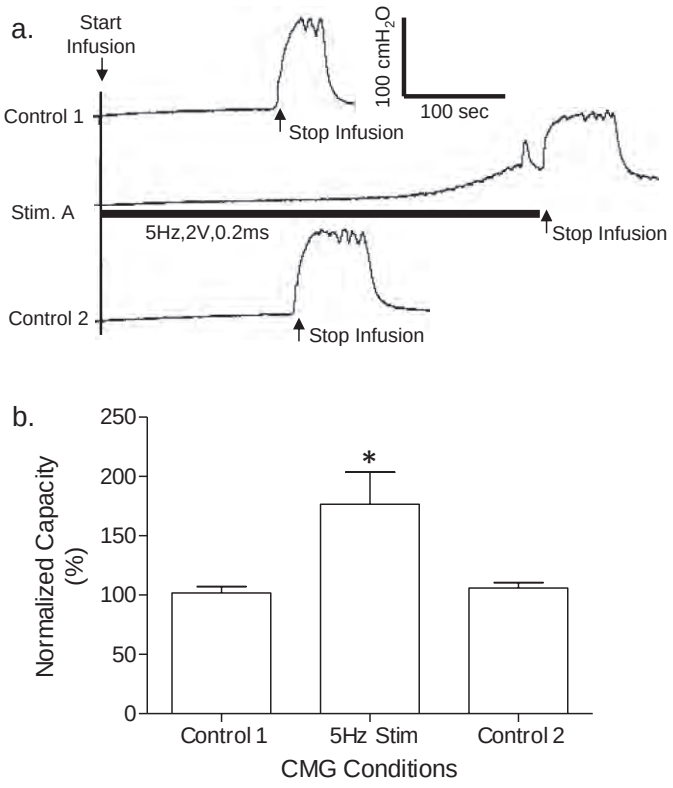

Figure 7. Increase in bladder capacity induced by 5 Hz unilateral pudendal nerve stimulation. (a) Repeated CMG recordings (infusion rate 2 mL/min in a female cat) showing in the middle trace the reversible increase in bladder capacity during stimulation. The black bar under the CMG trace indicates the stimulation duration. The Y-calibration bar indicates the bladder pressure in 100 cmH_2O and the X-calibration bar indicates the time in 100 sec. (b) Normalized bladder capacity measured during different CMGs. The capacity was normalized to the measurement from control 1 CMG. * indicates significantly different from the control 1. Stimulation: frequency 5 Hz, pulse width 0.2 msec, intensity 2–5 V. *N* = 4 cats. CMG—cystometrogram.

first step of our long-term effort in designing an implantable pudendal nerve stimulator for restoring bladder functions after SCI.

Authorship Statement

All authors designed and conducted the study. All authors approved the final manuscript. DOD and NIH provided the funding for the study. Dr. Tai had complete access to the study data.

How to Cite this Article:

Yang G., Wang J., Shen B., Roppolo J.R., de Groat W.C., Tai C. 2014. Pudendal Nerve Stimulation and Block by a Wireless-Controlled Implantable Stimulator in Cats. Neuromodulation 2014; 17: 490–496

REFERENCES

1. de Groat WC, Booth AM, Yoshimura N. Neurophysiology of micturition and its modification in animal models of human disease. In: Maggi CA, ed. *The autonomic nervous system, nervous control of the urogenital system*. London: Harwood Academic Publishers, 1993:227–289.
2. Burns AS, Rivas DA, Ditunno JF. The management of neurogenic bladder and sexual dysfunction after spinal cord injury. *Spine* 2001;26:S129–S136.
3. van Kerrebroeck PEV, Koldewijn EL, Rosier PFWM, Wijkstra H, Debruyne FMJ. Results of the treatment of neurogenic bladder dysfunction in spinal cord injury by sacral posterior root rhizotomy and anterior sacral root stimulation. *J Urol* 1996;155:1378–1381.
4. Tai C, Smerin SE, de Groat WC, Roppolo JR. Pudendal-to-bladder reflex in chronic spinal-cord-injured cats. *Exp Neurol* 2006;197:225–234.
5. Tai C, Wang J, Wang X, de Groat WC, Roppolo JR. Bladder inhibition and voiding induced by pudendal nerve stimulation in chronic spinal cord injured cats. *Neurourol Urodyn* 2007;26:570–577.
6. Tai C, Chen M, Shen B et al. Plasticity of urinary bladder reflexes evoked by stimulation of pudendal afferent nerves after chronic spinal cord injury in cat. *Exp Neurol* 2011;228:109–117.
7. Tai C, Roppolo JR, de Groat WC. Block of external urethral sphincter contraction by high frequency electrical stimulation of pudendal nerve. *J Urol* 2004;172:2069–2072.
8. Tai C, Roppolo JR, de Groat WC. Response of external urethral sphincter to high frequency biphasic electrical stimulation of pudendal nerve. *J Urol* 2005;174:782–786.
9. Tai C, Wang J, Chancellor MB, Roppolo JR, de Groat WC. Influence of temperature on pudendal nerve block induced by high frequency biphasic electrical current. *J Urol* 2008;180:1173–1178.
10. Tai C, Wang J, Wang X, Roppolo JR, de Groat WC. Voiding reflex in chronic spinal cord injured cats induced by stimulating and blocking pudendal nerves. *Neurourol Urodyn* 2007;26:879–886.
11. Thor KB, Hisamitsu T, Roppolo JR. Selective inhibitory effects of ethylketocyclazocine on reflex pathways to the external urethral sphincter of the cat. *J Pharmacol Exp Ther* 1989;248:1010–1025.
12. Woock JP, Yoo PB, Grill WM. Finite element modeling and in vivo analysis of electrode configurations for selective stimulation of pudendal afferent fibers. *BMC Urol* 2010;10:11.
13. Yoo PB, Woock JP, Grill WM. Bladder activation by selective stimulation of pudendal nerve afferents in cats. *Exp Neurol* 2008;212:218–225.
14. Sarr MG, Billington CJ, Brancatisamo R et al. The EMPOWER study: randomized, prospective, double-blind, multicenter trial of vagal blockade to induce weight loss in morbid obesity. *Obes Surg* 2012;22:1771–1782.
15. Waataja JJ, Tweden KS, Honda CN. Effects of high-frequency alternating current on axonal conduction through the vagus nerve. *J Neural Eng* 2011;8:056013.
16. van Kerrebroeck PEV, van Voskuilen AC, Heesakkers JPFA et al. Results of sacral neuromodulation therapy for urinary voiding dysfunctions: outcomes of a prospective, worldwide clinical study. *J Urol* 2007;178:2020–2034.
17. Peters KM, Feber KM, Bennett RC. Sacral versus pudendal nerve stimulation for voiding dysfunction: a prospective, single-blinded, randomized, crossover trial. *Neurourol Urodyn* 2005;24:643–647.
18. Peters KM, Feber KM, Bennett RC. A prospective, single-blinded, randomized crossover trial of sacral vs. pudendal nerve stimulation for interstitial cystitis. *BJU Int* 2007;100:835–839.

COMMENT

This is an important contribution to the goal of developing a wireless pudendal nerve stimulator for restoration of bladder function following an upper motoneuron spinal cord lesioned bladder.

Michael Ruggieri, MD
Philadelphia, PA, USA

Comments not included in the Early View version of this paper.

J Comput Neurosci (2014) 37:377–386
DOI 10.1007/s10827-014-0510-z

Effect of non-symmetric waveform on conduction block induced by high-frequency (kHz) biphasic stimulation in unmyelinated axon

Shouguo Zhao · Guangning Yang · Jicheng Wang · James R. Roppolo · William C. de Groat · Changfeng Tai

Received: 12 January 2014 / Revised: 2 May 2014 / Accepted: 5 June 2014 / Published online: 14 June 2014

Abstract The effect of a non-symmetric waveform on nerve conduction block induced by high-frequency biphasic stimulation is investigated using a lumped circuit model of the unmyelinated axon based on Hodgkin-Huxley equations. The simulation results reveal that the block threshold monotonically increases with the stimulation frequency for the symmetric stimulation waveform. However, a non-monotonic relationship between block threshold and stimulation frequency is observed when the stimulation waveform is non-symmetric. Constant activation of potassium channels by the high-frequency stimulation results in the increase of block threshold with increasing frequency. The non-symmetric waveform with a positive pulse 0.4–0.8 μs longer than the negative pulse blocks axonal conduction by hyperpolarizing the membrane and causes a decrease in block threshold as the frequency increases above 12–16 kHz. On the other hand, the non-symmetric waveform with a negative pulse 0.4–0.8 μs longer than the positive pulse blocks axonal conduction by depolarizing the membrane and causes a decrease in block threshold as the frequency increases above 40–53 kHz. This simulation study is important for understanding the potential mechanisms underlying the nerve block observed in animal studies, and may also help to design new animal experiments to further improve the nerve block method for clinical applications.

Keywords Nerve block · High-frequency · Stimulation · Sodium · Potassium

Action Editor: Arnd Roth

S. Zhao · G. Yang · J. Wang · C. Tai (✉)
Department of Urology, University of Pittsburgh,
700 Kaufmann Building, 15213 Pittsburgh, PA, USA
e-mail: cftai@pitt.edu

S. Zhao · G. Yang
Department of Biomedical Engineering, Beijing Jiaotong University,
Beijing, Peoples Republic China

J. R. Roppolo · W. C. de Groat · C. Tai
Department of Pharmacology and Chemical Biology,
University of Pittsburgh, Pittsburgh, PA, USA

1 Introduction

It has been known for about 80 years that high-frequency biphasic stimulation can block conduction of myelinated axons at a minimal frequency of approximately 5 kHz (Cattell and Gerard 1935; Reboul and Rosenblueth 1939; Rosenblueth and Reboul 1939). Recently this nerve block method has been applied to treat obesity (Camilleri et al. 2009; Wattaja et al. 2011), block chronic pain of peripheral origin (Cuellar et al. 2013; van Buyten et al. 2013), or restore urinary function after spinal cord injury (Gaunt and Prochazka 2009; Tai et al. 2004). However, the mechanisms underlying this conduction block are still unknown. It has been proposed that high-frequency biphasic stimulation causes extracellular accumulation of potassium (Cattell and Gerard 1935) or constant depolarization of the axonal membrane (Tanner 1962) to induce the block. Although the patch-clamp technique has significantly increased our understanding of sodium and potassium channel properties of the axonal membrane (Catterall 2012; Jan and Jan 2012; Schwarz et al. 1995; Vasylyev and Waxman 2012; Waxman 2012), it has not been used to investigate axonal responses to high-frequency (>5 kHz) biphasic stimulation leaving the above proposals unconfirmed.

Recent studies of unmyelinated axons using sea slugs and frogs (Joseph and Butera 2009, 2011) have further shown that the high-frequency biphasic stimulation has a maximal block threshold at 12–15 kHz. This observation provides a new challenge and/or opportunity for testing the different hypotheses regarding the blocking mechanism. It seems likely that a

single mechanism as proposed above (Cattell and Gerard 1935; Tanner 1962) would not explain the two critical frequencies (5 kHz and 12–15 kHz) of conduction block by high-frequency stimulation. Therefore, in this study we investigated the role that both sodium and potassium channel kinetics might play in the block of unmyelinated axons induced by high-frequency biphasic stimulation.

It is a technical challenge to generate a perfectly symmetric biphasic waveform due to the limitations of the electronic generators. Therefore, as the stimulation frequency becomes very high (>10 kHz), a small difference (<1 μs) in the duration of the positive and negative pulses of the biphasic waveform could lead to a significantly different response of the axonal membrane. In the present study we investigated the effect of a non-symmetric waveform on high-frequency nerve conduction block. Because it is technically difficult to measure sodium and potassium channel activity during the biphasic high-frequency stimulation due to the strong electrical artifacts, we used an axonal cable model based on Hodgkin-Huxley equations (Hodgkin and Huxley 1952) to simulate the response of an unmyelinated axon to high-frequency biphasic stimulation to determine: (1) whether the model can predict the minimal frequency (about 5 kHz) for nerve block and the frequencies (about 12–15 kHz) for a maximal block threshold; (2) whether sodium and/or potassium channel kinetics determine these critical blocking frequencies. Answering these questions might not only reveal the physiological mechanisms underlying nerve conduction block, but may also guide future animal experiments and clinical applications of nerve conduction block induced by high-frequency biphasic stimulation (Camilleri et al. 2009; Cuellar et al. 2013; Gaunt and Prochazka 2009; Tai et al. 2004; Wattaja et al. 2011; van Buyten et al. 2013).

2 Methods

The unmyelinated axon model (Fig. 1) consists of a 9-mm-long axon segmented into many small cylinders of length Δx=0.25 mm, each of which is modeled by a resistance-capacitance circuitry. The ionic currents passing through the variable membrane resistance are described by Hodgkin–Huxley equations (Hodgkin and Huxley 1952). Two mono polar electrodes (with the indifferent electrodes at infinity) are placed at 1 mm distance from the unmyelinated axon. One is the block electrode at the 6 mm location along the axon, where the high-frequency biphasic electrical current is delivered. The other is the test electrode at the 3 mm location, which delivers a uniphasic single pulse (pulse width: 0.1 ms; intensity: 10–15 mA) to evoke an action potential that can propagate through the site of the block electrode. The test electrode is always the cathode (negative pulse). The block electrode always delivers the high-frequency biphasic current with the cathodal phase first.

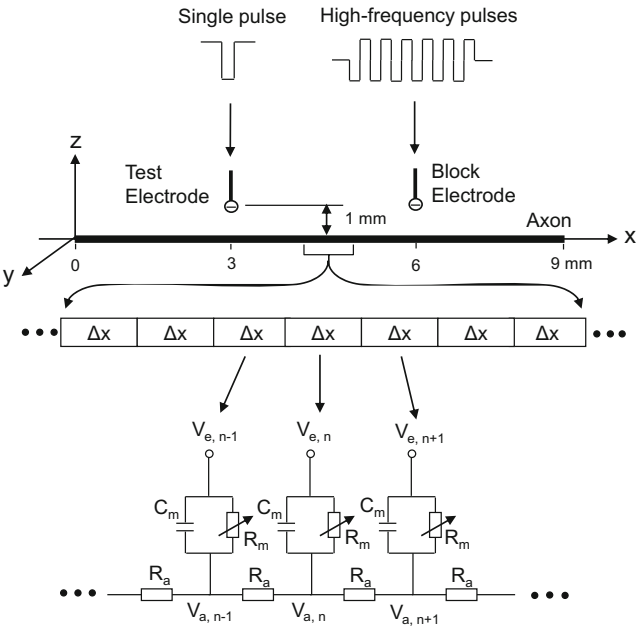

Fig. 1 Unmyelinated axon model to simulate conduction block induced by high-frequency biphasic electrical current. The unmyelinated axon is segmented into many small cylinders of length Δx, each of which is modeled by a resistance-capacitance circuit based on the Hodgkin–Huxley model. R_a: Axoplasm resistance. R_m: Membrane resistance. C_m: Membrane capacitance. V_a: Intracellular potential. V_e: Extracellular potential

We assume that the unmyelinated axon is in an infinite homogeneous medium (resistivity ρ_e=300 Ωcm). After neglecting the small influence of the axon in the homogeneous medium, the extracellular potential $V_{e,n}$ at the nth segment along the axon can be described by:

$$V_{e,n} = \frac{\rho_e}{4\pi}\left[\frac{I_{block}(t)}{\sqrt{(n\Delta x - x_0)^2 + z_0^2}} + \frac{I_{test}(t)}{\sqrt{(n\Delta x - x_1)^2 + z_1^2}}\right]$$

Where $I_{block}(t)$ is the high-frequency biphasic current delivered to the block electrode (at location x_0=6 mm, z_0=1 mm); $I_{test}(t)$ is the single test pulse delivered to the test electrode (at location x_1=3 mm, z_1=1 mm).

The change of the membrane potential V_n at the nth segment of the unmyelinated axon is described by:

$$\frac{dV_n}{dt} = \left[\frac{d}{4\rho_i}\left(\frac{V_{n-1} - 2V_n + V_{n+1}}{\Delta x^2} + \frac{V_{e,n-1} - 2V_{e,n} + V_{e,n+1}}{\Delta x^2}\right) - I_{i,n}\right] / c_m$$

Where $V_n = V_{a,n} - V_{e,n} - V_{rest}$; $V_{a,n}$ is the intracellular potential at the nth segment; $V_{e,n}$ is the extracellular potential at the nth segment; V_{rest} is the resting membrane potential; d is the

unmyelinated axon diameter; ρ_i is the resistivity of axoplasm (34.5 Ωcm); c_m is the capacity of the membrane (1 uF/cm^2); $I_{i,n}$ is the ionic current at the n^{th} segment described by Hodgkin–Huxley equations (Hodgkin and Huxley 1952; Rattay 1989; Rattay and Aberham 1993; Tai et al. 2005a, 2005b).

The model equations were solved by the Runge–Kutta method (Boyce and Diprima 1997) with a time step of 0.2 μsec. A smaller time step (0.05 μsec) or Runge–Kutta-Fehlberg method (Heinbockel 2005) with an adaptive time step was also used to confirm some of the key results. The temperature parameter was set at T=18.5 °C. The simulation was always started at initial condition V_n=0. The membrane potentials at the two end segments of the modeled axon were always equal to the membrane potentials of their closest neighbors, which implemented sealed boundary conditions (no longitudinal currents) at the two ends of the modeled axon. The block threshold intensity was determined with a resolution of 1 mA.

3 Results

3.1 Conduction block by symmetric and non-symmetric biphasic stimulation waveforms

Figure 2 shows that in an unmyelinated axon the Hodgkin–Huxley model can successfully simulate the conduction block induced by high-frequency (10 kHz) symmetric biphasic stimulation. In Fig. 2a the 10 kHz blocking stimulation (81 mA) generates an initial action potential propagating in both directions. At 5 ms after the start of blocking stimulation, the test electrode delivers a single pulse that generates another action potential propagating toward the block electrode (see the white arrow in Fig. 2a). This action potential fails to propagate through the block electrode due to the presence of the high-frequency biphasic stimulation. However, at a lower stimulation intensity (80 mA in Fig. 2b) the 10 kHz stimulation does not block nerve conduction and the action potential propagates through the site of the block

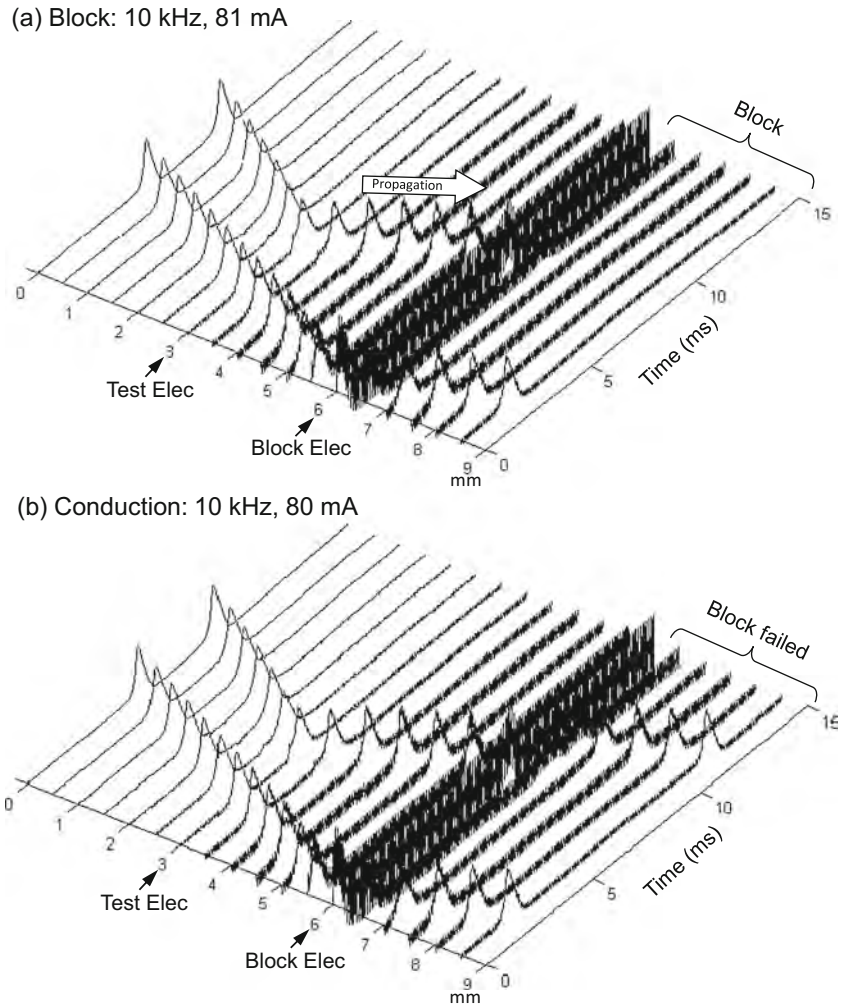

Fig. 2 Blocking the propagation of action potentials along an unmyelinated axon by high-frequency symmetric biphasic stimulation. High-frequency (10 kHz) stimulation is continuously delivered at the block electrode, which initiated an initial action potential. Another action potential is initiated via the test electrode at 5 ms after starting the high-frequency stimulation, and propagates towards both ends of the axon. The 10 kHz stimulation blocks nerve conduction at the intensity of 81 mA (**a**), but not at 80 mA (**b**). The *short arrows* mark the locations of test and block electrodes along the axon. The *white arrow* indicates propagation of the action potential to the location of the 10 kHz blocking stimulation. Axon diameter: 2 μm

electrode. Similar conduction block was also successfully simulated for non-symmetric biphasic stimulation waveforms where either the positive pulse is 0.4 or 0.8 μs longer than the negative pulse, or the reverse of this condition.

Figure 3 shows the intensity thresholds for inducing conduction block at different frequencies (5–100 kHz) for an unmyelinated axon of 2 μm diameter. For the symmetric biphasic waveform (Fig. 3a), the block threshold monotonically increases as the stimulation frequency increases. However, if the biphasic waveform is not symmetric (Fig. 3b and c), the block threshold increases initially and then decreases with increasing stimulation frequency, showing a non-monotonic relationship between block threshold and stimulation frequency. If the positive pulse is 0.4 or 0.8 μs longer than the negative pulse, the block threshold peaks between 12 kHz and 16 kHz (Fig. 3b). However, if the negative pulse is 0.4–0.8 μs longer than the positive pulse, the block threshold peaks at a frequency of 40–53 kHz (Fig. 3c). For the symmetric waveform, nerve block is not observed at frequencies below 5 kHz, indicating that the minimal frequency for inducing nerve block is about 5 kHz (Fig. 3). To evaluate the possibility that the numerical integration method might cause the effect of asymmetric stimulation waveform, we also calculated the result shown in Fig. 3b using a smaller time step of 0.05 μs or using Runge–Kutta-Fehlberg method with an adaptive time step. These methods did not change the results (see Fig. 3d).

3.2 Mechanisms of the conduction block by symmetric and non-symmetric waveforms

Figure 4 shows the same simulation as in Fig. 2a for the 10 kHz symmetric biphasic waveform but including more detailed information for the 3 consecutive axon segments at distances of 0–1 mm from the block electrode (the location at 6.0 mm is under the block electrode). Figure 4a-c show the action potential, sodium current, and potassium current at different locations approaching the block electrode. This action potential propagation is disrupted at the location (6.0 mm) under the block electrode, where axon membrane is alternately depolarized and hyperpolarized with large pulsed sodium and potassium currents. The behavior of the membrane potential and ionic currents can be further explained by the activation/inactivation of the sodium and potassium channels as shown in Fig. 4d-f. As the action potential propagates toward the block electrode, the activation (m) of sodium channels also changes at each location and becomes weaker and oscillatory at the location under the block electrode (Fig. 4d). Meanwhile, the inactivation of sodium channels is kept at a low level (i.e., h is a high value) under the block electrode (Fig. 4e). The combination of activation and inactivation of sodium channels (Fig. 4d-e) determines that the sodium current becomes a pulsed inward current under the block electrode (Fig. 4b). Therefore, the sodium channels are never completely blocked when conduction block occurs. However, the change in potassium activation (n) induced by the action potential becomes smaller under the block electrode

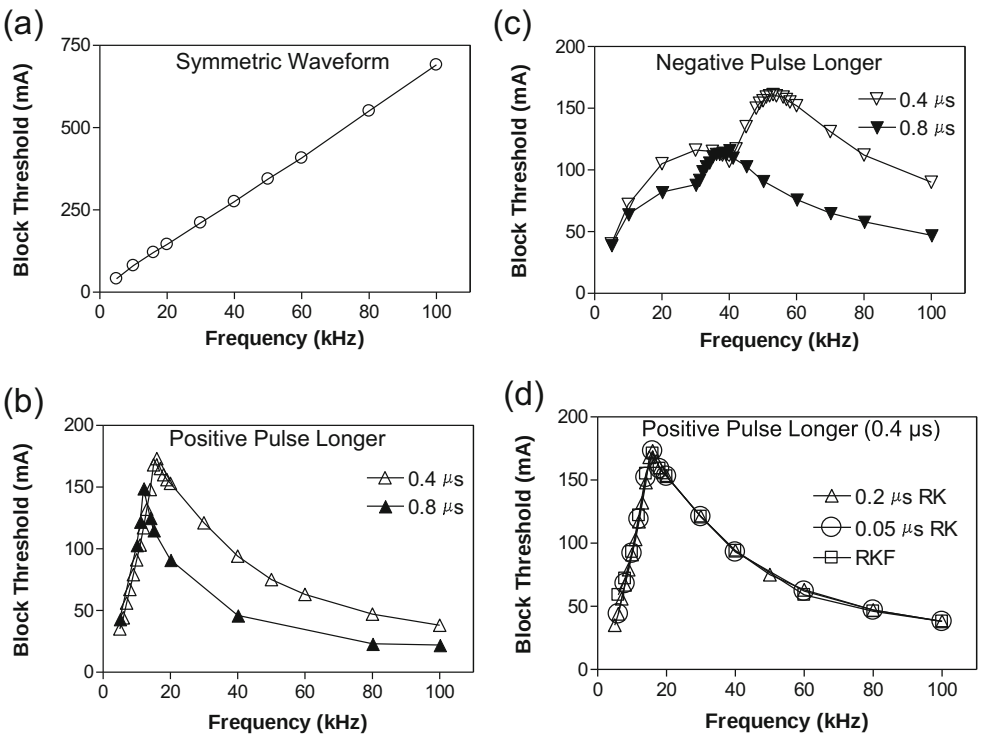

Fig. 3 The threshold intensity to block nerve conduction changes with the stimulation frequency. (**a**). For the symmetric waveform, the block threshold monotonically increases as the frequency increases. (**b**). If the positive pulse is longer (0.4 or 0.8 μs), the block threshold peaks at 12–16 kHz and then gradually decreases as the frequency increases. (**c**). If the negative pulse is longer (0.4 or 0.8 μs), the block threshold peaks at 40–53 kHz. (**d**). The same results were also obtained by Runge–Kutta (RK) numerical integration method with a smaller time step of 0.05 μs or by Runge–Kutta-Fehlberg (RKF) numerical integration method with an adaptive time step. Axon diameter: 2 μm

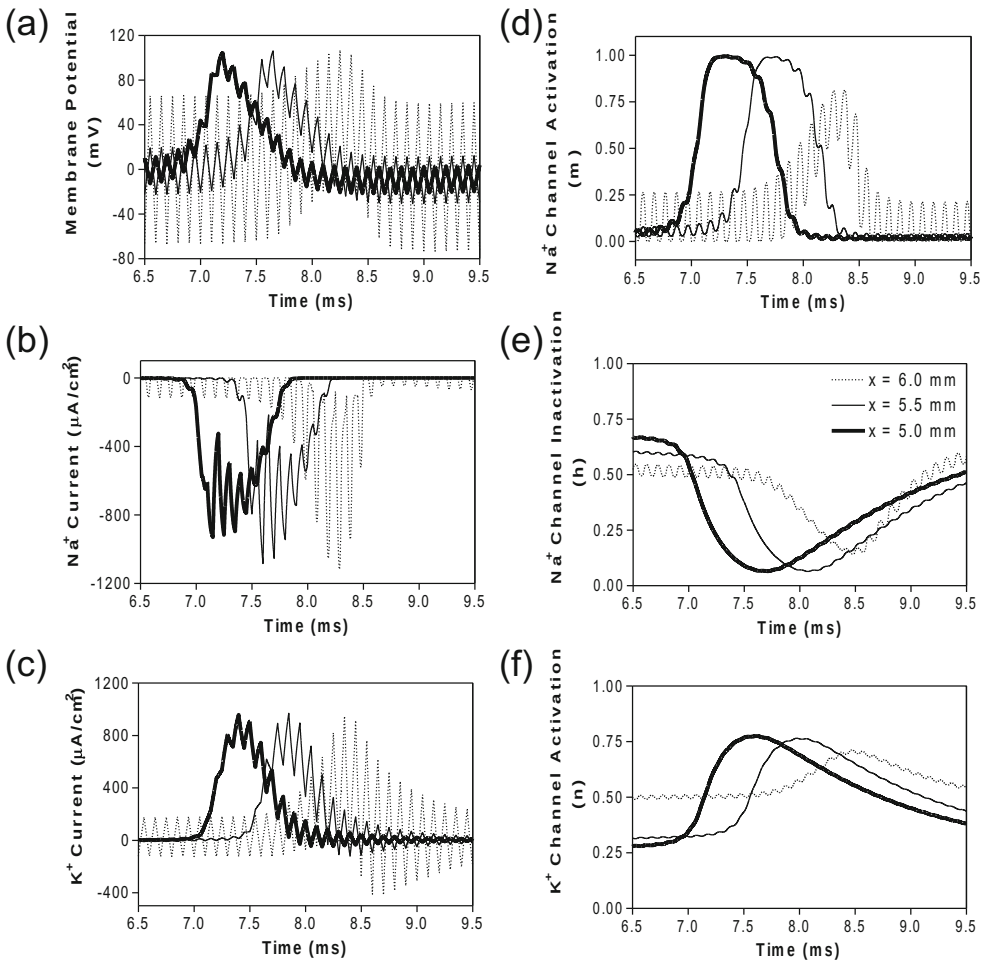

Fig. 4 The changes in membrane potential, ionic currents and activation/inactivation of ion channels near the block electrode when conduction block occurs as shown in Fig. 2 (**a**) during stimulation with a symmetric waveform. The legends in (**e**) indicate the location of each axon segment. Node at 6.0 mm is under the block electrode. (**a**) Change in membrane potential, (**b**) Na^+ current, (**c**) K^+ current, (**d**) Na^+ channel activation, (**e**) Na^+ channel inactivation, (**f**) K^+ channel activation. *Symmetric stimulation waveform*: 10 kHz, 81 mA. Axon diameter: 2 μm. *Abscissa*: time in ms after the start of blocking stimulation

(Fig. 4f) because potassium channels are constantly activated at this location, resulting in a large pulsed outward potassium current (Fig. 4c). This large outward potassium current opposes the large inward sodium current, causing the membrane under the block electrode to become un-excitable leading to the block of action potential conduction. This blocking mechanism is observed for the symmetric waveform in the frequency range of 5–100 kHz (Fig. 3a). Our previous simulation studies of an unmyelinated axon (Tai et al. 2005a, 2005b) also revealed that the constant activation of potassium channels by high-frequency symmetric biphasic stimulation requires higher stimulation intensity as the frequency increases, because a lower frequency can maintain a higher activation level of potassium channels than a higher frequency.

A similar blocking mechanism is also observed for non-symmetric waveforms at frequencies below the peak block threshold frequency (Fig. 3b and c). Figure 5 shows that at 10 kHz the symmetric and non-symmetric waveforms produce almost the same alternating membrane depolarization/hyperpolarization (Fig. 5a) and very similar ion channel activation/inactivation (Fig. 5b-d). It is also worth noting that the 0.4 μs difference between the positive and negative pulses produces no difference in potassium channel activation (Fig. 5d).

In order to understand why the block threshold with the non-symmetric waveform starts to decrease at frequencies above the peak block threshold frequency (Fig. 3b and c), we further investigated the changes in membrane potential, ionic currents, and activation/inactivation of the sodium and potassium channels at frequencies between 12–100 kHz. Figure 6 shows the conduction block by the 80 kHz non-symmetric waveform with a positive pulse 0.4 μs longer than the negative pulse. Action potential propagation is completely abolished at the location (6.0 mm) under the block electrode, where the axon membrane is hyperpolarized to about −120 mV [(−50 mV)+(−70 mV resting potential), see Fig. 6a]. This hyperpolarization is caused by the accumulation of 0.4 μs longer positive pulses, which completely deactivates both sodium and potassium channels (Fig. 6d and f) and eliminates both sodium and potassium currents (Fig. 6b and c) thereby resulting in a conduction block at the location (6.0 mm) under the block electrode. Meanwhile, inactivation (h) of sodium channels is minimal (≈1) under the block electrode (Fig. 6e). The same blocking mechanism is observed at frequencies greater than 12–16 kHz for non-symmetric waveforms with the positive pulse 0.4 or 0.8 μs longer than the negative pulse (Fig. 3b). As the frequency is increased, the accumulation of positive charges

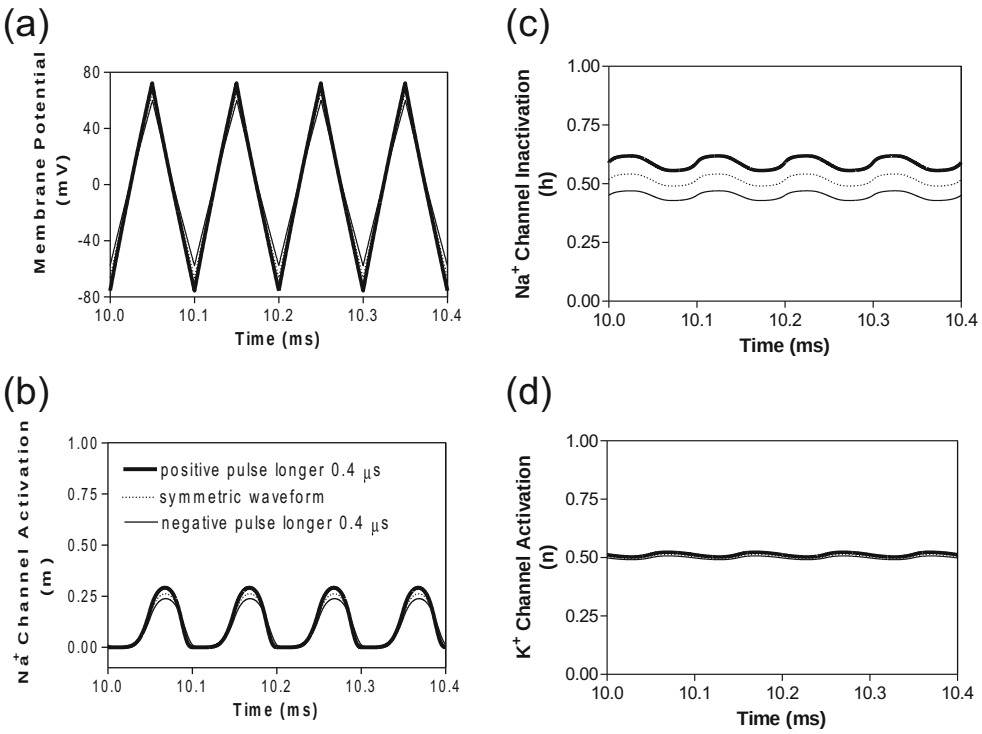

Fig. 5 The effects of non-symmetric waveforms on membrane potential and activation/inactivation of ion channels under the block electrode when stimulation frequency is 10 kHz. The legends in (**b**) indicate the types of waveform: symmetric and non-symmetric with a 0.4 μs difference in pulse width between the positive and negative pulses. (**a**) Change of membrane potential, (**b**) Na^+ channel activation, (**c**) Na^+ channel inactivation, (**d**) K^+ channel activation. *Stimulation waveforms*: 10 kHz at block threshold intensities. *Axon diameter*: 2 μm. *Abscissa*: time in ms after the start of blocking stimulation

due to the longer positive pulses is greater and produces the same level of hyperpolarization at a lower stimulus intensity. Therefore, the block threshold decreases as the frequency increases (Fig. 3b).

However, if the non-symmetric waveform has a longer negative pulse, it generates a constant depolarization under the block electrode instead of a hyperpolarization. Figure 7 shows the membrane potentials and ion channel activation/inactivation for the symmetric and non-symmetric waveforms at 80 kHz. Although the 0.4 μs difference between the positive and negative pulses does not produce a different membrane response at 10 kHz (Fig. 5), it can generate a significantly different response at 80 kHz (Fig. 7). The non-symmetric waveform with the negative pulse 0.4 μs longer than the positive pulse produces a constant depolarization about 20 mV (Fig. 7 a), which causes a significant inactivation of sodium channels (Fig. 7c) resulting in a conduction block. The accumulation of negative charges due to longer negative pulses is greater for a higher frequency, thereby producing the same level of depolarization at a lower block threshold (Fig. 3c).

4 Discussion

This study employed the Hodgkin–Huxley axonal model to simulate nerve conduction block by high-frequency (5–100 kHz) biphasic stimulation in an unmyelinated axon (Figs. 1–2). It revealed that the block threshold monotonically increases with the stimulation frequency if the biphasic stimulation waveform is symmetric (Fig. 3a). A non-monotonic relationship between block threshold and stimulation frequency can only be observed when the biphasic stimulation waveform is non-symmetric (Fig. 3b and c). Constant activation of potassium channels by high-frequency stimulation is the underlying mechanism for the increase of block threshold with increasing frequency (Figs. 4 and 5). The non-symmetric waveform consisting of longer positive pulses blocks axonal conduction by hyperpolarizing the membrane (Fig. 6), which causes a decrease in block threshold as the frequency increases above 12–16 kHz (Fig. 3b). On the other hand, the non-symmetric waveform consisting of longer negative pulses blocks axonal conduction by depolarizing the membrane (Fig. 7), which causes a decrease in block threshold as the frequency increases above 40–53 kHz (Fig. 3c).

This study and our previous studies (Tai et al. 2005a, 2005b) using the unmyelinated axonal model (Hodgkin–Huxley model) have successfully predicted the minimal blocking frequency (5 kHz) (Bowman and McNeal 1986; Reboul and Rosenblueth 1939; Rosenblueth and Reboul 1939). However, the peak block threshold frequencies (12–15 kHz) discovered recently in unmyelinated axons of sea-slugs and frogs (Joseph and Butera 2009, 2011) can only be observed in this simulation study using non-symmetric waveforms with a positive pulse 0.4 or 0.8 μs longer than the negative pulse (Fig. 3). Since the animal studies (Joseph and Butera 2009, 2011) did not report the accuracy of the stimulation waveform, it is difficult to know whether the peak block threshold frequencies

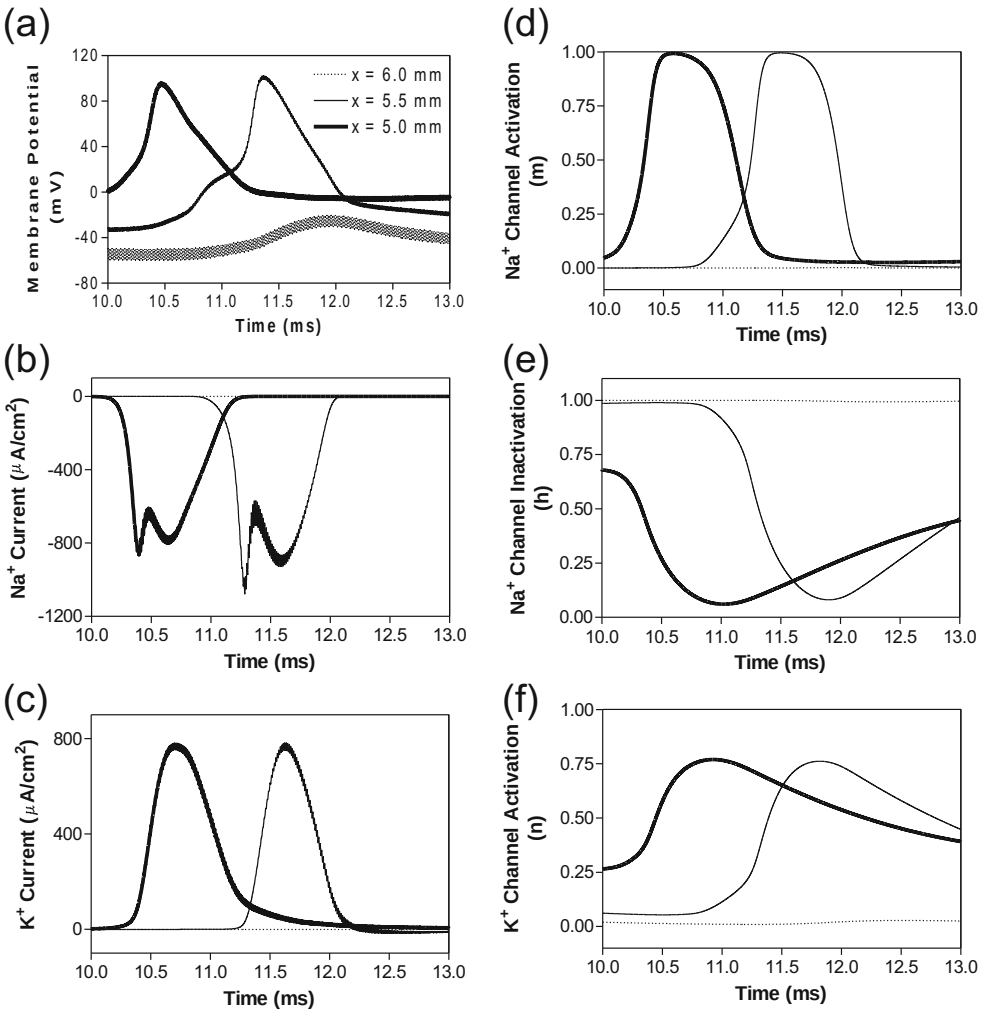

Fig. 6 The changes in membrane potential, ionic currents and activation/inactivation of ion channels near the block electrode when conduction block is induced by a 80 kHz non-symmetric waveform with the positive pulse 0.4 μs longer than the negative pulse. The legends in (**a**) indicate the location of each axon segment. Node at 6.0 mm is under the block electrode. (**a**) Change in membrane potential, (**b**) Na^+ current, (**c**) K^+ current, (**d**) Na^+ channel activation, (**e**) Na^+ channel inactivation, (**f**) K^+ channel activation. Non-symmetric stimulation waveform: 80 kHz, 48 mA. *Axon diameter*: 2 μm. *Abscissa*: time in ms after the start of blocking stimulation

(12–15 kHz) were caused by a slightly non-symmetric waveform used in those studies. Additional animal studies with accurate information about the symmetry of the stimulation waveform are needed in order to confirm the results from this simulation study.

However, the animal study (Joseph and Butera 2011) using the same stimulation waveform also showed that in a myelinated axon the block threshold monotonically increases with stimulation frequency up to 50 kHz. Our previous simulation study (Tai et al. 2011) using a myelinated axon model (Frankenhaeuser-Huxley model) showed the same monotonic increase in block threshold at frequencies up to 100 kHz for axons of diameter 10–20 μm. However, the effect of non-symmetric waveforms on conduction block of myelinated axon has not been investigated. Since the ion channels in myelinated axons (Frankenhaeuser 1960) have much faster kinetics than in unmyelinated axons (Hodgkin and Huxley 1952), it is possible that a frequency greater than 50 kHz might be needed in order to induce a constant hyperpolarization and a decrease in block threshold by the non-symmetric waveform with a slightly longer positive pulses. Therefore, more studies are warranted to investigate nerve conduction block in myelinated axons using non-symmetric stimulation waveforms.

The results in this study emphasize the importance of using a symmetric biphasic waveform for high-frequency nerve block, especially when the frequency is above 10 kHz. The small difference of 0.4 μs between the positive and negative pulses (less than 0.8 % difference in pulse width) may not make a difference in nerve block at frequencies below 10 kHz (Figs. 4–5), but can make a significant difference at frequencies of 20–100 kHz (1.6-8 % difference in pulse width) causing a decrease in block threshold (Fig. 3b and c) by constantly hyperpolarizing or depolarizing the axonal membrane (Figs. 6–7). The net effect of the non-symmetric waveform on axonal conduction is equivalent to that caused by direct current (DC). The non-symmetric waveform with a longer positive (or negative) pulse blocks nerve conduction by inducing a constant hyperpolarization (or depolarization) of the axon membrane, which is similar to the nerve conduction block induced by an anodal (or cathodal) DC (Tai et al. 2009). It is known that DC can damage nerves during long-

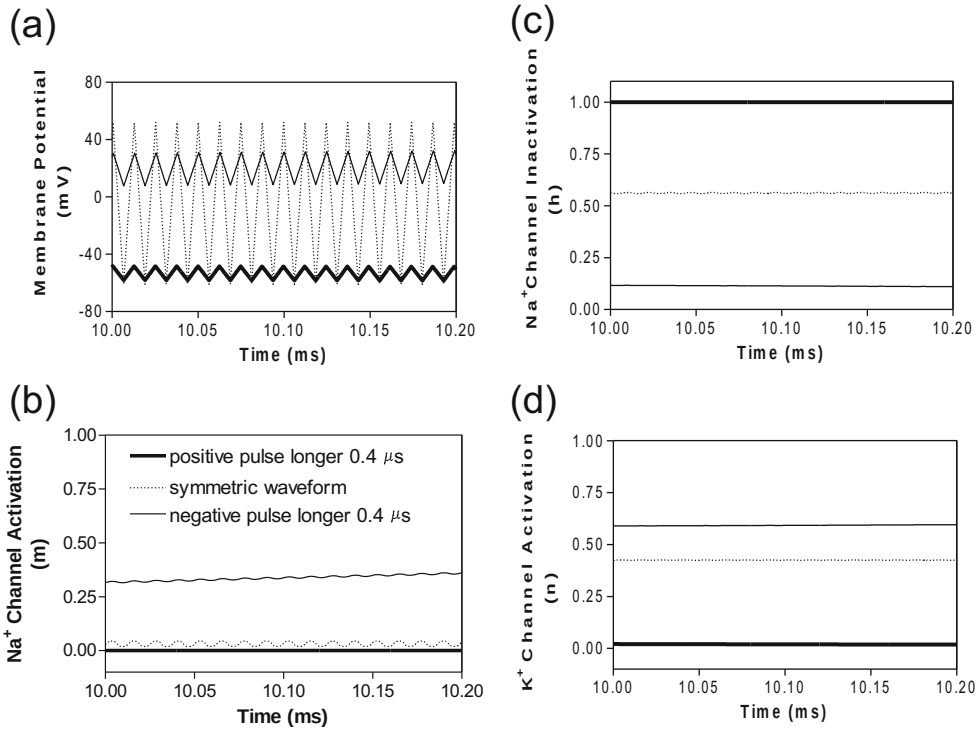

Fig. 7 The effects of non-symmetric waveforms on membrane potential and activation/inactivation of ion channels under the block electrode when stimulation frequency is 80 kHz. The legends in (**b**) indicate the types of waveform: symmetric and non-symmetric with a 0.4 μs difference in pulse width between the positive and negative pulses. (**a**) Change of membrane potentials, (**b**) Na^+ channel activation, (**c**) Na^+ channel inactivation, (**d**) K^+ channel activation. Stimulation waveforms: 80 kHz at block threshold intensities. *Axon diameter*: 2 μm. *Abscissa*: time in ms after the start of blocking stimulation

term application due to the accumulation of electrical charges that can cause irreversible chemical reactions. Electrical charges could accumulate more rapidly when the stimulation frequency is high (such as >10 kHz, see Fig. 7) even with a very small difference between the durations (such as 0.4 μs) of the positive and negative pulses of the non-symmetric waveform. Therefore, the results from this simulation study suggest that waveform symmetry needs to be carefully examined when the high-frequency (kHz) biphasic stimulation is to be used in clinical applications.

It has been proposed that high-frequency biphasic stimulation might induce block by producing a constant depolarization of the axonal membrane (Tanner 1962). However, the results in this simulation study show that a constant depolarization is only possible when the biphasic waveform is non-symmetric with a longer negative pulse than positive pulse (Fig. 7). If the biphasic waveform is symmetric (i.e., charge-balanced), it will not produce a constant depolarization. Instead, the axonal membrane will be alternately depolarized and hyperpolarized (Fig. 7a) causing a constant activation of the potassium channels (Fig. 4f and Fig. 7d). Therefore, it is possible that extracellular accumulation of potassium as proposed previously (Cattell and Gerard 1935) could contribute to the nerve conduction block. However, this blocking mechanism will depend on how fast the potassium can diffuse in the extracellular space. In this simulation study the extracellular accumulation of potassium is not considered but the nerve conduction block is still successfully simulated, indicating that the extracellular accumulation of potassium might not be a necessary factor in the block induced by high-frequency (kHz) biphasic stimulation.

The results in this study and our previous studies using an unmyelinated axonal model (Tai et al. 2005a, 2005b) indicate that the kinetics of ion channel gating play a major role in the conduction block induced by high-frequency biphasic stimulation. For example, the kinetics of the potassium channel are slow compared to the sodium channel. Therefore, opening and closing of the potassium channel cannot follow higher frequencies. Hence, it is constantly open as the frequency increases to the minimal blocking frequency of about 5 kHz (Fig. 4) (Tai et al. 2005a, 2005b), which results in a potassium current that opposes the sodium current induced by the arrival of the action potential and thereby elicits a conduction block (Fig. 4). This potassium channel mechanism causes the monotonic increase in block threshold as the stimulation frequency increases (Figs. 3–5) because a lower frequency can maintain a higher activation level of potassium channels (Tai et al. 2005a, 2005b). However, the blocking mechanisms identified in this simulation study still need to be confirmed by animal studies using patch-clamp techniques to examine the ion channel kinetics (Vasylyev and Waxman 2012). In addition, the responses of different subtypes of sodium and potassium channels to high-frequency biphasic stimulation also need to be investigated using patch-clamp techniques (Vasylyev and Waxman 2012) or by simulation studies using the kinetics of different subtypes of ion channels (Catterall 2012; Jan and Jan 2012; Waxman 2012).

It is worth noting that the block threshold calculated in this model study is much higher than the measurements from animal studies (Gaunt and Prochazka 2009; Joseph and Butera 2009, 2011). This is mainly due to the 1 mm distance between the block electrode and the axon (Fig. 1), while the electrode in animal studies is in close contact with the nerve. In addition, the extracellular medium resistivity (ρ_e=300 Ωcm) in this model study is probably higher than in animal studies, which can also cause a higher block threshold. Currently nerve conduction block by high-frequency biphasic stimulation has been shown both in small (<1 μm diameter) unmyelinated axons of rat vagus nerve (Wattaja et al. 2011) and in large (2–20 μm diameter) unmyelinated axons of Aplysia (Joseph and Butera 2009). Therefore, we chose an unmyelinated axon of 2 μm diameter as the representative in this study to investigate the effect of stimulation waveform asymmetry.

Nerve conduction block induced by high-frequency biphasic stimulation has many potential applications in both clinical medicine and basic neuroscience research (Camilleri et al. 2009; Gaunt and Prochazka 2009; Tai et al. 2004; Wattaja et al. 2011). The results about nerve block of umyelinated axons in this study are especially useful for clinical applications to block chronic pain (Cuellar et al. 2013; van Buyten et al. 2013). Understanding the mechanisms underlying this type of nerve block could improve the design of new stimulation waveforms (Roth 1994, 1995) and further promote clinical application (Leob 1989; Song et al. 2008). Simulation analysis using computer models provides a tool to reveal the possible blocking mechanisms and may help to design new animal experiments to further improve the nerve blocking method.

Acknowledgments This study is supported by DOD Spinal Cord Injury Program under grant W81XWH-11-1-0819 and by NIH under grant DK-068566.

Conflict of interest The authors declare that they have no conflict of interest.

References

Bowman, B. R., & McNeal, D. R. (1986). Response of single alpha motoneurons to high-frequency pulse train: firing behavior and conduction block phenomenon. *Applied Neurophysiology, 49*, 121–138.

Boyce WE, Diprima RC. Elementary differential equations and boundary value problems. *John Wiley & Sons Inc.* 6th ed: 436–457, 1997.

Camilleri, M., Toouli, J., Herrera, M. F., Kow, L., Pantoja, J. P., Billington, C. J., Tweden, K. S., Wilson, R. R., & Moody, F. G. (2009). Selection of electrical algorithms to treat obesity with intermittent vagal block using an implantable medical device. *Surgery for Obesity and Related Diseases, 5*, 224–230.

Cattell, M., & Gerard, R. W. (1935). The "inhibitory" effect of high-frequency stimulation and the excitation state of nerve. *Journal of Physiology, 83*, 407–415.

Catterall, W. A. (2012). Voltage-gated sodium channels at 60: structure, function and pathophysiology. *Journal of Physiology, 590*, 2577–2589.

Cuellar, J. M., Alataris, K., Walker, A., Yeomans, D. C., & Antognini, J. F. (2013). Effect of high-frequency alternating current on spinal afferent nociceptive transmission. *Neuromodulation, 16*, 318–327.

Frankenhaeuser, B. (1960). Quantitative description of sodium currents in myelinated nerve fibres of xenopus laevis. *Journal of Physiology (London), 151*, 491–501.

Gaunt, R. A., & Prochazka, A. (2009). Transcutaneously coupled, high-frequency electrical stimulation of the pudendal nerve blocks external urethral sphincter contractions. *Neurorehab. Neural Repair, 23*, 615–626.

Heinbockel JH. Numerical Methods for Scientific Computing. *Trafford Publishing*, 2005.

Hodgkin, A. L., & Huxley, A. F. (1952). A quantitative description of membrane current and its application to conduction and excitation in nerve. *Journal of Physiology (London), 117*, 500–544.

Jan, L. Y., & Jan, Y. N. (2012). Voltage-gated potassium channels and the diversity of electrical signalling. *Journal of Physiology (London), 590*, 2591–2599.

Joseph, L., & Butera, R. (2009). Unmyelinated aplysia nerves exhibit a nonmonotonic blocking response to high-frequency stimulation. *IEEE Trans Neural Syst Rehab Eng, 17*, 537–544.

Joseph, L., & Butera, R. (2011). High-frequency stimulation selectively blocks different types of fibers in frog sciatic nerve. *IEEE Trans Neural Syst Rehab Eng, 19*, 550–557.

Leob, G. E. (1989). Neural prosthetic interfaces with the nervous system. *Trends in Neurosciences, 12*, 195–201.

Rattay, F. (1989). Analysis of models for extracellular fiber stimulation. *IEEE Transactions on Biomedical Engineering, 36*, 676–682.

Rattay, F., & Aberham, M. (1993). Modeling axon membranes for functional electrical stimulation. *IEEE Transactions on Biomedical Engineering, 40*, 1201–1209.

Reboul, J., & Rosenblueth, A. (1939). The action of alternating currents upon the electrical excitability of nerve. *American Journal of Physiology, 125*, 205–215.

Rosenblueth, A., & Reboul, J. (1939). The blocking and deblocking effects of alternating currents on nerve. *American Journal of Physiology, 125*, 251–264.

Roth, B. J. (1994). Mechanisms for electrical stimulation of excitable tissue. *Critical Rev Biomed Eng, 22*, 253–305.

Roth, B. J. (1995). A mathematical model of make and break electrical stimulation of cardiac tissue by a unipolar anode or cathode. *IEEE Transactions on Biomedical Engineering, 42*, 1174–1184.

Schwarz, J. R., Reid, G., & Bostock, H. (1995). Action potentials and membrane currents in the human node of Ranvier. *Pflügers Archiv, 430*, 283–292.

Song, D., Raphael, G., Lan, N., & Loeb, G. E. (2008). Computationally efficient models of neuromuscular recruitment and mechanics. *Journal of Neural Engineering, 5*, 175–184.

Tai, C., Roppolo, J. R., & de Groat, W. C. (2004). Block of external urethral sphincter contraction by high frequency electrical stimulation of pudendal nerve. *Journal of Urology, 172*, 2069–2072.

Tai, C., de Groat, W. C., & Roppolo, J. R. (2005a). Simulation analysis of conduction block in unmyelinated axons induced by high-frequency biphasic electrical currents. *IEEE Transactions on Biomedical Engineering, 52*, 1323–1332.

Tai, C., de Groat, W. C., & Roppolo, J. R. (2005b). Simulation of nerve block by high-frequency sinusoidal electrical current based on the Hodgkin-Huxley model. *IEEE Trans Neural Syst Rehab Eng, 13*, 415–422.

Tai, C., Roppolo, J. R., & de Groat, W. C. (2009). Analysis of nerve conduction block induced by direct current. *Journal of Computational Neuroscience, 27*, 201–210.

Tai, C., Guo, D., Wang, J., Roppolo, J. R., & de Groat, W. C. (2011). Mechanism of conduction block in amphibian myelinated axon induced by biphasic electrical current at ultra-high frequency. *Journal of Computational Neuroscience, 31*, 615–623.

Tanner, J. A. (1962). Reversible blocking of nerve conduction by alternating-current excitation. *Nature, 195*, 712–713.

van Buyten, J. P., Al-Kaisy, A., Smet, I., Palmisani, S., & Smith, T. (2013). High-frequency spinal cord stimulation for the treatment of chronic back pain patients: results of a prospective multicenter European clinical study. *Neuromodulation, 16*, 59–65.

Vasylyev, D. V., & Waxman, S. G. (2012). Membrane properties and electrogenesis in the distal axons of small dorsal root ganglion neurons *in vitro*. *Journal of Neurophysiology, 108*, 729–740.

Wattaja, J. J., Tweden, K. S., & Honda, C. N. (2011). Effects of high frequency alternating current on axonal conduction through the vagus nerve. *Journal of Neural Engineering, 8*, 056031.

Waxman, S. G. (2012). Sodium channels, the electrogenisome and the electrogenistat: lessons and questions from the clinic. *Journal of Physiology (London), 590*, 2601–2612.

Medical & Biological Engineering & Computing

Conduction Block in Myelinated Axons Induced by High-Frequency (kHz) Non-symmetric Biphasic Stimulation

--Manuscript Draft--

Manuscript Number:	
Full Title:	Conduction Block in Myelinated Axons Induced by High-Frequency (kHz) Non-symmetric Biphasic Stimulation
Article Type:	Original article
Keywords:	nerve, block, simulation, high-frequency, model
Corresponding Author:	Changfeng Tai, Ph.D. University of Pittsburgh Pittsburgh, PA UNITED STATES
Corresponding Author Secondary Information:	
Corresponding Author's Institution:	University of Pittsburgh
Corresponding Author's Secondary Institution:	
First Author:	Shouguo Zhao
First Author Secondary Information:	
Order of Authors:	Shouguo Zhao
	Guangning Yang
	Jicheng Wang
	James R Roppolo
	William C de Groat
	Changfeng Tai, Ph.D.
Order of Authors Secondary Information:	
Abstract:	This study used the Frankenhaeuser-Huxley axonal model to analyze the effects of non-symmetric waveforms on conduction block of myelinated axons induced by high-frequency (10-300 kHz) biphasic electrical stimulation. The results predict a monotonic relationship between block threshold and stimulation frequency for symmetric waveform and a non-monotonic relationship for non-symmetric waveforms. The symmetric waveform causes conduction block by constantly activating both sodium and potassium channels at frequencies of 20-300 kHz, while the non-symmetric waveforms share the same blocking mechanism from 20 kHz up to the peak threshold frequency. At the frequencies above the peak threshold frequency the non-symmetric waveforms block axonal conduction by either hyperpolarizing the membrane (if the positive pulse is longer) or depolarizing the membrane (if the negative pulse is longer). This simulation study further increases our understanding of conduction block in myelinated axons induced by high-frequency biphasic electrical stimulation, and can guide future animal experiments as well as optimize stimulation parameters that might be used for electrically induced nerve block in clinical applications.
Suggested Reviewers:	Frank Rattay, PhD Professor, Technische Universitat Wien frank.rattay@tuwien.ac.at Dr. Rattay is an expert in electrical nerve stimulation.
	Bradley J Roth, PhD Professor, Oakland University roth@oakland.edu Dr. Roth is an expert on model analysis of electrical nerve stimulation

	Christopher N Honda, PhD Professor, University of Minnesota cnhonda@umn.edu Dr. Honda is an expert on high-frequency nerve block.
	Arthor Prochazka, PhD Professor, University of Alberta arthur.prochazka@ualberta.ca Dr. Prochazka is an expert on high-frequency nerve block.
	Gerald E Leob, PhD Professor, University of Southern California gloeb@usc.edu Dr. Leob is an expert on electrical nerve stimulation.

Conduction Block in Myelinated Axons Induced by High-Frequency (kHz) Non-symmetric Biphasic Stimulation

Shouguo Zhao [1,2], Guangning Yang [1,2], Jicheng Wang [1]
James R. Roppolo [3], William C. de Groat [3], Changfeng Tai [1,3]

[1] Department of Urology, University of Pittsburgh, Pittsburgh, PA
[2] Department of Biomedical Engineering, Beijing Jiaotong University, P.R. China
[3] Department of Pharmacology and Chemical Biology, University of Pittsburgh, PA

Total number of words: 5302
Number of words in abstract: 166
Number of figures: 7
Number of table: 0

Correspondence to:

Changfeng Tai, Ph.D.
Department of Urology
University of Pittsburgh
700 Kaufmann Building
Pittsburgh, PA15213, USA
Phone: 412-692-4142
Fax: 412-692-4380
Email: cftai@pitt.edu

ABSTRACT

This study used the Frankenhaeuser–Huxley axonal model to analyze the effects of non-symmetric waveforms on conduction block of myelinated axons induced by high-frequency (10-300 kHz) biphasic electrical stimulation. The results predict a monotonic relationship between block threshold and stimulation frequency for symmetric waveform and a non-monotonic relationship for non-symmetric waveforms. The symmetric waveform causes conduction block by constantly activating both sodium and potassium channels at frequencies of 20-300 kHz, while the non-symmetric waveforms share the same blocking mechanism from 20 kHz up to the peak threshold frequency. At the frequencies above the peak threshold frequency the non-symmetric waveforms block axonal conduction by either hyperpolarizing the membrane (if the positive pulse is longer) or depolarizing the membrane (if the negative pulse is longer). This simulation study further increases our understanding of conduction block in myelinated axons induced by high-frequency biphasic electrical stimulation, and can guide future animal experiments as well as optimize stimulation parameters that might be used for electrically induced nerve block in clinical applications.

Key Words: nerve, block, simulation, high-frequency, model.

I. INTRODUCTION

High-frequency (kHz) biphasic electrical stimulation has recently been investigated extensively due to its potential clinical application to block peripheral nerve conduction [7, 16, 29, 32]. Although the mechanisms underlying this nerve block are still unclear [1, 33], previous animal studies of myelinated axons have shown that the block threshold intensity monotonically increases as the stimulation frequency increases up to 50 kHz [2, 10, 13]. Our recent computer simulation study of large (10-20 μm diameter) myelinated axons further indicates a monotonic increase in block threshold up to 100 kHz [28]. However, recent animal studies [12, 13] revealed that this monotonic relationship does not hold in small unmyelinated axons where the block threshold current only increases with frequency up to about 12-15 kHz and then decreases as the stimulation frequency further increases. This discovery raises the question about what causes the difference of high-frequency block between myelinated and unmyelinated axons. Answering this question will help to understand the mechanisms underlying nerve conduction block induced by high-frequency biphasic electrical stimulation.

Due to the difficulties in recording ion channel activity in axonal nodes during high-frequency biphasic electrical stimulation, the mechanisms of nerve block have been mainly investigated by modeling and computer simulation. These simulation studies have been successful in reproducing many phenomena observed in animal experiments, for example the minimal block frequency, the influence of temperature on minimal block frequency, and the relationship between axon diameter and block threshold [1, 3, 15, 26,

27, 31, 28, 33]. The newly discovered non-monotonic relationship between block threshold and stimulation frequency was also successfully reproduced in our recent simulation study of unmyelinated axons [34]. This study indicates that the monotonic decrease in block threshold in unmyelinated axons at frequencies above 15 kHz is probably caused by a slightly (<1 μs in pulse width) non-symmetric waveform of the high-frequency stimulation, which constantly hyperpolarizes or depolarizes the axon as the frequency increases above 15 kHz.

Although our previous simulation study [28] of large (10-20 μm diameter) myelinated axons showed a monotonic increase in block threshold with stimulation frequency up to 100 kHz, the effect of a non-symmetric waveform on the block threshold was not investigated. Based on our recent simulation study of unmyelinated axons [34], we hypothesize that a non-symmetric waveform can also cause a decrease in block threshold as the frequency increases above a certain level in myelinated axons. It is known that the ion channel kinetics of myelinated axons is faster than unmyelinated axons [8, 11]. Therefore, it is reasonable to expect that a higher frequency would be required in myelinated axons than in unmyelinated axons in order to cause a constant hyperpolarization/depolarization by a non-symmetric stimulation waveform.

In this study we employed a myelinated axonal model (Frankenhaeuser–Huxley model) [9, 18, 19] to simulate high-frequency nerve block and to determine: (1) if a decrease in block threshold can be produced by high-frequency stimulation of a non-symmetric waveform; (2) At what frequency the decrease in block threshold can

occur; (3) what happens to the sodium and potassium channels when this decrease in block threshold occurs. Understanding the mechanisms of nerve conduction block induced by high-frequency biphasic electrical stimulation will be very useful in developing new nerve blocking methods, optimizing stimulation parameters, or improving the efficacy of blocking nerves in different clinical applications.

II. METHODS

The myelinated axon model used in our study is showed in Fig.1. A 40 mm long, myelinated axon is modeled with the inter-node length $\Delta x=100d$ (d is the myelinated axon diameter). Each node (nodal length: L=2.5 um) is modeled by a membrane capacitance (C_m) and a variable membrane resistance (R_m). The ionic currents passing through the variable membrane resistance are described by Frankenhaeuser–Huxley equations [9, 18, 19]. Two monopolar point electrodes (with the indifferent electrode at infinity) are placed at 1 mm distance from the axon. One is the block electrode at the 30 mm location along the axon, where the high frequency biphasic current is delivered (Fig.1). The other is the test electrode at 10 mm location, which delivers a uniphasic single pulse (pulse width 0.1 ms and intensity 0.5-2mA) to evoke an action potential and test whether this action potential can propagate through the site of the block electrode. The test electrode is always the cathode (negative pulse), and the block electrode delivers biphasic pulses with the cathodal phase first.

We assume that the myelinated axon is in an infinite homogeneous medium

(resistivity $\rho_e = 300\ \Omega$cm). After neglecting the small influence of the axon in the homogeneous medium, the extracellular potential $V_{e,n}$ at the nth node along the axon can be described by:

$$V_{e,n} = \frac{\rho_e}{4\pi}\left[\frac{I_{block}(t)}{\sqrt{(n\Delta x - x_0)^2 + z_0^2}} + \frac{I_{test}(t)}{\sqrt{(n\Delta x - x_1)^2 + z_1^2}}\right]$$

where $I_{block}(t)$ is the high-frequency biphasic current delivered to the block electrode (at location x_0 = 30 mm, z_0 = 1 mm); $I_{test}(t)$ is the single test pulse delivered to the test electrode (at location x_1 = 10 mm, z_1 = 1 mm).

The change of the membrane potential V_n at the nth node of the myelinated axon is described by:

$$\frac{dV_n}{dt} = \left[\frac{d\Delta x}{4\rho_i L}\left(\frac{V_{n-1} - 2V_n + V_{n+1}}{\Delta x^2} + \frac{V_{e,n-1} - 2V_{e,n} + V_{e,n+1}}{\Delta x^2}\right) - I_{i,n}\right] / c_m$$

where V_n=$V_{a,n}$-$V_{e,n}$-V_{rest}; $V_{a,n}$ is the intracellular potential at the nth node; $V_{e,n}$ is the extracellular potential at the nth node; V_{rest} is the resting membrane potential; ρ_i is the resistivity of axoplasm (100 Ωcm); c_m is the capacity of the membrane (2 uF/cm^2); $I_{i,n}$ is the ionic current density at the nth node described by Frankenhaeuser–Huxley equations [9, 18, 19] (see appendix).

The myelinated axon model was solved by Runge-Kutta method [5] with a time step of 0.5 μsec. The simulation was always started at initial condition $V_n = 0$. The membrane potentials at the two end nodes of the modeled axon were always equal to the membrane potentials of their closest neighbors, which implemented sealed boundary conditions (no longitudinal currents) at the two ends of the modeled axon. The block threshold current

was determined with a resolution of 0.1 mA. The simulation was performed on a myelinated axon of diameter 2 μm with the temperature parameter set at 37 °C.

III. RESULTS

A. Conduction block by symmetric and non-symmetric biphasic stimulation waveforms

Fig.2 shows that in a myelinated axon the Frankenhaeuser–Huxley model can successfully simulate the conduction block induced by high-frequency (30 kHz) symmetric biphasic stimulation. In Fig.2 (a) the 30 kHz blocking stimulation (10 mA) generates an initial action potential propagating in both directions. At 5 ms after the start of blocking stimulation, the test electrode delivers a single pulse that generates another action potential propagating toward the block electrode [see the white arrow in Fig.2 (a)]. This action potential fails to propagate through the block electrode due to the presence of the high-frequency biphasic stimulation. However, at a lower stimulation intensity [9.9 mA in Fig.2 (b)] the 30 kHz stimulation does not block nerve conduction and the action potential propagates through the site of the block electrode. Similar conduction block was also successfully simulated for non-symmetric biphasic stimulation waveforms where either the positive pulse is 1 or 2 μs longer than the negative pulse, or the reverse of this condition.

Fig.3 shows the intensity thresholds for inducing conduction block at different frequencies (10-300 kHz) for a myelinated axon of 2 μm diameter. For the symmetric biphasic waveform [Fig.3 (a)], the block threshold monotonically increases as the

stimulation frequency increases. However, if the biphasic waveform is not symmetric [Fig.3 (b) and (c)], the block threshold increases initially and then decreases with increasing stimulation frequency, showing a non-monotonic relationship between block threshold and stimulation frequency. If the positive pulse is 1-2 μs longer than the negative pulse, the block threshold peaks between 60 kHz and 80 kHz [Fig.3 (b)]. However, if the negative pulse is 1-2 μs longer than the positive pulse, the block threshold peaks at a frequency of 40-70 kHz [Fig.3 (c)].

B. Mechanisms of the conduction block by symmetric and non-symmetric waveforms

Fig.4 shows the same simulation as in Fig.2 (a) for the 30 kHz symmetric biphasic waveform but including more detailed information for the 4 consecutive axon nodes at distances of 0-1.2 mm from the block electrode (the location at 30.0 mm is under the block electrode). Figs.4 (a)-(c) show the action potential, sodium current, and potassium current at different locations approaching the block electrode. This action potential propagation is disrupted at the location (30.0 mm) under the block electrode, where axon membrane potential is oscillating with large pulsed sodium and potassium currents. The behavior of the membrane potential and ionic currents can be further explained by the activation/inactivation of the sodium and potassium channels as shown in Fig.4 (d)-(f). As the action potential propagates toward the block electrode, the activation (m) of sodium channels also changes at each location and becomes almost constant (about 0.4) at the location under the block electrode [Fig.4 (d)]. Meanwhile, the inactivation of

sodium channels is kept at a low value (about 0.1) under the block electrode [Fig.4 (e)]. The combination of activation and inactivation of sodium channels [Fig.4 (d)-(e)] determines that the sodium channel becomes constantly open and results in a pulsed inward sodium current under the block electrode [Fig.4 (b)]. Therefore, the sodium channels are never completely blocked when conduction block occurs. However, the change in potassium activation (n) induced by the action potential becomes smaller under the block electrode [Fig.4 (f)] because potassium channels are constantly activated at this location, resulting in a large pulsed outward potassium current [Fig.4 (c)]. This large outward potassium current opposes the large inward sodium current, causing the membrane under the block electrode to become un-excitable leading to the block of action potential conduction. This blocking mechanism is observed for the symmetric waveform in the frequency range of 20-300 kHz [Fig.3 (a)]. Our previous simulation study (Zhang et al, 2006) has shown that at frequency range of 5-10 kHz the potassium channel but not the sodium channel is constantly open, which causes the conduction block.

Similar blocking mechanisms are also observed for non-symmetric waveforms at frequencies below the peak block threshold frequency [Fig.3 (b) and (c)]. Fig.5 shows that at 30 kHz the symmetric and non-symmetric waveforms produce almost the same oscillating membrane potential [Fig.5 (a)] and very similar ion channel activation/inactivation [Fig.5 (b)-(d)]. It is also worth noting that the 1 μs difference between the positive and negative pulses does not change potassium channel activation

[Fig.5 (d)].

In order to understand why the block threshold with the non-symmetric waveform starts to decrease at frequencies above the peak block threshold frequency [Fig.3 (b) and (c)], we further investigated the changes in membrane potential, ionic currents, and activation/inactivation of the sodium and potassium channels at frequencies between 50-300 kHz. Fig.6 shows the conduction block by the 120 kHz non-symmetric waveform with a positive pulse 1 μs longer than the negative pulse. Action potential propagation is completely abolished at the location (30.0 mm) under the block electrode, where the axon membrane is hyperpolarized to about -120 mV [(-50 mV) + (-70 mV resting potential), see Fig.6 (a)]. This hyperpolarization is caused by the accumulative effect of 1 μs longer positive pulses, which significantly deactivates both sodium and potassium channels [Fig.6 (d) and (f)], dramatically reduces sodium current [Fig.6 (b)], and eliminates potassium currents [Fig.6(c)] thereby resulting in a conduction block at the location (30.0 mm) under the block electrode. Meanwhile, inactivation (h) of sodium channels is minimal (≈ 1) under the block electrode [Fig.6 (e)]. The same blocking mechanism is observed at frequencies greater than 60-80 kHz for non-symmetric waveforms with the positive pulse 1-2 μs longer than the negative pulse [Fig.3 (b)]. As the frequency is increased, the accumulation of positive charges due to the longer positive pulses is greater and produces the same level of hyperpolarization at a lower stimulus intensity. Therefore, the block threshold decreases as the frequency increases [Fig.3 (b)].

However, if the non-symmetric waveform has a longer negative pulse (1-2 μs longer),

it generates a constant depolarization under the block electrode instead of a hyperpolarization when stimulation frequency increases higher than 40-70 kHz [Fig.3(c)]. The non-symmetric waveform with the negative pulse 1 μs longer than the positive pulse produces a constant depolarization about 20 mV at the blocking electrode [Fig.7 (a)], which causes a significant inactivation of sodium channels [Fig.7 (e)] resulting in very small sodium current [Fig.7(b)] during stimulation thereby a conduction block. The accumulation of negative charges due to longer negative pulses is greater for a higher frequency, thereby producing the same level of depolarization at a lower block threshold [Fig.3 (c)]. It is worth noting that symmetric waveform can induce pulsed inward sodium currents during the stimulation [Fig.4 (b)], while non-symmetric waveforms can not induce pulsed inward sodium currents either due to sodium channel deactivation by a constant hyperpolarization [Fig.6 (a) and (b)] or sodium channel inactivation by a constant depolarization [Fig.7 (a) and (b)].

IV. DISCUSSION

This study using the Frankenhaeuser–Huxley axonal model successfully simulated nerve conduction block in myelinated axons during high-frequency (10-300 kHz) biphasic electrical stimulation (Fig.2). It predicted a monotonic relationship between block threshold and stimulation frequency for a symmetric waveform [Fig.3(a)] and a non-monotonic relationship for non-symmetric waveforms [Fig.3 (b) and (c)]. The results reveal that the symmetric waveform causes conduction block by constantly activating

both sodium and potassium channels (Fig.4) at frequencies of 20-300 kHz, while the non-symmetric waveforms share the same blocking mechanism as the symmetric waveform from 20 kHz up to the peak threshold frequency (Fig.5). However, at the frequencies above the peak threshold frequency the non-symmetric waveforms cause either hyperpolarization (Fig.6, positive pulse longer) or depolarization (Fig.7, negative pulse longer) and thereby conduction block. These results have significant implications for future animal experiments and for clinical applications of the nerve block methods.

This study predicts in myelinated axons that the block threshold will reach a peak and then gradually decrease when the stimulation frequency increases above approximately 50 kHz for non-symmetric waveforms (Fig.3). A similar non-monotonic block response has been observed in unmyelinated axons of sea slugs and frogs with the block threshold peaks ranging between 12-15 kHz [12, 13] and in our recent simulation study of unmyelinated axons [34]. Previous animal studies that examined block of myelinated axons [2, 10, 13] only tested frequencies up to 50 kHz and showed a monotonic increase in block threshold as the frequency increases same as our simulation results at frequencies below 50 kHz (Fig.3). The results in this simulation study further suggest that additional animal studies should be conducted to examine higher frequencies (50-300 kHz) in myelinated axons and to confirm the different block responses for symmetric and non-symmetric waveforms.

This study emphasizes the importance of using a symmetric biphasic waveform for high-frequency nerve block of myelinated axons, especially when the frequency is above

50 kHz. The small difference of 1 μs between the positive and negative pulses (less than 19% difference in pulse width) may not make a difference in nerve block at frequencies below 50 kHz (Figs.4-5), but can make a significant difference at frequencies of 50-300 kHz (19-50% difference in pulse width) causing a decrease in block threshold [Fig.3 (b) and (c)] by constantly hyperpolarizing (Fig.6) or depolarizing (Fig.7) the axonal membrane. The net effect of the non-symmetric waveform on axonal conduction is equivalent to that caused by direct current (DC). The non-symmetric waveform with a longer positive (or negative) pulse blocks nerve conduction by inducing a constant hyperpolarization (or depolarization) of the axon membrane, which is similar to the nerve conduction block induced by an anodal (or cathodal) DC [31]. It is known that DC can damage nerves during long-term application due to the accumulation of electrical charges that can cause irreversible chemical reactions. Electrical charges could accumulate more rapidly when the stimulation frequency is high (such as >50 kHz, see Figs.6-7) even with a very small difference (such as 1 μs) between the durations of the positive and negative pulses of the non-symmetric waveform. Therefore, the results from this simulation study suggest that waveform symmetry needs to be carefully examined when the high-frequency biphasic stimulation is to be used in clinical applications at a frequency greater than 50 kHz.

This study and our previous studies [28, 33] using the myelinated axonal model (Frankenhaeuser–Huxley model) have revealed several different blocking mechanisms for different stimulation frequencies. These studies indicate that the kinetics of ion

channel gating play a major role in the conduction block induced by high-frequency biphasic electrical stimulation. The kinetics of the potassium channel are slow compared to the sodium channel [8, 11], and therefore this channel does not follow high-frequencies very well. Thus, the potassium channel becomes constantly open as the frequency increases to the minimal blocking frequency of about 4 kHz [15, 33]. This potassium channel opening mechanism governs the monotonic increase in block threshold at the frequency range of 4-10 kHz [15, 33]. As the frequency increases further (>20 kHz), it saturates the faster kinetics of the sodium channel causing the channel to be constantly open [Fig.4(d) and Fig.5(b)] and lose its ability to regulate sodium current during action potential generation [Fig.4(b)] resulting in a conduction block [Fig.4(a)] (also see Tai et al. 2011). This sodium channel opening mechanism governs the monotonic increase in block threshold from 20 kHz to 300 kHz for a symmetric waveform [Fig.3(a)], but only to the frequency at which the block threshold peaks for non-symmetric waveforms [Fig.3 (b) and (c)]. Further increasing the stimulation frequency above the peak threshold frequency will cause either hyperpolarization (Fig.6) or depolarization (Fig.7) by the non-symmetric waveforms, which is responsible for the monotonic decrease in block threshold (Fig.3). The ion channel kinetic mechanisms are supported by evidence from animal studies indicating that the minimal blocking frequency is about 4 kHz [4, 20, 22] and that the block threshold monotonically increases in the frequency range of 4-50 kHz [2, 10, 13]. However, these ion channel kinetic mechanisms revealed by model analysis still need to be confirmed directly by animal studies in the future.

This study used the Frankenhaeuser–Huxley axonal model that has fixed parameters independent of stimulation frequency and is suitable for the temperature range of 20-37 °C [9, 18, 19]. The stimulation amplitudes used in this study are well within the model's range, since they never cause the simulation to overflow and steady state responses were always achieved (Figs.2-7). Although the model parameters were obtained from voltage clamp experiments (low frequency response), the Frankenhaeuser–Huxley axonal model has been used successfully to simulate axonal responses for stimulation up to 50 kHz [6, 17, 21]. Our previous studies using the Frankenhaeuser–Huxley axonal model [28, 31, 33] have also successfully simulated high-frequency nerve block up to 100 kHz and reproduced many phenomena observed in animal experiments, for example the minimal block frequency, the influence of temperature on minimal block frequency, and the relationship between axon diameter and block threshold. However, whether the simulation results obtained in this study for stimulation frequency up to 300 kHz predict the real axonal block effect can only be confirmed by animal studies using myelinated nerve. This simulation study provides the rationale for and the expected results for future animal studies.

Nerve conduction block induced by high-frequency biphasic electrical stimulation has many potential applications in both clinical medicine and basic neuroscience research [7, 16, 29, 32]. Understanding the mechanisms underlying this type of nerve block could improve the design of new stimulation waveforms [23, 24] and further promote clinical application [14, 25]. Simulation analysis using computer models provides a tool to reveal

the possible blocking mechanisms and may help to design new animal experiments to further improve the nerve blocking method.

APPENDIX

The ionic current density $I_{i,n}$ at n^{th} node is described as:

$$I_{i,n} = i_{Na} + i_K + i_P + i_L$$

$$i_{Na} = P_{Na} m^2 h \frac{EF^2}{RT} \frac{[Na]_0 - [Na]_i e^{EF/RT}}{1 - e^{EF/RT}}$$

$$i_K = P_K n^2 \frac{EF^2}{RT} \frac{[K]_0 - [K]_i e^{EF/RT}}{1 - e^{EF/RT}}$$

$$i_P = P_P p^2 \frac{EF^2}{RT} \frac{[Na]_0 - [Na]_i e^{EF/RT}}{1 - e^{EF/RT}}$$

$$i_L = g_L \left(V_n - V_L \right)$$

$$E = V_n + V_{rest}$$

where P_{Na} (0.008 cm/s), P_K (0.0012 cm/s) and P_P (0.00054 cm/s) are the ionic permeabilities for sodium, potassium and nonspecific currents respectively; g_L (30.3 $k\Omega^{-1}$ cm^{-2}) is the maximum conductance for leakage current. V_L (0.026 mV) is reduced equilibrium membrane potential for leakage ions, in which the resting membrane potential V_{rest} (-70 mV) has been subtracted. $[Na]_i$ (13.7 mmole/l) and $[Na]_o$ (114.5 mmole/l) are sodium concentrations inside and outside the axon membrane. $[K]_i$ (120 mmole/l) and $[K]_o$ (2.5 mmole/l) are potassium concentrations inside and outside the axon membrane. F (96485 c/mole) is Faraday constant. R (8314.4 mJ/K/mole) is gas constant.

m, h, n and p are dimensionless variables, whose values always change between 0 and 1. m and h represent activation and inactivation of sodium channels, whereas n represents activation of potassium channels. p represents activation of non-specific ion channels. The evolution equations for m, h, n and p are the following:

$$dm/dt = [\alpha_m(1-m) - \beta_m m]k_m$$

$$dh/dt = [\alpha_h(1-h) - \beta_h h]k$$

$$dn/dt = [\alpha_n(1-n) - \beta_n n]k$$

$$dp/dt = [\alpha_p(1-p) - \beta_p p]k$$

and

$$\alpha_m = \frac{0.36(V_n - 22)}{1 - \exp(\frac{22 - V_n}{3})}$$

$$\beta_m = \frac{0.4(13 - V_n)}{1 - \exp(\frac{V_n - 13}{20})}$$

$$\alpha_h = -\frac{0.1(V_n + 10)}{1 - \exp(\frac{V_n + 10}{6})}$$

$$\beta_h = \frac{4.5}{1 + \exp(\frac{45 - V_n}{10})}$$

$$\alpha_n = \frac{0.02(V_n - 35)}{1 - \exp(\frac{35 - V_n}{10})}$$

$$\beta_n = \frac{0.05(10 - V_n)}{1 - \exp(\frac{V_n - 10}{10})}$$

$$\alpha_p = \frac{0.006(V_n - 40)}{1 - \exp(\frac{40 - V_n}{10})}$$

$$\beta_p = -\frac{0.09(V_n + 25)}{1 - \exp(\frac{V_n + 25}{20})}$$

$$k_m = 1.8^{(T-293)/10}$$

$$k = 3^{(T-293)/10}$$

where T is the temperature in °Kelvin, which is 310 °Kelvin or 37°C in this study. The initial values for m, h, n and p (when $V_n = 0$ mV) are 0.0005, 0.0268, 0.8249 and 0.0049 respectively.

ACKNOWLEDGEMENTS

This study is supported by the NIH under grants DK-068566, DK-090006, DK-091253, and by DOD under grant W81XWH-11-1-0819.

REFERENCES

1. Ackermann DM, Bhadra N, Gerges M, Thomas PJ (2011) Dynamics and sensitivity analysis of high-frequency conduction block. *Journal of Neural Engineering* 8, 1-14.
2. Bhadra, N, Kilgore K (2005) High-frequency electrical conduction block of mammalian peripheral motor nerve. *Muscle Nerve* 32, 782–790.
3. Bhadra N, Lahowetz E, Foldes S, Kilgore K (2007). Simulation of high-frequency sinusoidal electrical block of mammalian myelinated axons. *Journal of Computational Neuroscience* 22, 313-326.
4. Bowman BR, McNeal DR (1986) Response of single alpha motoneurons to

high-frequency pulse train: Firing behavior and conduction block phenomenon. *Applied Neurophysiology* 49, 121–138.

5. Boyce WE, Diprima RC (1997) Elementary Differential Equations and Boundary Value Problems. John Wiley & Sons, Inc., 6th ed., pp.436-457.
6. Bromm B (1975) Spike frequency of the nodal membrane generated by high-frequency alternating current. *Pfluger Archive* 353, 1–19.
7. Camilleri M, Toouli J, Herrera MF, Kow L, Pantoja JP, Billington CJ, Tweden KS, Wilson RR, Moody FG (2009) Selection of electrical algorithms to treat obesity with intermittent vagal block using an implantable medical device. Surgery *for Obesity and Related Diseases* 5, 224-230.
8. Frankenhaeuser B (1960) Quantitative description of sodium currents in myelinated nerve fibres of xenopus laevis. *Journal of Physiology (Lond.)* 151, 491-501.
9. Frankenhaeuser B, Huxley AF (1964) The action potential in the myelinated nerve fibre of Xenopus Laevis as computed on the basis of voltage clamp data. *Journal of Physiology (Lond.)* 171, 302-315.
10. Graunt RA, Prochazka A (2009) Transcutaneously coupled, high-frequency electrical stimulation of the pudendal nerve blocks external urethral sphincter contractions. *Neurorehabiliation and Neural Repair* 23, 615-626.
11. Hodgkin AL, Huxley AF (1952) A quantitative description of membrane current and its application to conduction and excitation in nerve. *Journal of Physiology (Lond.)* 117, 500–544.

12. Joseph L, Butera R (2009) Unmyelinated aplysia nerves exhibit a nonmonotonic blocking response to high-frequency stimulation. *IEEE Transactions on Neural System and Rehabilitation Engineering* 17, 537–544.
13. Joseph L, Butera R (2011) High-frequency stimulation selectively blocks different types of fibers in frog sciatic nerve. *IEEE Transactions on Neural System and Rehabilitation Engineering* 19, 550–557.
14. Leob GE (1989) Neural prosthetic interfaces with the nervous system," *Trends on Neuroscience* 12, 195-201.
15. Liu H, Roppolo JR, de Groat WC, Tai C (2009) The Role of slow potassium current in nerve conduction block induced by high-frequency biphasic electrical current. *IEEE Transactions on Biomedical Engineering* 56, 137-146.
16. Nashold BS, Goldner JL, Mullen JB, Bright DS (1982) Long-term pain control by direct peripheral-nerve stimulation. *Journal of Bone Joint Surgery* 64A, 1–10.
17. Rattay F (1986) High frequency electrostimulation of excitable cells. Journal of Theoretical Biology 123, 45–54.
18. Rattay F (1989) Analysis of models for extracellular fiber stimulation," *IEEE Transactions on Biomedical Engineering* 36, 676-682.
19. Rattay F, Aberham M (1993) Modeling axon membranes for functional electrical stimulation. *IEEE Transactions on Biomedical Engineering* 40, 1201-1209.
20. Reboul J, Rosenblueth A (1939) The action of alternating currents upon the electrical excitability of nerve. *American Journal of Physiology* 125, 205–215.

21. Reilly JP, Freeman VT, Larkin WD (1985) Sensory effects of transient electrical stimulation – evaluation with a neuroelectric model. *IEEE Transactions on Biomedical Engineering* 32, 1001–1011.

22. Rosenblueth A, Reboul J (1939) The blocking and deblocking effects of alternating currents on nerve. *American Journal of Physiology* 125, 251–264.

23. Roth BJ (1994) Mechanisms for electrical stimulation of excitable tissue," *Critical Review on Biomedical Engineering* 22, 253-305.

24. Roth BJ (1995) A mathematical model of make and break electrical stimulation of cardiac tissue by a unipolar anode or cathode. *IEEE Transactions on Biomedical Engineering* 42, 1174-1184.

25. Song D, Raphael G, Lan N, Loeb GE (2008) Computationally efficient models of neuromuscular recruitment and mechanics. *Journal of Neural Engineering* 5, 175-184.

26. Tai C, de Groat WC, Roppolo JR (2005) Simulation analysis of conduction block in unmyelinated axons induced by high-frequency biphasic electrical currents. *IEEE Transactions on Biomedical Engineering* 52, 1323–1332.

27. Tai C, de Groat WC, Roppolo JR (2005) Simulation of nerve block by high-frequency sinusoidal electrical current based on the Hodgkin-Huxley model. *IEEE Transactions on Neural System and Rehabilitation Engineering* 13, 415-422.

28. Tai C, Guo D, Wang J, Roppolo JR, de Groat WC (2011) Mechanism of conduction block in amphibian myelinated axon induced by biphasic electrical current at

ultra-high frequency. *Journal of Computational Neuroscience* 31, 615-623.

29. Tai C, Roppolo JR, de Groat WC (2004) Block of external urethral sphincter contraction by high frequency electrical stimulation of pudendal nerve. *Journal of Urology* 172, 2069–2072.

30. Tai C, Roppolo JR, de Groat WC (2009). Analysis of nerve conduction block induced by direct current. *Journal of Computational Neuroscience,* 27: 201-210.

31. Tai C, Wang J, Roppolo JR, de Groat WC (2009) Relationship between temperature and stimulation frequency in conduction block of amphibian myelinated axon. *Journal of Computational Neuroscience* 26, 331-338.

32. Wattaja JJ, Tweden KS, Honda CN (2011) Effects of high frequency alternating current on axonal conduction through the vagus nerve. *Journal of Neural Engineering* 8, 056031, 2011.

33. Zhang X, Roppolo JR, de Groat WC, Tai C (2006) Mechanism of nerve conduction block induced by high- frequency biphasic electrical currents. *IEEE Transactions on Biomedical Engineering* 53, 2445–2454.

34. Zhao S, Yang G, Wang J, Roppolo .R, de Groat WC, Tai C (2014) Effect of non-symmetric waveform on conduction block induced by high-frequency (kHz) biphasic stimulation in unmyelinated axon. *Journal of Computational Neuroscience* 37: 377-386.

FIGURE CAPTIONS

Fig.1. Myelinated axonal model used to simulate conduction block induced by

high-frequency biphasic electrical current. The inter-node length $\Delta x = 100d$; d is the axon diameter. L is the nodal length. Each node is modeled by a resistance-capacitance circuit based on the FH model. R_a: inter-nodal axoplasmic resistance; R_m: nodal membrane resistance; C_m: nodal membrane capacitance; $V_{a,n}$: intracellular potential at the nth node; $V_{e,n}$: extracellular potential at the nth node.

Fig.2. Blocking the propagation of action potentials along a myelinated axon by high-frequency symmetric biphasic stimulation. High-frequency (30 kHz) stimulation is continuously delivered at the block electrode, which initiated an initial action potential in (a) and two initial action potentials in (b). Another action potential is initiated via the test electrode at 5 ms after starting the high-frequency stimulation, and propagates towards both ends of the axon. The 30 kHz stimulation blocks nerve conduction at the intensity of 10 mA (a), but not at 9.9 mA (b). The short arrows mark the locations of test and block electrodes along the axon. The white arrow indicates propagation of the action potential to the location of the 30 kHz blocking stimulation. Axon diameter: 2 μm.

Fig.3. The threshold intensity to block nerve conduction changes with the stimulation frequency. (a). For the symmetric waveform, the block threshold monotonically increases as the frequency increases. (b). If the positive pulse is longer (1 or 2 μs), the block threshold peaks at 60-80 kHz and then gradually decreases as the frequency increases. (c). If the negative pulse is longer (1 or 2 μs), the block threshold peaks at 40-70 kHz. Axon diameter: 2 μm.

Fig.4. The changes in membrane potential, ionic currents and activation/inactivation of

ion channels near the block electrode when conduction block occurs as shown in Fig.2 (a) during stimulation with a symmetric waveform. The legends in (e) indicate the locations along the axon. The location at 30.0 mm is under the block electrode. (a) Change in membrane potential, (b) Na^+ current, (c) K^+ current, (d) Na^+ channel activation, (e) Na^+ channel inactivation, (f) K^+ channel activation. Symmetric stimulation waveform: 30 kHz, 10 mA. Axon diameter: 2 μm. Abscissa: time in ms after the start of blocking stimulation.

Fig.5. The effects of non-symmetric waveforms on membrane potential and activation/inactivation of ion channels under the block electrode when stimulation frequency is 30 kHz. The legends in (c) indicate the types of waveforms: symmetric and non-symmetric with a 1 μs difference in pulse width between the positive and negative pulses. (a) Change of membrane potential, (b) Na^+ channel activation, (c) Na^+ channel inactivation, (d) K^+ channel activation. Stimulation waveforms: 30 kHz at block threshold intensities. Axon diameter: 2 μm. Abscissa: time in ms after the start of blocking stimulation.

Fig.6. The changes in membrane potential, ionic currents and activation/inactivation of ion channels near the block electrode when conduction block is induced by a 120 kHz non-symmetric waveform with the positive pulse 1 μs longer than the negative pulse. The legends in (d) indicate the locations along the axon. The location at 30.0 mm is under the block electrode. (a) Change in membrane potential, (b) Na^+ current, (c) K^+ current, (d) Na^+ channel activation, (e) Na^+ channel inactivation, (f) K^+ channel activation. Non-symmetric stimulation waveform: 120 kHz, 19.2 mA. Axon diameter: 2 μm.

Abscissa: time in ms after the start of blocking stimulation.

Fig.7. The changes in membrane potential, ionic currents and activation/inactivation of ion channels near the block electrode when conduction block is induced by a 120 kHz non-symmetric waveform with the negative pulse 1 μs longer than the positive pulse. The legends in (d) indicate the locations along the axon. The location at 30.0 mm is under the block electrode. (a) Change in membrane potential, (b) Na^+ current, (c) K^+ current, (d) Na^+ channel activation, (e) Na^+ channel inactivation, (f) K^+ channel activation. Non-symmetric stimulation waveform: 120 kHz, 8.7 mA. Axon diameter: 2 μm. Abscissa: time in ms after the start of blocking stimulation.

Figure
Click here to download Figure: Figure1.pdf

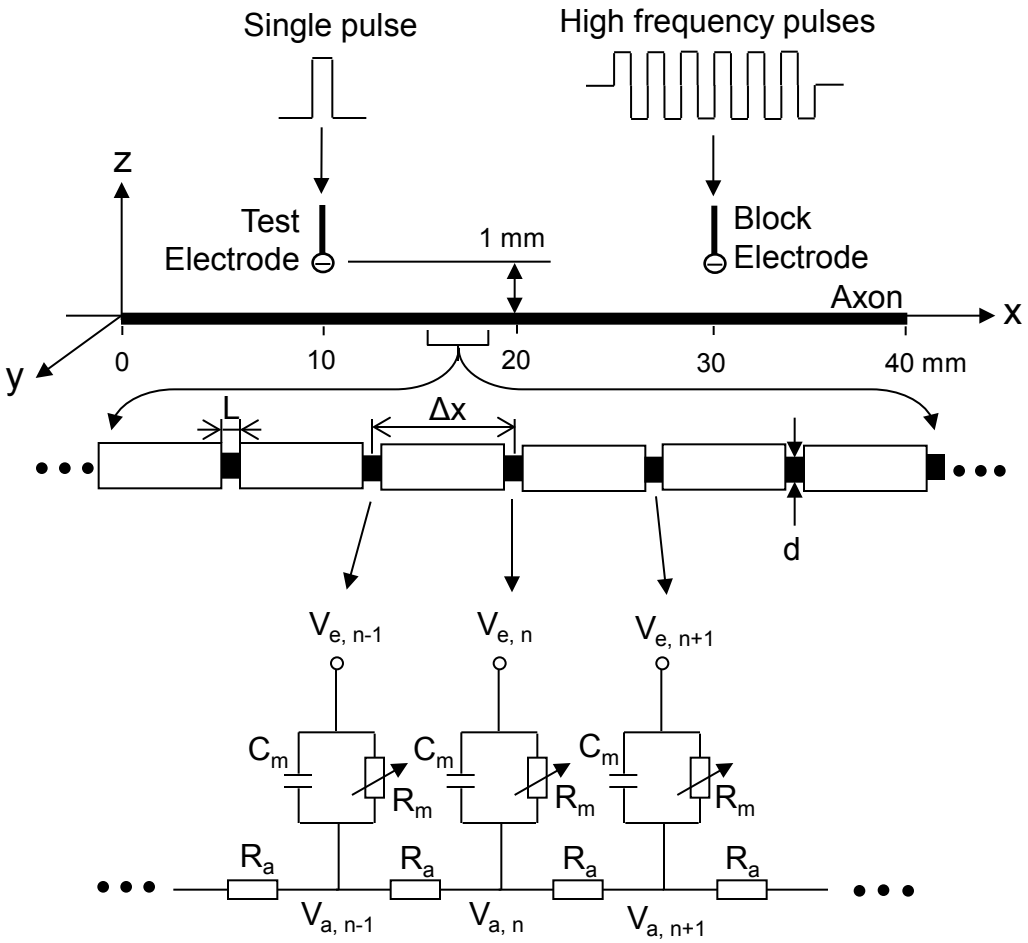

Fig.1. Myelinated axonal model used to simulate conduction block induced by high-frequency biphasic electrical current. The inter-node length $\Delta x = 100d$; d is the axon diameter. L is the nodal length. Each node is modeled by a resistance-capacitance circuit based on the FH model. R_a: inter-nodal axoplasmic resistance; R_m: nodal membrane resistance; C_m: nodal membrane capacitance; $V_{a,n}$: intracellular potential at the n^{th} node; $V_{e,n}$: extracellular potential at the n^{th} node.

Figure
Click here to download Figure: Figure2.pdf

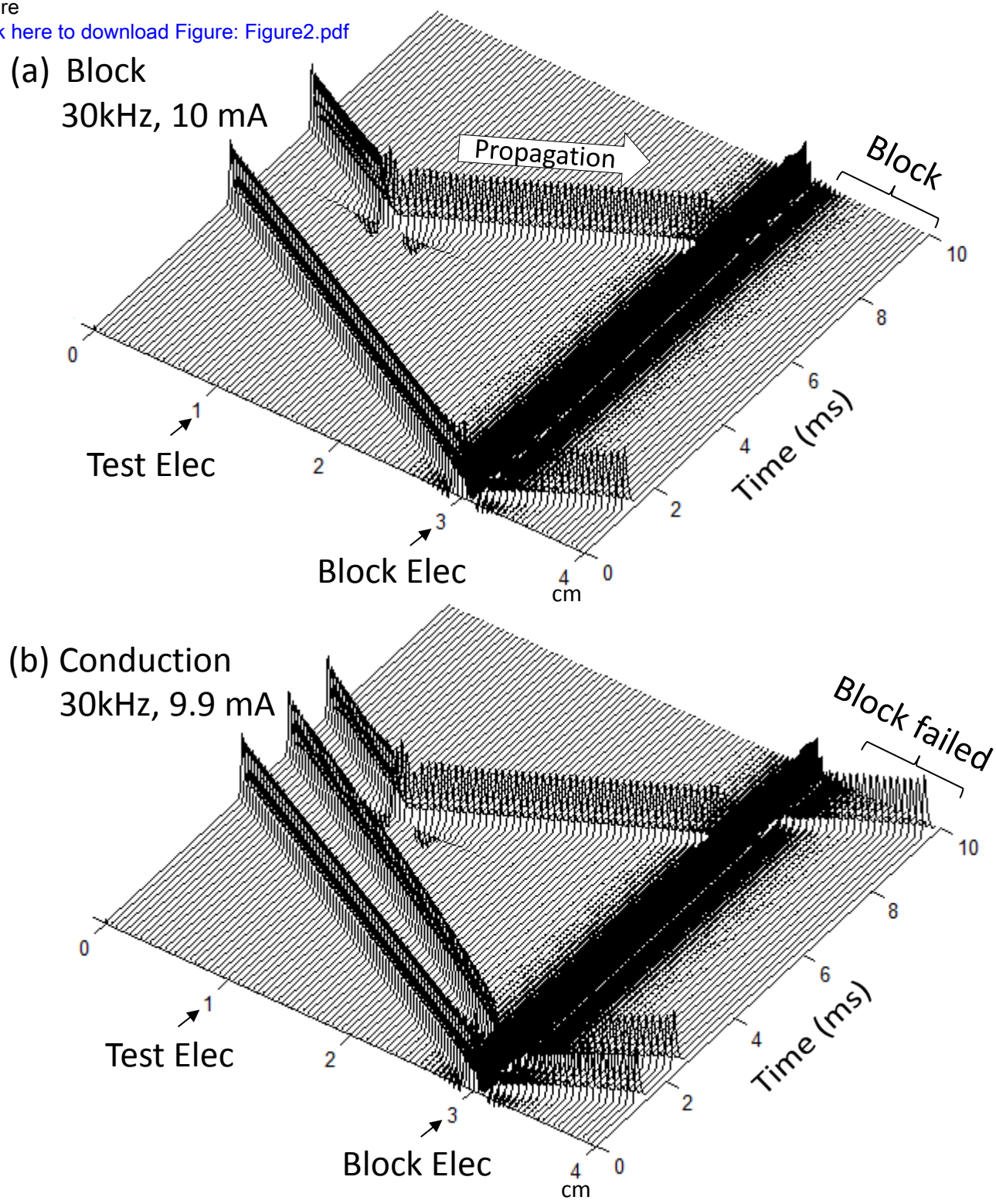

Fig.2. Blocking the propagation of action potentials along an myelinated axon by high-frequency symmetric biphasic stimulation. High-frequency (30 kHz) stimulation is continuously delivered at the block electrode, which initiated an initial action potential in (a) and two initial action potentials in (b). Another action potential is initiated via the test electrode at 5 ms after starting the high-frequency stimulation, and propagates towards both ends of the axon. The 30 kHz stimulation blocks nerve conduction at the intensity of 10 mA (a), but not at 9.9 mA (b). The short arrows mark the locations of test and block electrodes along the axon. The white arrow indicates propagation of the action potential to the location of the 30 kHz blocking stimulation. Axon diameter: 2 μm.

Figure
Click here to download Figure: Figure3.pdf

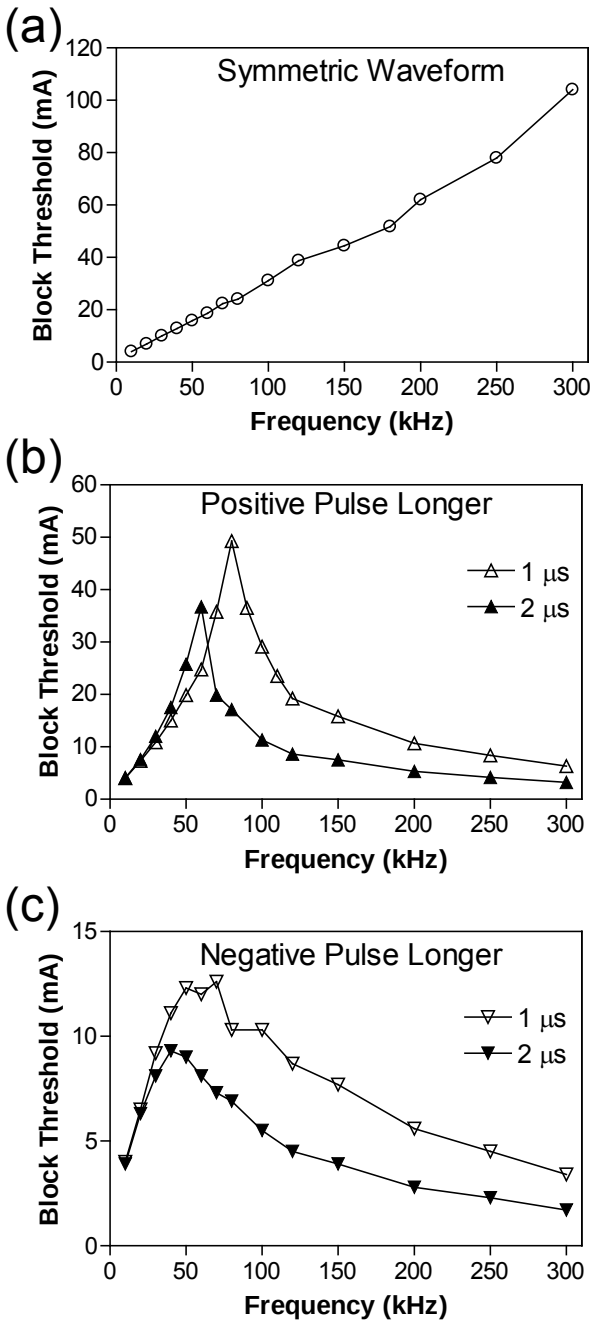

Fig.3. The threshold intensity to block nerve conduction changes with the stimulation frequency. (a). For the symmetric waveform, the block threshold monotonically increases as the frequency increases. (b). If the positive pulse is longer (1 or 2 μs), the block threshold peaks at 60-80 kHz and then gradually decreases as the frequency increases. (c). If the negative pulse is longer (1 or 2 μs), the block threshold peaks at 40-70 kHz. Axon diameter: 2 μm.

Figure
Click here to download Figure: Figure4.pdf

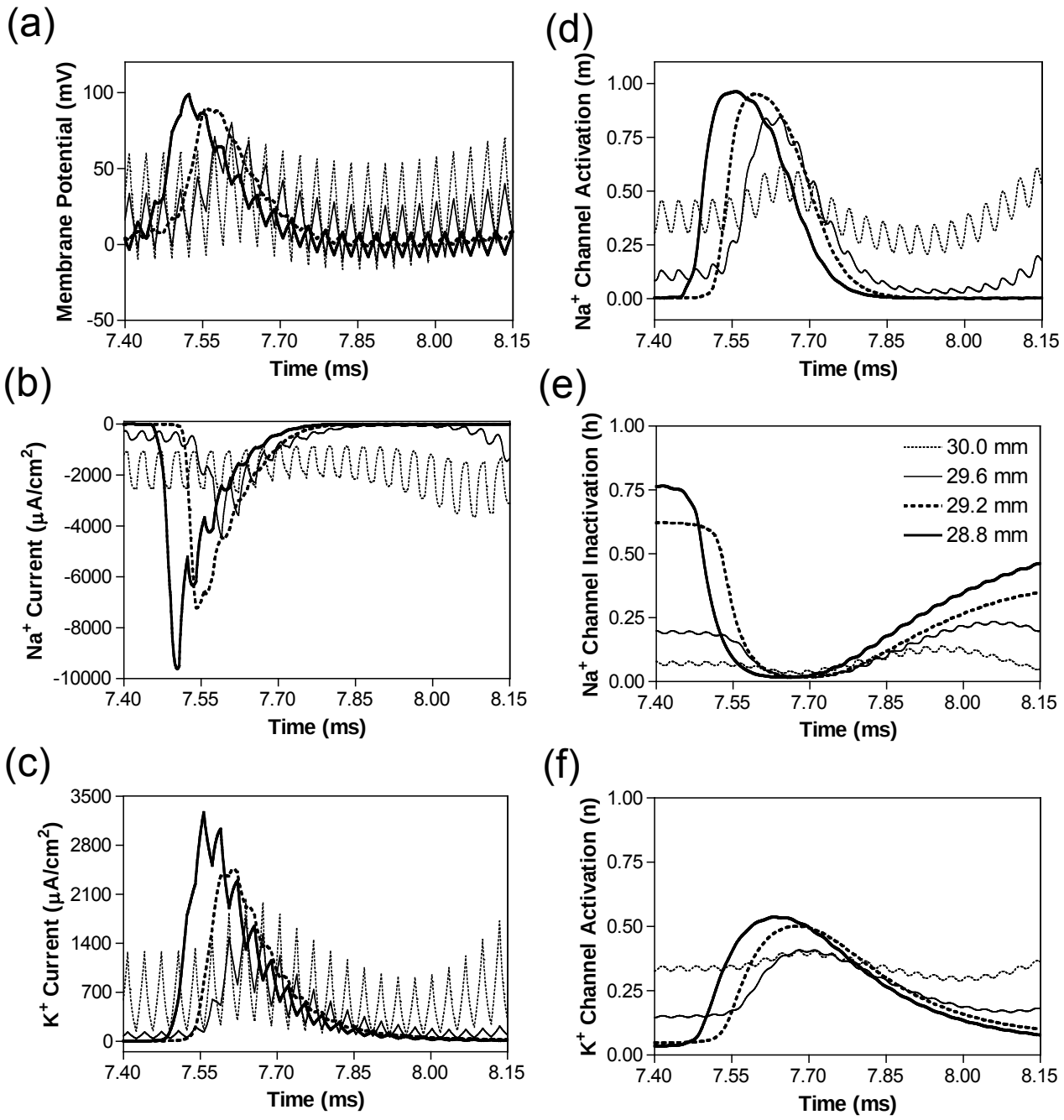

Fig.4. The changes in membrane potential, ionic currents and activation/inactivation of ion channels near the block electrode when conduction block occurs as shown in Fig.2 (a) during stimulation with a symmetric waveform. The legends in (e) indicate the locations along the axon. The location at 30.0 mm is under the block electrode. (a) Change in membrane potential, (b) Na^+ current, (c) K^+ current, (d) Na^+ channel activation, (e) Na^+ channel inactivation, (f) K^+ channel activation. Symmetric stimulation waveform: 30 kHz, 10 mA. Axon diameter: 2 μm. Abscissa: time in ms after the start of blocking stimulation.

Figure
Click here to download Figure: Figure5.pdf

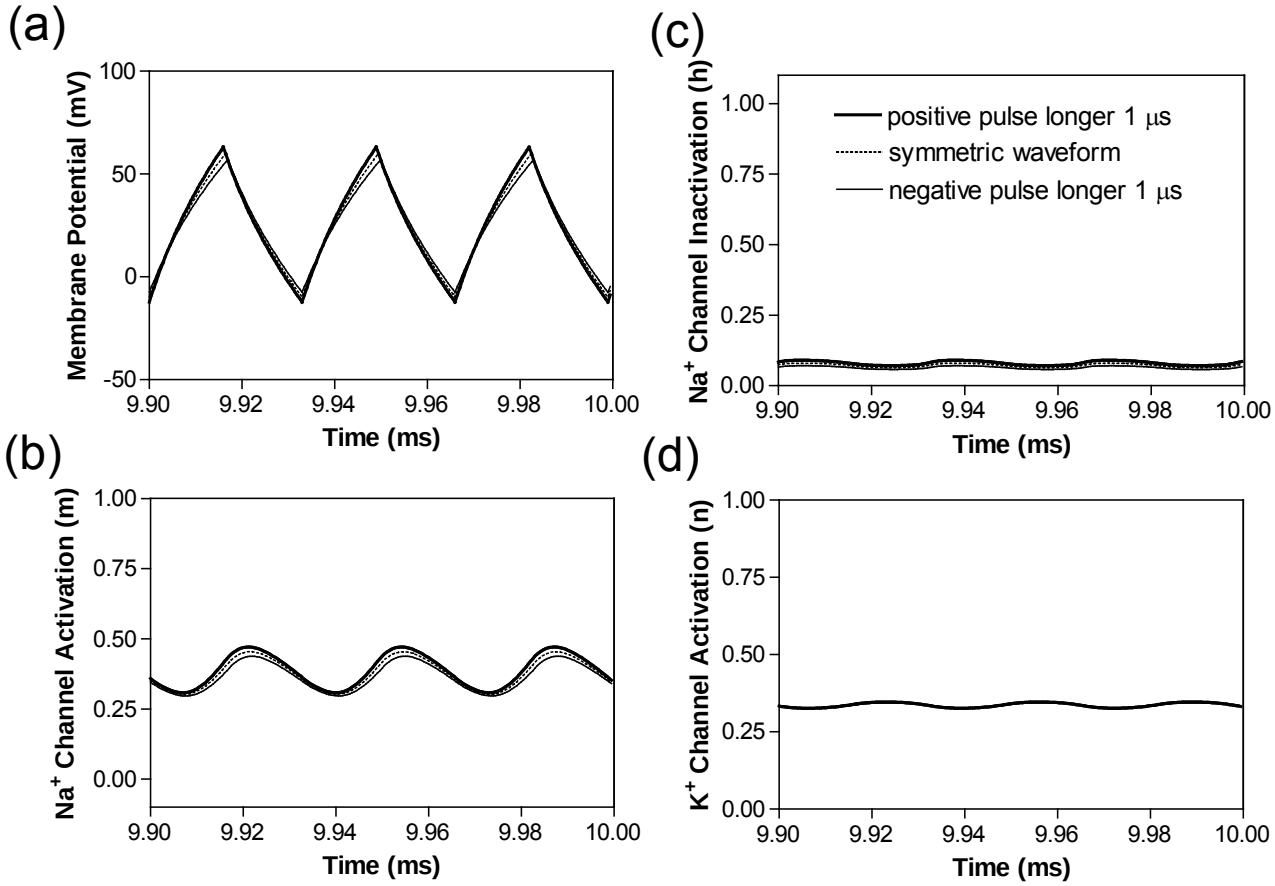

Fig.5. The effects of non-symmetric waveforms on membrane potential and activation/inactivation of ion channels under the block electrode when stimulation frequency is 30 kHz. The legends in (c) indicate the types of waveforms: symmetric and non-symmetric with a 1 μs difference in pulse width between the positive and negative pulses. (a) Change of membrane potential, (b) Na^+ channel activation, (c) Na^+ channel inactivation, (d) K^+ channel activation. Stimulation waveforms: 30 kHz at block threshold intensities. Axon diameter: 2 μm. Abscissa: time in ms after the start of blocking stimulation.

Figure
Click here to download Figure: Figure6.pdf

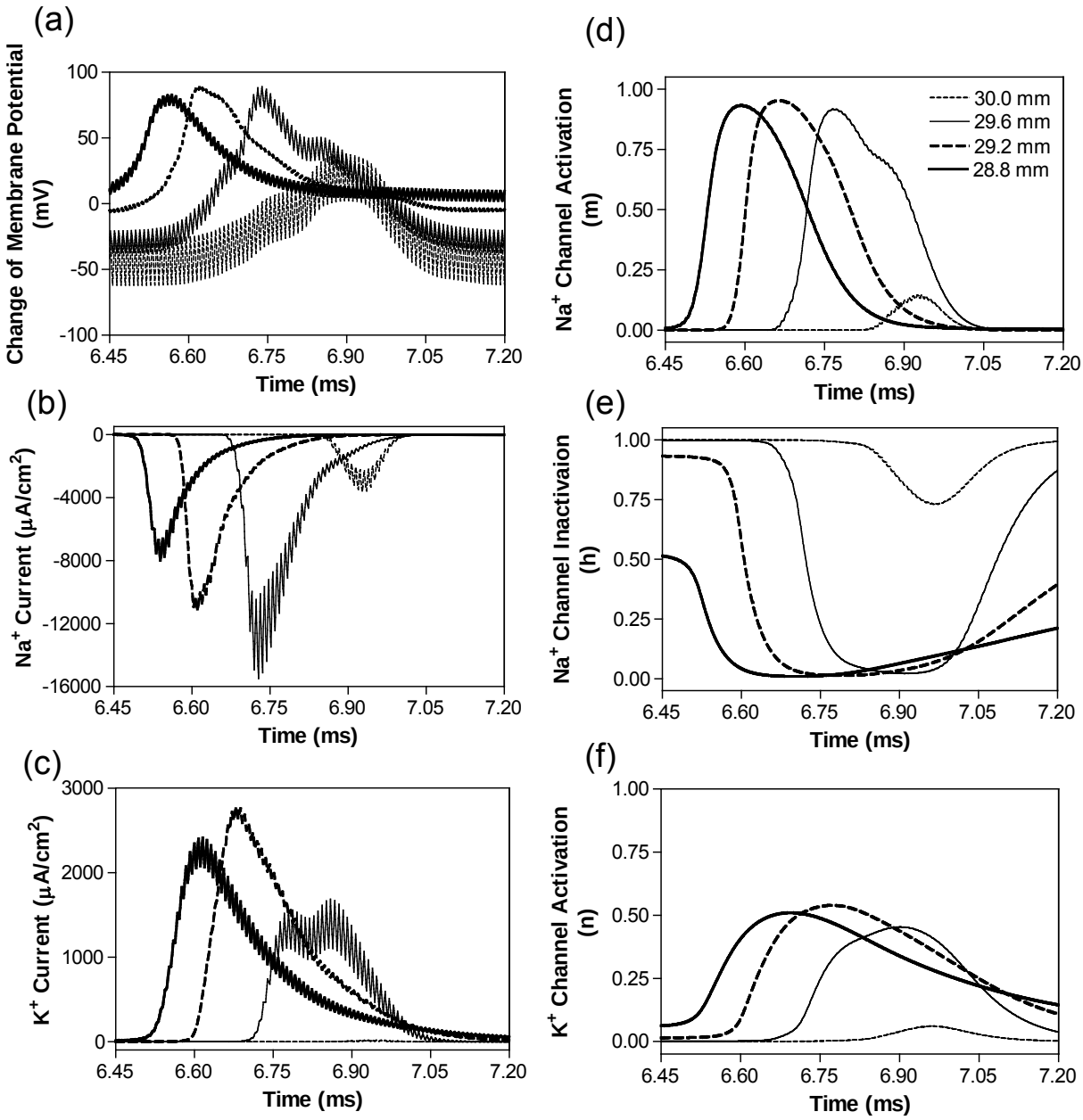

Fig.6. The changes in membrane potential, ionic currents and activation/inactivation of ion channels near the block electrode when conduction block is induced by a 120 kHz non-symmetric waveform with the positive pulse 1 μs longer than the negative pulse. The legends in (d) indicate the locations along the axon. The location at 30.0 mm is under the block electrode. (a) Change in membrane potential, (b) Na^+ current, (c) K^+ current, (d) Na^+ channel activation, (e) Na^+ channel inactivation, (f) K^+ channel activation. Non-symmetric stimulation waveform: 120 kHz, 19.2 mA. Axon diameter: 2 μm. Abscissa: time in ms after the start of blocking stimulation.

Figure
Click here to download Figure: Figure7.pdf

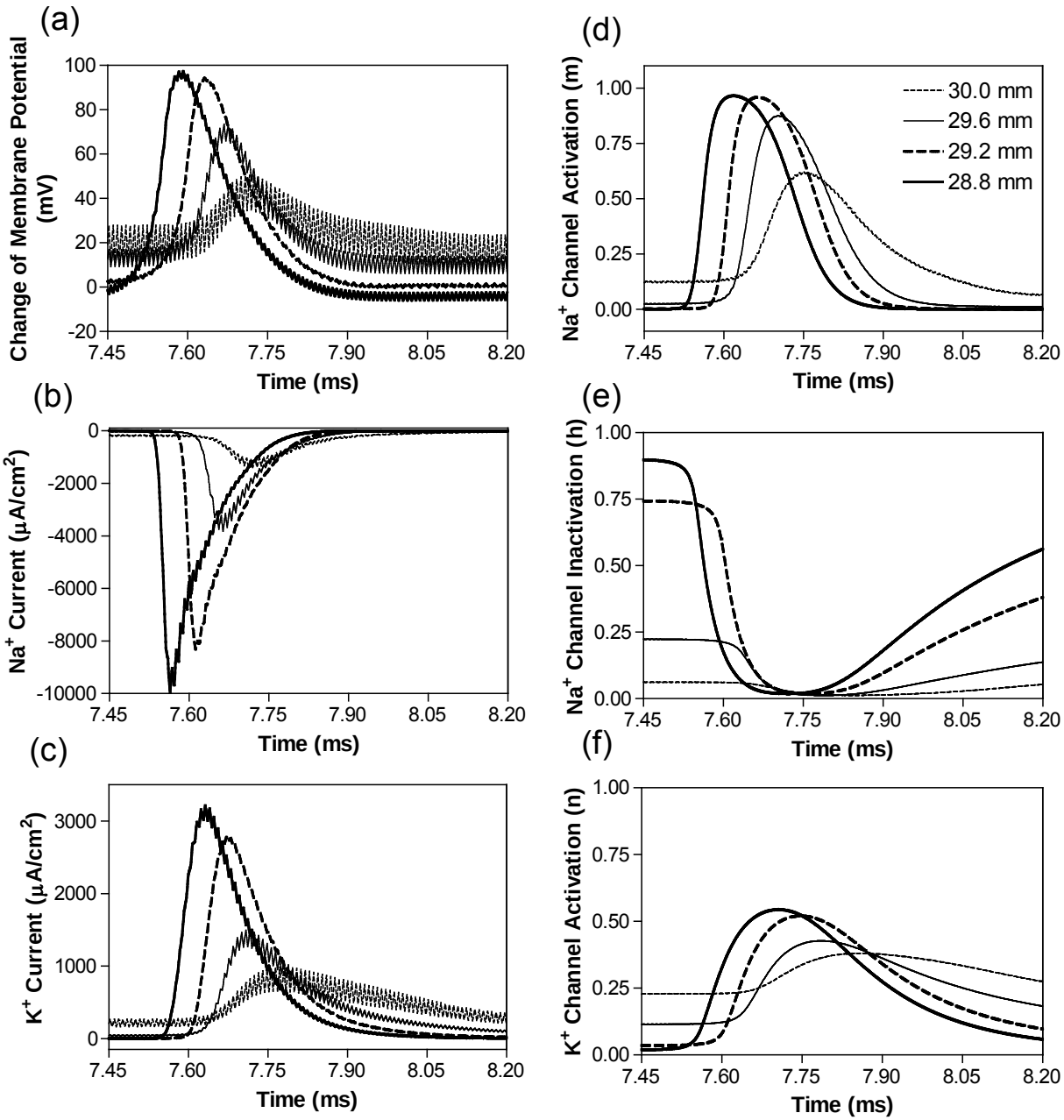

Fig.7. The changes in membrane potential, ionic currents and activation/inactivation of ion channels near the block electrode when conduction block is induced by a 120 kHz non-symmetric waveform with the negative pulse 1 μs longer than the positive pulse. The legends in (d) indicate the locations along the axon. The location at 30.0 mm is under the block electrode. (a) Change in membrane potential, (b) Na^+ current, (c) K^+ current, (d) Na^+ channel activation, (e) Na^+ channel inactivation, (f) K^+ channel activation. Non-symmetric stimulation waveform: 120 kHz, 8.7 mA. Axon diameter: 2 μm. Abscissa: time in ms after the start of blocking stimulation.

Pudendal Nerve Stimulation and Block by a Wireless-Controlled Implantable Stimulator in Cats

Guangning Yang, Jicheng Wang, Bing Shen, James R. Roppolo, William C. de Groat, Changfeng Tai
University of Pittsburgh

Background: To determine the functionality of a wireless controlled implantable stimulator designed for stimulation and block of the pudendal nerve.
Methods: In 5 cats under α-chloralose anesthesia, the stimulator was implanted underneath the skin on the left side in the lower back along the sacral spine. Two tripolar cuff electrodes were implanted bilaterally on the pudendal nerves in addition to one bipolar cuff electrode that was implanted on the left side central to the tripolar cuff electrode. The stimulator provided high frequency (5-20 kHz) biphasic stimulation waveforms to the two tripolar electrodes and low frequency (1-100 Hz) rectangular pulses to the bipolar electrode. Bladder and urethral pressures were measured to determine the effects of pudendal nerve stimulation (PNS) or block.
Results: The maximal (70-100 cmH_2O) urethral pressure generated by 20 Hz PNS applied via the bipolar electrode was completely eliminated by the pudendal nerve block induced by the high frequency stimulation (6-15 kHz, 6-10 V) applied via the two tripolar electrodes. In a partially filled bladder 20-30 Hz PNS (2-8 V, 0.2 ms) but not 5 Hz stimulation applied via the bipolar electrode elicited a large sustained bladder contraction (45.9±13.4 to 52.0±22 cmH_2O). During cystometry, the 5 Hz PNS significantly ($P<0.05$) increased bladder capacity to 176.5±27.1% of control capacity.
Conclusions: The wireless controlled implantable stimulator successfully generated the required waveforms for stimulation and block of pudendal nerve, which will be useful for restoring bladder functions after spinal cord injury (SCI).

FUNDING: This study is funded by DOD Spinal Cord Injury Research Program (SCIRP) under contract number W81XWH-11-1-0819.

Simulation Analysis of Conduction Block in Unmyelinated Axon after High-Frequency Electrical Stimulation

G. Yang [1], J. Wang [1], J. R. Roppolo [2], W. C. de Groat [2], C. Tai [1,2]

[1] Department of Urology, University of Pittsburgh, Pittsburgh, PA
[2] Department of Pharmacology and Chemical Biology, University of Pittsburgh, PA

Nerve conduction block induced by high frequency (>5 kHz) electrical stimulation have many potential clinical applications. Although the original Hodgkin-Huxley model can successfully simulate the conduction block in unmyelinated axon during the stimulation, it failed to simulate the conduction block during the period after the stimulation. In this study, the Hodgkin-Huxley model was modified to include an electrogenic sodium-potassium pump and successfully simulated the post-stimulation conduction block. Simulation analysis indicates that high frequency electrical stimulation causes continuous sodium influx and increases intra-axonal sodium concentration that can only recover slowly after the stimulation, causing conduction block during the post-stimulation period. The duration of the post-stimulation block is proportional to the duration and intensity of high frequency electrical stimulation. Understanding the mechanisms underlying high frequency block is important to further promote its clinical applications.

This study is funded by DOD Spinal Cord Injury Research Program (SCIRP) under contract number W81XWH-11-1-0819

Index Terms—Na-K pump, recovery period, sodium concentration, High-frequency.

Military Health System Research Symposium, Fort Lauderdale, Florida, 2012

AN IMPLANTABLE NEUROPROSTHETIC DEVICE TO RESTORE BLADDER FUNCTION AFTER SCI

Changfeng Tai, PhD
Assistant Professor, University of Pittsburgh

PURPOSE/AIMS: The purpose of this research is to design and develop an implantable neuroprosthetic device to restore urinary bladder function after spinal cord injury (SCI).

DESIGN: We hypothesize that bladder function can be normalized by electrical stimulation and/or blockade of pudendal nerves after chronic SCI using an implantable neuroprosthetic device. Experiments were conducted in cats under both anesthetic and awake conditions to validate our hypothesis. A small (4x5.5x1.4 cm), wireless controlled, wireless chargeable, implantable stimulator was developed for this purpose.

POPULATION/SAMPLE STUDIED: Total 7 cats with chronic SCI were used under α-chloralose anesthesia in this study. One of the cats was also tested under awake condition with the stimulator implanted chronically.

METHODS: Under anesthesia, bladder infusion and pressure measurement was performed via a catheter inserted through the bladder dome. Voiding was induced by slow infusion (0.5-4 ml/min) of the bladder or by electrically stimulating/blocking the pudendal nerves. Under awake condition, bladder empting was performed either by manual expression or by the chronically implanted pudendal nerve stimulator.

DATA ANALYSIS: Voiding efficiency (voided volume/total bladder volume) was compared between bladder distention-induced voiding and pudendal nerve stimulation-induced voiding under anesthesia, and between manual expression and chronically implanted stimulator-induced voiding under awake condition.

FINDINGS: Voiding induced by bladder distention had a very low efficiency (7.3±0.9%) in chronic SCI cats. Electrically stimulating/blocking the pudendal nerves induced efficient (80-90%) voiding under both anesthesia and awake condition.

CONCLUSIONS/RECOMMENDATIONS: Electrically stimulating/blocking the pudendal nerves in cats can successfully restore bladder functions after chronic SCI.

IMPLICATIONS: This animal study indicates that an implantable stimulator might be developed to restore bladder function after chronic SCI in human subjects by electrically stimulating/blocking the pudendal nerves.

FROM/TO TIME PERIOD OF STUDY: September 22, 2011 – October 21, 2014

FUNDING: This study is funded by DOD Spinal Cord Injury Research Program (SCIRP) under contract number W81XWH-11-1-0819.

42nd Annual Meeting of Society for Neuroscience, New Orleans, 2012.

Mechanisms Underlying Non-monotonic Block of Unmyelinated Axons by High-Frequency Biphasic Stimulation

J. Wang [1], S. Zhao [1,2], J. R. Roppolo [3], W. C. de Groat [3], C. Tai [1]

[1] Department of Urology, University of Pittsburgh, Pittsburgh, PA
[2] Department of Biomedical Engineering, Beijing Jiaotong University, P.R. China
[3] Department of Pharmacology and Chemical Biology, University of Pittsburgh, PA

Axonal conduction block induced by high-frequency biphasic electrical current is investigated using a lumped circuit model of the unmyelinated axon based on Hodgkin-Huxley equations. Axons of different diameters (1 and 2 μm) can be blocked completely when the stimulation frequency is between 5 kHz and 100 kHz. The non-monotonic relationship between block threshold and stimulation frequency, recently discovered in unmyelinated axons of sea-slugs and frogs, is successfully reproduced. Our simulation reveals that complete deactivation of sodium channels by the high-frequency blocking stimulation is the mechanism underlying the decrease in block threshold as the frequency increases above 20 kHz. At a relatively higher frequency (>30 kHz), the high-frequency blocking stimulation can quickly deactivate the sodium channels at the beginning of the stimulation, thereby avoiding the generation of initial action potentials. This simulation study further increases our understanding of conduction block in unmyelinated axons induced by high-frequency biphasic electrical current, and can guide future animal experiments as well as optimize stimulation parameters that might be used for electrically induced nerve block in clinical applications.

Key words: nerve, block, simulation, high-frequency, model.

Supported by: DOD Spinal Cord Injury Research Program (SCIRP) under contract number W81XWH-11-1-0819.